INTERNATIONAL UNION OF PURE AND APPLIED CHEMISTRY
IUPAC Secretariat: Back Court Chambers, 2-3 Pound Way,
Cowley Centre, Oxford OX4 3YF, UK

Organizing Committee

President: H. Akamatu
Vice-Presidents: T. Asahara
M. Matsui
S. Shibata
General Secretary: M. Ōki
Members:

Y. Ban
T. Fujinaga
M. Fujimaki
T. Hino
Y. Inubuse
Y. Ishii
S. Itô
Y. Kanda
O. Kammori
T. Mukaibo
S. Nagakura
A. Nakajima
H. Negita
T. Okamoto
S. Okamura
K. Saito
N. Saito
S. Shibata
N. Takahashi
T. Takeuchi
I. Tanaka
N. Tanaka
N. Tokura
T. Tsuruta
S. Yoshizawa
Y. Yukawa

International Union of Pure and Applied Chemistry
in conjunction with
Science Council of Japan
The Chemical Society of Japan
Pharmaceutical Society of Japan
and
The Agricultural Chemical Society of Japan

Physical Chemistry

Session lectures presented at the
Twentysixth International Congress of
Pure and Applied Chemistry
Tokyo, Japan, 4-10 September 1977

Symposium Editor:

S. Nagakura
University of Tokyo, Japan

PERGAMON PRESS
OXFORD · NEW YORK · TORONTO · SYDNEY · PARIS · FRANKFURT

U.K.	Pergamon Press Ltd., Headington Hill Hall, Oxford OX3 0BW, England
U.S.A.	Pergamon Press Inc., Maxwell House, Fairview Park, Elmsford, New York 10523, U.S.A.
CANADA	Pergamon of Canada, Suite 104, 150 Consumers Road, Willowdale, Ontario M2J 1P9, Canada
AUSTRALIA	Pergamon Press (Aust.) Pty. Ltd., P.O. Box 544, Potts Point, N.S.W. 2011, Australia
FRANCE	Pergamon Press SARL, 24 rue des Ecoles, 75240 Paris, Cedex 05, France
FEDERAL REPUBLIC OF GERMANY	Pergamon Press GmbH, 6242 Kronberg-Taunus, Pferdstrasse 1, Federal Republic of Germany

Printed in Great Britain by A. Wheaton & Co. Ltd., Exeter

ISBN 0 08 022036 3

Pure & Appl. Chem., Vol.50, pp. 743-758.
Pergamon Press Ltd.1978. Printed in Great Britain.

0033-4545/78/0801-0743 $02.00/0

CONTEMPORARY PERSPECTIVES IN PHYSICAL CHEMISTRY

Charles A. McDowell

Department of Chemistry, The University of British Columbia,
2075 Wesbrook Place, Vancouver, British Columbia, V6T 1W5
Canada

Abstract - Physical Chemistry has undergone a renaissance in the past few years because of the introduction of many new techniques. Many of these novel advances rely on the application of electronic developments, or the application of newer computing methods. In addition the introduction of lasers has led to a number of important developments which are likely to have a lasting impact on the whole field of Physical Chemistry.
Of the areas which owe most to developments in electronics and computing techniques we discuss some important advances in (a) electron and photoelectron spectroscopy; (b) magnetic resonance techniques, particularly those involving multiple-pulse techniques and multiple-quantum transitions; and (c) pico-second time resolved phenomena which have led to interesting developments in the study of vibrational energy transfer, relaxation phenomena, and very fast reactions.
Lasers have given rise to new areas of spectroscopy based on two quantum and multiple-quantum transitions. The use of dye lasers has led to several important new advances. Laser photochemistry, particularly, the observation of multiple-quantum photodissociation of molecules has opened up new exciting areas for study. Many of these studies have presented important new possibilities for the photochemical separation of isotopes.
Many interesting double resonance techniques have led to many new important details about molecular structure and have considerably increased the sensitivity and range of spectroscopic methods. Those which are discussed in this lecture include laser magnetic resonance spectroscopy and laser microwave optical double resonance.

When the organizers of this Congress wrote to me some considerable time ago inviting me to present an opening lecture in the Physical Chemistry Section, I hesitated for some time before accepting the invitation. In the meantime, Professor Nagakura sent me a brief outline of the various topics which were to be discussed in this session. After surveying the range of topics to be discussed, it was with some trepidation that I finally decided to accept the invitation.

The reason for my concern will be obvious to anyone who has attempted to follow closely the developments in Physical Chemistry during the past several years. A decade or so ago, Physical Chemistry seemed to have reached a point when the subject seemed to be well defined and fairly settled. Then, suddenly, there was the introduction of lasers and at the same time there came considerable developments in the application of computers, and also the application of various pulse techniques for measuring very fast processes. These new developments have completely revolutionalized the subject, so that we have had during the past five years or so, a complete revitalization of the whole field of Physical Chemistry. Not only have new areas of activity developed, but many older areas have been rejuvenated by the introduction of these new experimental techniques.

In attempting to survey these many interesting new developments I have, of course, been forced to read more carefully the recent literature. That discipline has been a most rewarding educational experience for me, and to that extent I am grateful to the Organizing Committee for causing me to be a more diligent student.

In this lecture I propose to make a quick survey of the more exciting recent and novel developments in various areas of Physical Chemistry. After that I shall deal in a little more detail with certain topics which seem to me to be most likely to lead to significant advances in the immediate future. In doing this I am, of course, mindful that I may omit some topics, and areas of the subject, which will seem to be of great importance to some persons. That some will be disappointed because the topic of their interest is omitted is inevitable. I am most conscious that to some extent I am in the position of the guest at a very large and beautiful buffet-style banquet, who having made his choice of the delicacies which appeal to him reaches the end of the buffet table to find some of the chefs staring at the guest's plate and exclaiming loudly, "But you have not chosen my favourite speciality".

Now may I offer by way of the hors d'ouvre, a quick survey of some important and novel developments in chosen areas of Physical Chemistry. In the area of Molecular Spectroscopy the introduction of lasers has changed that field completely. There have been developed new methods which have led to ultra high resolution spectroscopy; and even to spectroscopy without spectrographs or spectrometers! In addition, many multiple resonance techniques and multi-photon techniques have been developed. Whole new areas of spectroscopy have been revitalized. For example, some years ago it seemed that we had reached almost the limits of resolution in molecular spectroscopy, both in the ultra violet and in the infrared regions. In many cases Doppler broadening was the limiting factor determining the resolution which could be obtained by using the then available high resolution spectrographic methods. Various molecular beam techniques enabled certain Doppler spectra to be measured but the method is rather difficult to apply in many cases. The introduction of lasers and the discovery of multi-photon spectra, as well as various double resonance techniques, has led to the development of a Doppler free spectroscopy which presents us with the possibility of ultra high resolution studies widely applicable in both atomic and molecular spectroscopy. The extent to which the realizable resolution of spectra lines has been enhanced by the introduction of these newer methods is shown in Fig. 1.

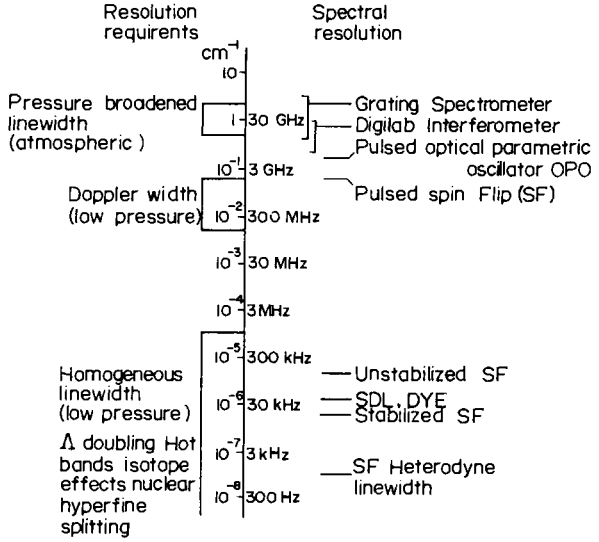

Fig. 1 Resolution requirements and attainable resolution from conventional instruments and tunable lasers.

Considerable improvements in the design of electron energy analysers have led to much higher resolution studies in Photoelectron Spectroscopy and Electron Spectroscopy. Both of these methods continue to yield results of importance in the study of molecular structure, both in the gaseous phase and in the solid state. Other interesting developments have occurred with Auger Spectroscopy and in the applications of Penning Ionization methods. Later I shall discuss some recent developments in the application of photoelectron spectroscopy to the study of free radicals and transient molecules, and the application of newer methods of electron spectroscopy to the study of ionization phenomena in gaseous molecules, and in particular, to the study of inner

shell excitation, and the determination of binding energies and momentum distributions of valence electrons which have been carried out in our Department.

Multi-photon techniques have also been of great importance recently in the study of photoionization phenomena, and these will undoubtedly lead to interesting developments in photoelectron spectroscopy. In the latter field, use of various types of lasers has led to many interesting new studies, not only of the photo-decomposition of molecular ions, but also a new area, Laser Detachment Photoelectron Spectroscopy. These studies have given us much new spectroscopic information concerning the energy levels and the structure of molecular ions. In addition, this latter technique has led to the very precise determination of electron affinities of a large number of radicals and molecules.

We have also seen important developments because of new discoveries in the area of Raman Spectroscopy. Laser Raman Spectroscopy has, of course, been an important new area of study, but in addition, newer Raman effects, such as Coherent Anti-Stokes Raman Spectroscopy have already become most important. Moreover, a new type of laser, called a Spin Flip Raman Laser, promises to lead to ultra high resolution infra-red spectroscopy, particularly when it is combined with optical-acoustical detection. A listing of the more important developments in this field from a physical chemistry viewpoint, is given in Table 1, shown on the following page. Of the topics listed in Table 1, we shall later discuss in more detail only two, namely, Coherent Anti-Stokes Raman Scattering (CARS) and the Spin Flip Raman Laser. Both of these will obviously be of great importance in Physical Chemistry.

TABLE 1. Developments in Raman scattering

Laser Resonance Raman Spectroscopy Inverse Raman Effect
Coherent Anti-Stokes Raman Scattering (CARS)
Coherent Stokes Raman Spectroscopy CSRS (SCISSORS)
Higher Order Raman Spectral Excitation Studies (HORSES)
Stimulated Raman Emission
Slip Flip Raman Laser (SFRL)

In the field of Chemical Kinetics, it is clear that great progress has been made studying the details of collision processes in gas phase reactions. Already there is much knowledge on a microscopic scale concerning the exchange of vibrational and rotational energy and the details of interactions and reactions in various chemical processes. Many of these researches are of considerable importance for the development of chemical lasers, a field in which there is at present tremendous activity. Our understanding of reaction dynamics from features of a potential energy surface has improved greatly in recent years. With simple systems such as $X+H_2$ accurate calculations of the potential energy surfaces are possible (Ref. 1), and molecular beam experiments provide accurate values for the angular (Ref. 2), and energy distribution (Ref. 3), which can be explained satisfactorily by the existing theories.

Most modern work has shown the importance of "sticky" intermediate complexes, e.g., I_2F in biomolecular reactions such as $F+I_2 \rightarrow IF+I$. These have been identified in the gas phase by using mass spectrometric techniques (Ref. 4).

There are now available two different methods using crossed molecular beams for obtaining information about the stability of these collision complexes, the study of which is likely to be of considerable importance. The first method is to study the lifetime of the complex by measuring the angular distribution of the products. The second method involves the synthesis of the radical molecules through erdoergic molecule-molecule reactions (Ref. 5).

The development of Picosecond Techniques has, of course, given us a method for studying very fast chemical reactions and processes particularly in the liquid phase. Not only has this been of great importance in studying relaxation processes in chemical systems, but it has also led to many interesting and important new developments in various branches of Physical Chemistry and Biophysics.

Apart from the obvious use of picosecond techniques in measuring the rates of ultra fast reactions, there are other important applications in chemistry. One of these is the study of the degradation of energy within a molecule.

Because many of these energy exchange processes occur so very rapidly and lie within the picosecond time domain, it is obvious that there are likely to be important developments from studies using these ultra fast measuring techniques.

In the case of photodissociation processes in liquids, there arises the well known 'cage effect'. Studies of the photodissociation of I_2 in various solvents using picosecond techniques have yielded much new information. An important finding was the first direct observation of the dynamics of a collision-induced predissociation in the liquid state with a pseudo-first-order constant $\sim 10^{11} sec^{-1}$ (Ref. 6).

Charge-transfer processes and the subsequent energy dissipation are important processes in chemistry. Picosecond studies on the anthracene diethyl aniline systems provide new views of the electron-transfer process and test theories of diffusion-controlled chemical processes (Ref. 7). It is also shown by these studies that there are strong geometrical requirements for electron transfer in non-polar solvents. Time dependent fluorescence depolarization measurements in the picosecond domain have been used by Fleming et al. (8) for the direct observation of the rotational diffusion of molecules. Picosecond methods have been applied to study the kinetics of the photosynthetic process (Ref. 9). Much progress has been made in unravelling the details of the photosynthetic reaction centre of bacteriochlorophyll, particularly those reaction processes which occur in times 5 picoseconds after the primary stimulus.

Magnetic Resonance Spectroscopy continues to be an area in which there is much innovation. Numerous multi-resonance techniques have been introduced and these have led to the solution of many problems in Molecular Structure and to the measurement of various relaxation processes of interest in all aspects of physical and biophysical chemistry. These new techniques have also had some important applications in chemical analysis. Multiple resonance techniques have been found to be widely applicable in Electron Paramagnetic Resonance, Nuclear Magnetic Resonance as well as in Nuclear Quadrupole Resonance Spectroscopy. We thus now have Electron-Electron Double Resonance (ELDOR), Electron-Nuclear Double Resonance (ENDOR) and Internuclear-Nuclear Double Resonance (INDOR), etc.

The continued application of pulse techniques deriving from the work of Hahn (Ref. 10), Carr-Purcell (Ref. 11), and Meiboom and Gill (Ref. 12), has led not only to important methods for the determination of relaxation mechanisms and relaxation times, but with the introduction of fast Fourier transform techniques has led to a whole new method, namely Fourier Transform Nuclear Magnetic Resonance Spectroscopy. This will continue to have many important applications in all branches of chemistry.

Perhaps the development of new methods for high resolution NMR of solids represent some of the more important recent developments. The perfection of certain of these newer methods will undoubtedly have a great impact on our subject. Earlier methods based on the high speed spinning of samples at the so-called 'magic angle' (Ref. 13) seem recently to be replaced by multiple pulse methods followed by Fourier transform techniques. The most promising of these seems to be the four pulse sequence introduced by Waugh, Huber and Haeberlen (Ref. 14) which is sometimes jocularly called the Wahuha sequence.

The increased availability of superconducting magnets together with double resonance techniques has led to the development of the proton-enhanced NMR method (Ref. 15) which has permitted the observation of ^{13}C resonances in natural abundance in organic solids. The application of this method has been developed by Haeberlen et al. (16) and extended not only to ^{13}C measurements but also to protons. An important new method called High-Resolution Fourier-Transform Double-Quantum Magnetic Resonance Spectroscopy has been introduced by Pines et al. (17). This double quantum method has already been successfully applied to obtain measurements of the chemical shift of deuterium atoms in organic single crystals.

Here we may perhaps also mention the introduction of Laser Magnetic Resonance Spectroscopy (Ref. 18), which has proved to be of considerable importance in the study of the structure of free radicals in the gas phase. We shall discuss this topic in more detail later.

Because of the development of ultra-high vacuum techniques and their applications there have been impressive advances in the field of Surface Chemistry.

These new ultra-high vacuum techniques ($\sim 10^{-11}$ torr) have led to the introduction of Low Energy Electron Diffraction (LEED) and Auger Spectroscopy, as well as the application of the methods of photoelectron and electron spectroscopy to the study of very clean surfaces. There are now so many different techniques available for the experimental investigation of surfaces that it is literally impossible for any single person to discuss them adequately. Because of this variety of techniques this field has itself something of an acronymic dictionary.

The results of LEED and Auger studies show markedly different adsorption structures for the same gas adsorbed on different crystal faces of a material. The presence of surface steps has been shown to have an important influence on the nature of the reactions which occur after chemisorption.

The technique of Extended X-ray Absorption Fine Structure (EXAFS) has recently been applied to surfaces and is seen as an ideal complement to LEED. The advantage is that while LEED characterizes the overall symmetry of the surface structure, EXAFS can quantitatively reveal details of the local structure around a given atom. A technique has recently been developed which enhances the sensitivity of EXAFS for surface studies. This involves measuring the Auger electrons as a function of the X-ray photon energy. This new technique has not only led to results of considerable interest and significance, but has added a new aeronym, namely, SEXAFS.

Raman scattering processes

In this section of the paper we shall deal in a little more detail with some specially selected topics. These have been chosen as representing some of the more interesting and important developments in recent times and are techniques which seem likely to have profound impact on many facets of Physical Chemistry. Of the many interesting developments which we mentioned as having taken place in the field of Raman Spectroscopy, we draw attention to two of the techniques which have novel features and such special properties that they seem likely to lead to interesting new developments in the field of Physical Chemistry. These two phenomena are: (a) Coherent Anti-Stokes Raman Scattering (CARS), and, (b) the Spin Flip Raman Laser.

Coherent anti-Stokes Raman scattering (CARS). As is well known, Raman scattering is an incoherent process, but Coherent Anti-Stokes Raman Scattering (CARS) is a four-wave mixing process which arises from the parametric nature of this process. The advantage over the normal spontaneous Raman scattering is that the scattered light in a CARS experiment is well collimated, and its intensity some 5 to 10 orders magnitude greater than the normal Raman scattering process. The transitions leading to Coherent Anti-Stokes Raman Scattering are illustrated in the diagram shown below. The scattering process is initiated by a pulsed tunable laser and interference filters permit the Anti-Stokes pulses of frequency $\omega_4 = (2\omega_1 - \omega_2)$ to be transmitted (Ref. 19). A schematic diagram of the experimental arrangement is shown in the following Fig. 2. Because of the intensity of the CARS lines, (in the case of nitrogen they have in fact been seen by the unaided human eye), the technique is immediately aplicable to the determination of low concentrations of compounds. In that regard it might be important as a non-destructive method for the analysis of biological as well as ordinary materials (Ref. 20). Another advantage is, of course, the enhanced resolution obtainable in a CARS experiment because the laser linewidth can produce to approximately 15 MHz. Because of this resolution precise measurements of rotational vibrational frequencies can be made on molecules for which the relevant data are not available from microwave spectroscopy. Already the technique has been applied to study temperature distributions in flames, and also for the analysis of combustion processes (Ref. 21).

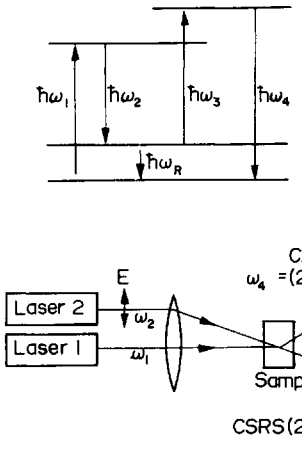

Fig. 2 Coherent Anti-Stokes Raman Spectroscopy CARS

The use of synchronized picosecond pulsed lasers in a CARS experiment enables this method to measure relaxation processes with high accuracy.

Although we have made reference above to the use of pulse techniques in obtaining the CARS radiation, recently c.w. lasers have been used, and in that case the two-branched spectrum of atmospheric pressure nitrogen was recorded in 10 ml/sec.

Spin flip Raman laser. The process of stimulated spin flip Raman scattering by conduction electrons in semiconductors, in particular InSb, has led to an important new spectroscopic method which continues to show that it is likely to be of considerable importance. The Raman scattering process for the spin flip excitation is not markedly different from the ordinary Raman scattering. In the spin flip Raman process the spin of a conduction electron in a semiconductor is reversed with respect to an external supplied magnetic field H. Figure 3 shows an idealized representation of the spin flip Raman scattering. The wavelength of the scattered radiation is magnetically tunable since the energy of the magnetic excitation given by the spin reversal process is dependent upon the value of the applied field H by the equation:- $h\omega_e = |g^*|\beta H$, where β is the usual Bohr magneton, eh/2 MC, but the effective conduction electron g factor, g*, is no longer ∿2 in a crystal environment. In the semi-conductor InSb the strong spin-orbit interaction and small energy gap led to g* values as large as -50. This large g* factor in InSb means that the scattered radiation output is tunable over a range of about 160 cm^{-1} for field strengths up to 10 T, or about 60 MHz per gauss. The spin flip Raman laser is therefore a tunable infra-red source and provides an alternative to other non-linear processes, such as parametric osulation and frequency mixing.

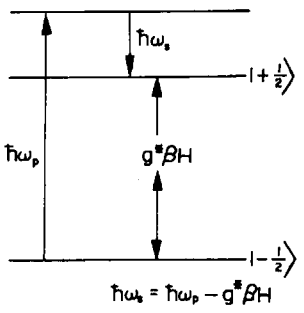

Fig. 3 Idealized energy level diagram for Spin-Flip Raman Scattering

Even with its normal resolution, tunable spin flip Raman spectroscopy has enormous potentiality. Doppler limited spectra can be obtained which reveal Λ-doubling, and nuclear quadrupole splittings in NO (Refs. 22,23). In addition, using the optical acoustic detection method, mentioned below, it has been possible also to study the Zeeman spectroscopy of the v = 1→2 vibrational-rotational transitions of the $^2\Pi_{1\,2}$ and $^2\Pi_{3\,2}$ states of NO. High resolution spectra of other molecules such as OCS, SbH_3, H_2O, etc. (Ref. 22) and C_2H_4 (Ref. 24) have also been obtained. That this technique can be used for ultra-high resolution studies has been demonstrated by Patel (25), who studied the saturation spectroscopy of water vapour and observed Lamb-dip width of the order of 200 kHz, a resolution of ∿3×10^8.

A typical experimental arrangement for the use of a c.w. spin flip Raman laser in molecular spectroscopy is shown below in Fig. 4.

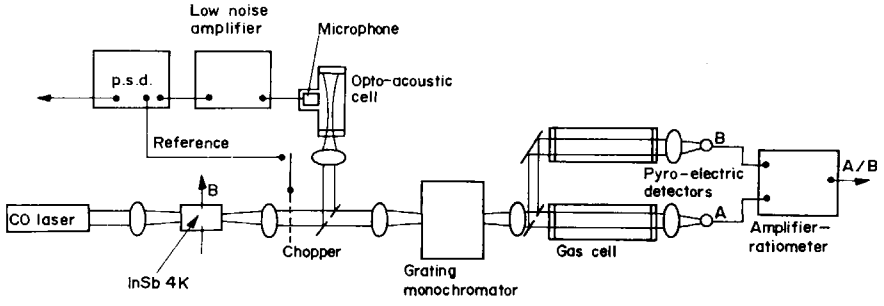

Fig. 4 Schematic diagram of the c.w. spin-flip Raman laser and the arrangement used for molecular spectroscopy.

Two different types of detection are commonly employed. In the double beam arrangement the radiation from both beams is focussed on pyroelectric detectors and the ratio of the signal recorded. Optical-acoustical detection can also be employed with considerable advantage. This latter is made possible because of the large spectral brightness of the SFRL, conservatively estimated as a factor of 10^{10} times above that from a conventional black-body source. This technique is particularly useful as it discriminated against amplitude

fluctuations in the SFRL output because it responds only when the molecules absorb the radiation. Patel and Kerl (26) have recently described a novel miniature optical acoustical cell which can measure absorption coefficients of $\sim 10^{10}\,cm^{-1}$. With this new cell and a SFRL spectrometer, they could detect NO concentrations as low as 1.0×10^{7} molecules cm^{-3}.

A tunable 5-μm spin flip Raman laser and a carbon monoxide laser have been set in a narrow wave guide to perform two-photon absorption spectroscopy on the NO molecule (Ref. 27). Coherent two-photon Doppler-free absorption (see later) and stepwise multiphoton absorption were observed. Measurements of the Λ doublet splitting was readily accomplished and very narrow Doppler free resonances of $v = 0$ to $v = 2$ were observed.

Multiphoton transitions

Two-photon transitions. The simultaneous emission or absorption of two photons of the same frequency is generally known as a two-photon transition. Simultaneous absorption or emission of two photons of different frequencies is sometimes also called a two-photon transition, and at other times a double-quantum transition. The theory of two-photon transitions was given first by Göppert-Meyer in 1931. She showed that from second-order perturbation theory, the probability amplitude for two-photon absorption from level 1 to level 2 (Fig. 5), when an atom, or molecule, is excited by radiation at frequency ω, about half the value of $\omega_0 = (\omega_2 - \omega_1)/\hbar$ is given by

$$a(t) = \frac{\hbar^2}{2} \sum_j \frac{x_{2j} - x_{j1}}{\omega_j - \omega_1 - \hbar\omega} \qquad \frac{e^{i(\omega_0 - 2\omega)t} - 1}{\omega_2 - \omega_1 - 2\hbar\omega}$$

where j represents all of the possible intermediate states.

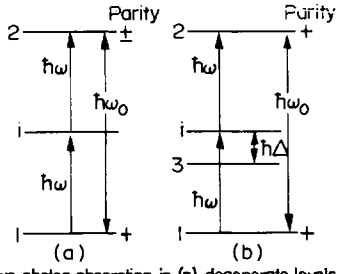

Fig. 5 Two-photon absorption in (a) degenerate levels, and (b) nondegenerate levels.

When all the j levels are distant from the virtual intermediate level i, the transition probability is quite small. Calculation shows that $|a(t)|^2 \approx f(E)^4$, so a very strong incident excitation is necessary for the observation of two-photon transitions, and thus the experimental investigation of this interesting phenomena in the spectra of atoms and molecules had to await the advent of lasers. Furthermore, the frequency of the laser must be adjustable if the two-photon transition occurs between sharp energy levels and no accidental coincidences between the laser frequency and the energy separation exists. It is, therefore, understandable that two-photon spectroscopy could not fully develop until high power tunable dye lasers became available.

The first observation of two-photon transitions was on atomic C_s (Ref. 28). With the development of tunable dye lasers it was not long before two-photon transitions were observed in molecular systems (Refs. 29-33), both in the gas and crystalline phases. Hampf, et al. (34) have used two tunable dye lasers with different wavelengths and polarizations, synchronized to produce a two-photon spectrum of benzene in the gas phase. Resolved single vibronic level fluorescence following two-photon excitation of benzene vapour has been used (Ref. 35) to confirm earlier work of Hochstrasser, et al. (29-31).

Two-photon sequential absorption spectroscopy as applied to the I_2 molecule has been described by Danyluk and King (36). It is apparent that this method has some advantages over the usual double-photon spectroscopy. It is more selective and produces much simpler spectra. Also as will be seen later, the two laser beams used in the experiment can be propagated in opposite directions through the absorption cell, so that the residual Doppler broadening is proportional to the difference in frequency between them, and consequently high resolution can be achieved.

Twarowski and Kliger (37) have used the technique of thermal blooming to observe the two-photon absorption spectrum of liquid benzene. This work seems to establish the ordering of the states in benzene as $^1B_{2u} < {}^1B_{iu} < {}^1E_{1g}$ (Rydberg) $< {}^1E_u < {}^1E_{2g}$. The authors modestly suggest the interesting acronym of MASTER spectroscopy for this technique; this being derived from the description Multiphoton Absorption Spectroscopy from Thermal Effects of Radiation.

The absorption of two microwave photons of the same frequency was first observed by Oka and Shimizu (38). The effect was first observed for the molecule CD_3CN and PF_3.

A further interesting example of two-photon absorption is the work of Oka and Shimizu (39) on the infra-red microwave two-photon transitions in NH_3. In this work a tunable frequency of microwave radiation was added to a fixed frequency of laser radiation utilizing the nonlinearity of the molecular absorption.

Later work by Oka, et al. (40) has led to the observations of infra-red radio frequency two-photon and multiphoton Lamb-dips in CH_3F which are caused by multiphoton processes. This method is obviously of significance for further ultra-high resolution spectroscopy of complex molecules.

Doppler free two-photon processes. An atom of molecule moving with velocity $\bar{v}$ and and absorb radiation of frequency ω has a Doppler shift of $\omega_o = \omega \pm \bar{k}\bar{v}$. It is known that for Raman scattering, which is a special type of two-photon process, that the Doppler broadening is less for the forward scattering than for the backward scattering. Chebotayev, et al. (41) proposed a method for eliminating the Doppler broadening in two-photon spectroscopy. This involved the two photons being used in a counterlinear absorption. The consequences of this are indicated in Fig. 6. Experimental demonstrations of this was first given by Cagnac, et al. (42). Doppler-free spectra attainable with two and multiphoton has great potential in the field of molecular spectroscopy. Cagnac, et al. (43) have also reported the observation of a three-photon Doppler-free spectrum. The first application to complex molecules was the detection of two-photon infra-red absorption in CH_3F by Bischel, et al. (44,45).

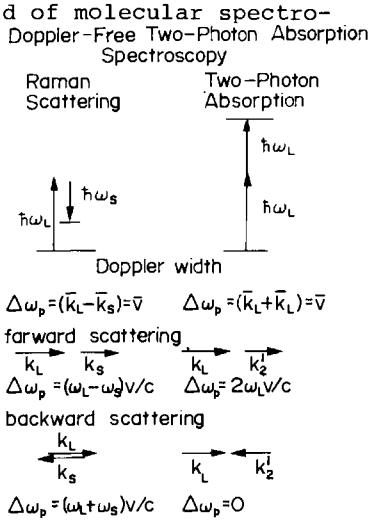

Fig. 6 Comparison of the energy and momentum relations for Raman and two-photon absorption processes

Multiphoton dissociation processes. The discovery that molecules could undergo multiphoton absorption of infra-red radiation from a high powered TEA carbon dioxide laser was one of the most exciting events in Physical Chemistry in recent years (Refs. 46,47). That this multiphoton absorption leads to dissociation and that the process is photo-selective has heightened the interest in these studies. Thus these powerful CO_2 lasers offer the possibility of controlling the specificity of chemical reactions by choosing the energy of the laser beams so as to cause the dissociation of particular bonds. More attractive is that it has been shown (Refs. 48,49) that isotopic enrichment can be achieved by the laser dissociation of polyatomic molecules like BCl_3, SF_6, O_sO_4, MoF_6, etc.

Kompa, et al. (50) have used this method to synthesize isosaborane ($B_{20}H_{16}$) from diborane, and carried out other similar reactions. Other work on photodecomposition and photosynthesis of complex molecules has been extensively persued by Ambartzumian, et al. (51).

The molecule most extensively studied has been SF_6 and there is as yet no agreement as to the exact mechanism of the photo induced dissociation. Amongst many other studies we may mention that crossed molecular and CO_2 laser beams have been used to study the collisionless multiphoton dissociation of SF_6 (Ref. 52). These authors established that the molecule does accumulate energy by sequential absorption of photons and were able to elucidate many of the details of the mechanism. An interesting and detailed theoretical discussion has been given by Mukamel and Jortner (53). A schematic quantum energy diagram based on their work is given in Fig. 7. The energy levels in Fig. 7 are divided into three groups denoted by the Roman numerals. Region I is

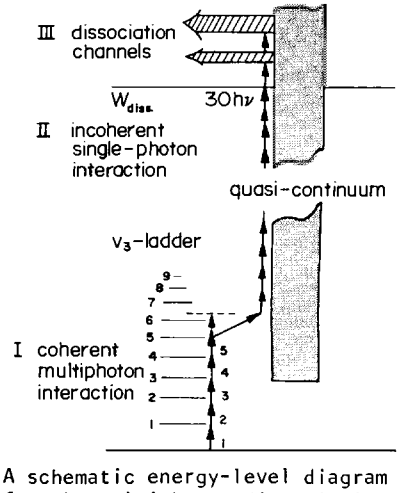

Fig. 7 A schematic energy-level diagram for the multiphoton dissociation of SF_6.

characterized by coherent interaction, discrete energy levels, the anharmonicity 'bottleneck', isotopic selectivity and resonant enhanced multiphoton absorption. Region II is characterized by incoherent simple-photon interactions. Region III is the true continuum of levels above the dissociation limit. A detailed consideration of this model by Black, et al. (54) shows that the collisionless multiphoton dissociation of SF_6 is a statistical thermodynamic process. The standard Rice-Ramsberger-Kassel-Marcus theory of unimolecular reactions provides a quantitative explanation of the dissociation.

Multiphoton Ionizations. (a) Multiphoton ionization processes in atoms. Multiphoton ionizations of atoms and molecules have been observed and these studies are likely to be of considerable importance. The wavelength dependence of the multiphoton ionization cross sections near the resonance threshold can be studied in detail by the use of tunable dye lasers. This type of study was first proposed by Ambartzumian, et al. (47,55) who were able to achieve selective two step ionization of rubidium atoms using a ruby-pumped dye laser and a doubled ruby laser radiation. Later, similar experiments were performed on caesium atoms by Popescu, et al. (56). They observed two-photon transitions from the $6^2S_{\frac{1}{2}}$ ground state to resonant n^2D and n^7S intermediated states, followed by either association ionization or by association followed by dissociative attachment. In addition, direct three-photon ionizations were also observed. Figure 8 shows an energy level diagram for the Cs atoms and indicates the multiphoton ionization processes. The two-step photoionization of sodium atoms was studied by Duong, et al. (57). These authors used a dye laser and radiation from a mercury vapour lamp to ionize the atoms. The method was used to detect optical resonances with a resolution of about 50 MHz.

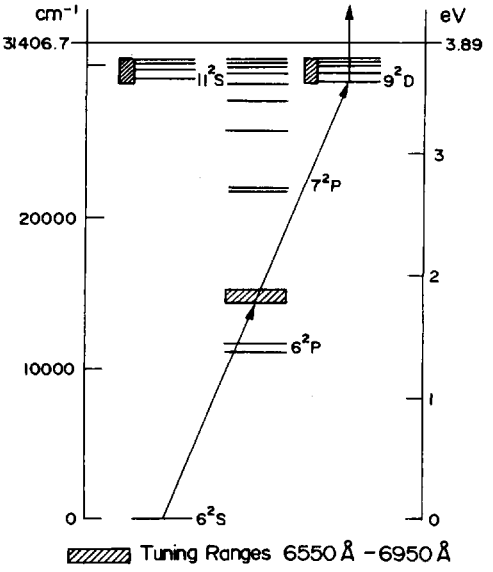

Fig. 8 Energy-level diagram of the states of atomic Cs relevant to three-photon photoionization over the 6550-6950 Å range of wavelengths covered in this experiment.

Two-photon ionization probabilities for atomic caesium have been measured at nine wavelengths of an Argon ion laser by Granneman and Van der Wiel (58). Hurtst, et al. (59) have studied the two-photon ionization of helium (2'S) atoms using a dye laser. The selective photoionization of uranium atoms has been studied in detail by Tuccio and co-workers (60). This may form the basis of a method for the separation of uranium isotopes and is thus of considerable industrial interest. The two-photon ionization is performed using a xenon laser operating at 3781 Å uranium atoms are excited from a metastable state 620 cm^{-1} above the ground state, to an energy level at 27,068 cm^{-1}, approximately one-half of the ionization energy. Excited atoms are then ionized using a krypton laser operation at 3507 Å and 3564 Å.

Ionization has also been observed in the case of calcium atoms following two-photon absorption to the bound, even-parity J=0 and J=2 states (Ref. 61). These authors used a nitrogen-laser-pumped dye laser to excite and ionize atoms in calcium vapour.

(b) Multiphoton ionization of molecules. The application of the multiphoton ionization technique to molecular systems promises to be of interest not only because by that means we can obtain more accurate values for the ionization potential of molecules, but also because it presents us with the possibilities of obtaining more accurate and precise photoionization cross-section data. It also gives us a method to study the energy levels of molecular ions with high accuracy. Moreover, as we shall see, it has opened up the possibilities of enhancing the resolution of molecular photoelectron spectroscopy.

The first report of a multiphoton ionization in a molecule was the observation of resonant two-photon photodetachment of electrons from the C_2^- reported by Lineberger and Patterson (62). These workers used a tunable dye laser to

photodetach electrons from framed mass-analysed beam of C_2^- ions. From their results they were able to show that the ground state of the C_2^- ion was a $^2\Sigma_g$ state. The technique employed can obviously be applied to many molecular positive ions, as well as negative ions, provided that single photon photodissociation from the lower (ground) state is energetically impossible.

A somewhat similar technique was used by Johnson to study multiple photoionization processes in benzene (Ref. 63) and trans-1,3-butadiene (Ref. 64). In the case of benzene a resonance seen in the multiphoton ionization spectrum at 391.4 nm was identified as a two-photon resonance with a bound state of symmetry E_2g as indicated by an active e_2g vibration. Three-photon resonances with various Rydberg states were also observed. Thus both three- and four-photon ionization processes were found in this study. Laser studies by Arikawa, Shindo and Izawa (65), using a crossed beam apparatus, confirmed the above observations and showed that the two-photon absorption was to the E_2g state the only one allowed by the symmetry (even parity) selection rate.

In the case of trans-1,3-butadiene again many three-photon resonances with various Rydberg states were found; these correspond to four-photon ionizations.

Three-photon ionizations of molecular iodine I_2, with resonance in an intermediate state excited by two-photons has been studied in some detail by Dalby and co-workers (66,67). These workers use an ionization cell to detect the photo ions and photoelectrons and obtain high resolutions, photoelectron and photoionization spectra of the iodine molecule. This work demonstrates the importance and power of multiphoton molecular photoelectron spectroscopy.

A two step photoionization of formaldehyde (H_2CO) molecules has been reported (Refs. 68,69). It takes place by the simultaneous action of a radiation pulse of a N_2-laser (λ = 3371 Å), which excites the $^1A_2$ state of the H_2CO and of a H_2-laser (λ = 1600 Å) which photoionizes the excited $^1A_2$ molecules. This method of selective photoionization through an intermediate electron state has many possible applications. A tunable dye laser could be used to populate particular states of molecules from which photoionizations may be induced by radiation from a second laser. This could be the basis of an extremely sensitive and selective photoionization mass spectrometric method. It could also be used to provide very high resolution molecular photoelectron spectra. By making use of the possibility of Doppler-free two or three photon processes leading to ionization, it may be possible to observe extremely high resolution photoionizations and photoelectron spectra of molecules. It has also been suggested that by the use of a tunable IR laser it should be possible to carry out the selective detection of complex molecules because the two-step molecular ionization could involve intermediate vibrational states (Ref. 70). An interesting and important application of the above techniques has been described by Hurst, et al. (59). These authors used two synchronized pulsed lasers to induce the resonance ionization of caesium atoms. Sensitive ionization counting methods enabled them to detect a single C_s atom even in the presence of 10^{19}, or more, atoms of another kind. This ultra-sensitive method is likely to have many applications in various areas of science and medicine. It may also be of considerable technological importance.

Attention may perhaps also be drawn to a related technique which should be of general applicability. This is the Stark-field induced ionization of high-lying states of atoms which was first applied to sodium by Ducas, et al. (71). The method is quite straightforward and depends on the fact that atoms (or molecules) excited by multiphoton transitions to high Rydberg states can be ionized with high efficiency by the application of an electric field. In most cases quite modest Stark fields of $\sim$500 volts/cm^{-1} are sufficient to cause ionization.

Electron Spectroscopy and Photoelectron Spectroscopy

Many new techniques have been introduced to the area of Electron and Photoelectron Spectroscopy which have led to experimental results not previously available because of limitations of wavelength, or radiation intensity. The recent developments in the design of electron energy analysers have increased markedly the resolution of spectrometers. In addition, many new and more sensitive detectors have been developed (Ref. 72). These two factors have meant that more detailed high resolution photoelectron and electron spectra can now be obtained on a more or less routine basis in many laboratories.

Photoelectron spectroscopy. With regard to radiation sources for photoelectron spectroscopy, there have also been many developments. In the case of u.v. photoelectron spectroscopy, as we have mentioned earlier, the intro-

duction of lasers has not only permitted the development of Laser Detachment Spectroscopy, of which we shall say something later, but quite recently the use of multiphoton techniques points the way to the possibility of obtaining quite high resolution spectra, particularly if two or more lasers are used in a counter-linear fashion to remove Doppler broadening. Synchrotron radiation sources are now commonly used for photoelectron spectroscopic studies in the VUV and every X-ray region and have opened up a whole new aspect of this form of electron spectroscopy (Ref. 73).

The application of photoelectron spectroscopic techniques to the study of surfaces has been most fruitful in that it has, together with LEED and Auger spectroscopic studies, completely revolutionalized the whole of surface chemistry and physics. Photoelectron emission studies on organic crystals has also been an interesting field in recent years (Ref. 74), which has given much new knowledge concerning the catalytic activity of organic semiconductors.

As mentioned earlier, the application of photoelectron spectroscopy continues to be most important in the study of molecular structure and related phenomena. The field is too active to be surveyed fully here, and so one can only mention a few areas in which significant advances have been made recently, and from which developments it is likely that new information will continue to come forth.

Recent work on the X-ray photoelectron spectroscopy of metal compounds has shown that satellite phenomena is quite general (Refs. 75,76,77). There have been developed, several theories to explain the results, and it now seems clear that not only does metal-ligand but also ligand-metal transfer processes also occur. The general principles of shake-up and shake-off phenomena are becoming clear. In the case of X-ray photoelectron spectra of simpler substances, we may mention the rather interesting and detailed study of the M_1 and M_3 levels in bromine and krypton. Svensson, et al. (78) also studied the $M_1M_{2,3}$ and $M_{2,3}$ super Coster-Kronig transitions for these and also for chlorine. Several discrete configuration interaction resonances were observed and the occurrence of these was reflected in the lifetime broadening of the lines in the spectra.

The power of recent high resolution studies is perhaps best seen in the work of Karlsson, et al. (72) who reported on the He(I) photoelectron study of the valence electron spectra of C_6H_6, and the hexafluorides of sulphur, molybdenum, tungsten, uranium and SiF_4 (Ref. 79). They obtained high resolution for benzene comparable with the work reported earlier by Åsbrink, et al. (80). An interesting recent high resolution analysis of the He(I) photoelectron spectrum of HCN has been reported by Friedh and Åsbrink (81).

Gas phase X-ray photoelectron spectroscopy has continued to be a fruitful area of investigation and amongst recent studies which show the power of this method when combined with detailed theoretical calculations as a way to reveal the electronic structure of many molecular systems. Examples of recent studies carried out in this way are given in Refs. 82-84.

U.V. photoelectron spectroscopy (Ref. 85), as has been mentioned, has continued to be a method which yields considerable important information about the electronic structures of molecules. There has recently been much interest in the application of this method to the study of conformational problems, to monomer-dimer equilibria, to transient molecules and free radicals. A good example of one of these topics is the recent detailed studies of the He(I) photoelectron spectra of NO_2 and N_2O_4 (Refs. 86,87). In the case of the study of transient molecules and free radicals, this area has developed so rapidly, and the number of species which have recently been investigated is so large, that it is impossible to describe the work in any detail here. We shall perhaps do best by simply referring to our own recent work on the diazine molecule N_2H_2 (Ref. 88). One facet of the well resolved spectrum of this molecule is shown in Figs. 9 and 10. We show this to illustrate the detailed resolution which can be obtained in the photoelectron spectra of transient species using modern techniques. It also serves as an example of the interesting interplay between experiment and recent developments in theoretical chemistry studies of the electronic structure of molecules. It is well known that calculations utilizing Koopman's Theorem are not always applicable to the interpretation of the photoelectron spectra of many compounds. The difficulties in the application of Koopman's Theorem and the calculation of the expected theoretical photoelectron spectra of a

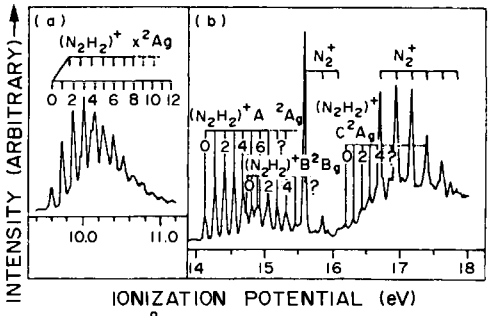

Fig. 9 The 584 Å photoelectron bands of N_2H_4 in detail.

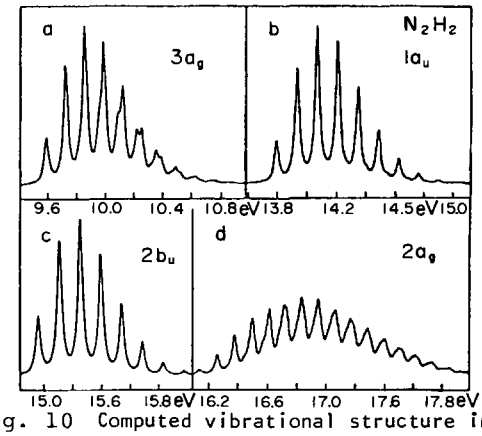

Fig. 10 Computed vibrational structure in the first four bands of *trans*-HNNH.

given molecule have largely been overcome by recent developments in theoretical chemistry. One of these, and the most extensive, is the Green's Function Method largely developed by Cederbaum, et al. (89-92). The other method which relies on third order perturbation theory calculations (Ref. 93) is most successful when applied to small molecules. Figures 9 and 10 show excellent agreement between the experimental spectrum and the theoretically calculated spectra of N_2H_2, and is a nice illustration of how far these newer theoretical methods have developed. They have, in fact, become the preferred method for interpreting the detailed structure of well resolved photoelectron spectra.

Perhaps the most interesting and exciting development in photoelectron spectroscopy in the past few years has been the use of dye-lasers in the study of photodetachment from negative ions. This work has largely been developed by Lineberger and his colleagues, and has, in fact, opened up a new field of spectroscopy. The amount of detailed information which has been obtained by this novel technique would have been unimaginable some five years ago. Because of these new studies, we now have extremely accurate values for the electron affinities of a vast number of atomic (Ref. 94) and molecular negative ions (Refs. 95-97).

In addition, it has been possible to obtain other important structural details about molecular negative ions which could not be got by any other experimental method available at present. An interesting recent development has been the observation of window (Fano) resonances in the photodetachment processes from C_S^- and Rb^-. In both cases, the photodetachment cross section exhibits a sharp minimum at a certain frequency which corresponds to very weak absorption by the negative ion concerned. In the case of caesium, a deep second minimum occurs due to excitation of a second autodetaching state.

Electron spectroscopy. As mentioned above, developments in experimental methods, and in particular in the design of electron energy analysers, has led to the marked improvement of the resolution of electron impact spectrometers. In the more recent developments in this field, many new types of experiments have become possible and these have led to much valuable information concerning the electronic structure of molecules, molecular ions, and in particular, the details of inner-shell ionization phenomena.

The most direct of these newer methods is called Electron Energy Loss Spectroscopy (EELS). The basis of this type of study lies in the application of the Bethe Theory, using the Born approximation, to electron-atom or electron-molecule collisions. If we consider the process $e + M \rightarrow M^+ + 2e$, we can write the differential cross section $d\sigma$ as a function of the scattering angle Ω as $\frac{d\sigma}{d\Omega} = \frac{2}{E}\frac{k_n}{k_o}\frac{1}{K^2}\frac{df(k)}{dE}$ from which it can readily be shown that $\frac{d\sigma}{d\theta} = \frac{2}{E}\frac{k_n}{k_o}\frac{1}{K^2}\frac{df_o}{dE} = \frac{2}{E}\frac{k_n}{k_o}\frac{1}{K^2}\frac{m_c}{\pi e^2 h}\sigma_{\text{photons}}$. Therefore, using fast electrons at the optical limit (i.e., $K^2 \rightarrow 0$), it becomes possible to have what is called "spectroscopy in the dark", i.e., to make quantitative "optical" measurements in which the energy loss simulates the "photon" energy. At low electron impact energy and large scattering angles, the momentum transfer is large and non dipole (i.e., optically forbidden) transitions dominate the spectrum.

In particular, Brion, et al. have developed a variety of electron impact coincidence experiments which simulate photoionization mass spectrometry and photoelectron spectrometry. With these new developments they have been able to obtain, via the Bethe-Born relation, partial photoionization cross-sections, branching ratios and photoionization efficiencies for a number of molecules (Refs. 98,99). Brion and his colleagues have developed a new (e,2e) ionization method which makes use of coincidence detection and energy analysis of the two electrons. In this method the cross-section σ, is determined as a function of the scattering angle ϕ, by the coincident count rate and thus gives a direct measurement of the momentum distribution of the ionized electron. This is potentially a most important new development since it enables one to probe the spacial distribution of the orbital wavefunction of a molecule, and determines the order and symmetry of the orbitals. It also permits the measurement of the binding energies corresponding to single and multiple electron ionization processes (Ref. 100).

Laser magnetic resonance spectroscopy

The general technique of laser magnetic resonance is very similar to other magnetic resonance methods such as electron paramagnetic resonance or nuclear magnetic resonance. As is well known, NMR uses radio frequency radiation to produce transitions between nuclear spin levels, and EPR uses microwave radiation to produce transitions between electron spin levels, in laser magnetic resonance radiation (Refs. 101,102) from infra-red lasers is used to produce transitions between rotational levels in paramagnetic atoms or molecular species such as free radicals. Absorption of the laser radiation photons is accomplished by tuning the paramagnetic molecular rotational levels with resonance by varying an applied magnetic field.

A simplified rotational energy level diagram which illustrates the principles of laser magnetic resonance absorption is shown in Fig. 11. Note that not all the levels which arise from Λ doubling and nuclear spin are shown. The near coincidence of the laser photon E_L with the field free rotational transition E(J=5/2 ← J=3/2) is shown on the left.

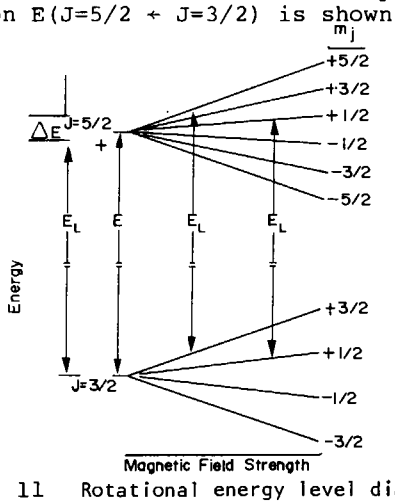

Fig. 11 Rotational energy level diagram showing near coincidence of laser line E_L with rotational transition E(J=5/2←J=3/2).

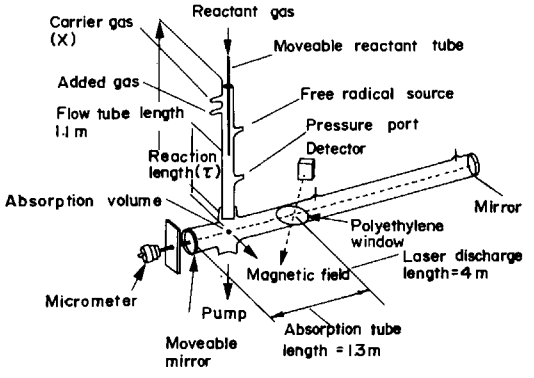

Fig. 12 Schematic diagram of laser magnetic resonance apparatus.

To the right of Fig. 11 (Fig. 12), is a sketch of the apparatus used for the observation of the laser magnetic resonance spectra of paramagnetic species and free radicals generated by chemical reaction in a flow system. Other methods such as a microwave discharge or photolysis can be used to generate the free radicals required for particular studies.

What is of great interest is the enormous sensitivity which this method presents for the study of the details of the rotational fine structure of free radicals and atoms. Because of the great increase in the availability of infra-red lasers covering quite a range of frequencies, the method has become a most powerful spectroscopic technique which will obviously continue to be of considerable importance in the structural studies on free radicals in the gas phase (Refs. 103,104). It has also been shown to be of much promise for the measurement of gas phase free radical reaction rates. In particular, it has been used by Howard and Evenson (105) to measure the rates of the reaction of the OH radical with CO, NO, and NO_2 296°K and over

a pressure range of 0.4-5 torr. More recently it has proved to be satisfactory for the measurement of the rates of reaction of the NO_2 radical with HO and O atoms (Ref. 106). This is a most important chemical reaction in the upper atmosphere and is of considerable importance in the sequence of reactions which are involved in the expected depletion of stratospheric ozone by nitrogen oxides released by high flying aircraft, and by chlorine species from the photodecomposition of halocarbons.

Acknowledgement - We wish to thank the National Research Council of Canada for financial support for some aspects of the work described in this paper.

REFERENCES

1. C.F. Bander, P.K. Bearson, S.V.-O'Neil and H.F. Schaefer, J. Chem. Phys. 56, 4624 (1972); J.C. Polanyi and J.L. Schreiber, Disc. Farad. Soc. 62, 267 (1977).
2. J.M. Farrar and Y.T. Lee, J. Chem. Phys. 63, 3639 (1975).
3. M.J. Berry, J. Chem. Phys. 59, 6229 (1973); J.C. Polanyi and K.B. Woodall, J. Chem. Phys. 57, 1574 (1972).
4. J.J. Valenti, M.J. Coggiola and Y.T. Lee, J. Amer. Chem. Soc. 98, 853 (1976).
5. J.M. Farrar and Y.T. Lee, J. Amer. Chem. Soc. 96, 7570 (1976).
6. T.J. Chuang, G.W. Hoffman and K.B. Eisenthal, Chem. Phys. Lett. 25, 201 (1974).
7. T.J. Chuang and K.B. Eisenthal, J. Chem. Phys. 62, 2213 (1975).
8. G.R. Fleming, J.M. Morris and G.W. Robinson, Chem. Phys. 17, 91 (1976).
9. K. Kaufmann, P.C. Dutton, T.C. Netzel, J.S. Leigh and P.M. Rentzopis, Science 188, 1301 (1975).
10. E.L. Hahn, Phys. Rev. 70, 460 (1946).
11. H.Y. Carr and E.M. Purcell, Phys. Rev. 94, 630 (1954).
12. S. Meiboom and D. Gill, Rev. Sci. Instrum. 29, 688 (1958).
13. E.A. Andrew, Y. Apaydin and W.S. Moore, Phys. Lett. 25A, 44 (1967).
14. J.S. Waugh, L.M. Huber and U. Haeberlen, Phys. Rev. Lett. 20, 180 (1968).
15. A. Pines, M.G. Gibby and J.S. Waugh, J. Chem. Phys. 56, 1776 (1972); 59, 569 (1973).
16. U. Haeberlen, U. Kohlschutte, H.W. Spiess and H. Zimmerman, Chem. Phys. 3, 284 (1974); 4, 269 (1974). Proceedings XIXth Congress Ampere, Heidelberg, p. C11 (1976).
17. S. Vega, T.W. Shattuck and A. Pines, Phys. Rev. Lett. 37, 43 (1976); S. Vega and A. Pines, J. Chem. Phys. 62, 5624 (1977).
18. K.M. Evenson, J.S. Wells and H.E. Radford, Phys. Rev. Lett. 25, 199 (1970); H.E. Radford, K.M. Evenson and C.J. Howard, J. Chem. Phys. 60, 3178 (1974); P.B. Davies, D.K. Russell, B.A. Thrush and F.D. Wayne, J. Chem. Phys. 62, 3739 (1975).
19. M.D. Levelson, C. Flytzanis and N. Bloembergen, Phys. Rev. 6, 3962 (1972).
20. W.M. Tolles and R.D. Turner, Applied Spectroscopy, 31, 96 (1977).
21. F. Moya, S.A.J. Drnet and J.P.E. Taran, Laser Spectroscopy, Springer-Verlag, New York, p. 66 (1975).
22. R.J. Butcher, R.B. Dennis and S.D. Smith, Proc. Roy. Soc. 344A, 541 (1975).
23. C.K.N. Patel, R.J. Kerl and E.G. Burkhardt, Phys. Rev. Lett. 38, 1204 (1977).
24. J. Häger, W. Hinz, W. Walther and G. Strey, Applied Physics 9, 35 (1976).
25. C.K.N. Patel, App. Phys. Lett. 25, 112 (1974).
26. C.K.N. Patel and R.K. Kerl, App. Phys. Lett. 30, 578 (1977).
27. M.A. Guerra, A. Sanchez and A. Javan, Phys. Rev. Lett. 38, 482 (1977).
28. I.D. Abella, Phys. Rev. Lett. 9, 453 (1962).
29. R.G. Bray, R.M. Hochstrasser and J.E. Wessel, Chem. Phys. Lett. 27, 167 (1974).
30. R.M. Hochstrasser, J.E. Wessel and H.N. Sung, J. Chem. Phys. 60, 317 (1974).
31. R.G. Bray, R.M. Hochstrasser and H.N. Sung, Chem. Phys. Lett. 33, 1 (1975).
32. L. Wunsch, H.J. Neusser and E.W. Schlag, Chem. Phys. Lett. 31, 433 (1975).
33. L. Wunsch, H.J. Neusser and E.W. Schlag, Chem. Phys. Lett. 32, 210 (1975).
34. W. Hampf, H.J. Neusser and E.W. Schlag, Chem. Phys. Lett. 46, 406 (1977).
35. A.E.W. Knight and C.S. Parmenter, Chem. Phys. Lett. 43, 359 (1974).
36. M.D. Danyluk and G.W. King, Chem. Phys. 22, 59 (1977).
37. A.J. Twarowski and D.S. Kliger, Chem. Phys. 20, 259 (1977).
38. T. Oka and T. Shimizu, Phys. Rev. A2, 587 (1970).

39. T. Oka and T. Shimizu, Appl. Phys. Lett. 19, 99 (1971).
40. S.M. Freund, M. Römheld and T. Oka, Phys. Rev. Lett. 35, 1497 (1975).
41. L.S. Vasilenko, V.P. Chebotayev and A.V. Shishaer, Sov. Phys. JETP Lett. 12, 113 (1970).
42. B. Cagnac, G. Grynberg and F. Biraben, J. Phys. (Paris), 34, 56 (1973).
43. G. Grynberg, F. Biraben, M. Bassini and B. Cagnac, Phys. Rev. Lett. 37, 283 (1976).
44. W.K. Bischel, P.J. Kelley and C.K. Rhodes, Phys. Rev. Lett. 34, 300 (1975).
45. W.K. Bischel, P.J. Kelley and C.K. Rhodes, Phys. Rev. A13, 1817 (1976).
46. N.R. Isenor and M.C. Richards, App. Phys. Lett. 18, 225 (1971).
47. R.V. Ambartzumian, V.P. Kalinin and V.S. Letokhov, Soc. Phys. JETP Lett. 13, 217 (1971).
48. R.V. Ambartzumian, V.S. Letokhov, G.N. Makarov and A.A. Puretzkii, Zh. Eksp, Teor. Fiz. 15, 709 (1972); 17, 91 (1973).
49. V.S. Letokhov, Chem. Phys. Lett. 15, 221 (1972).
50. H.R. Bachmann, R. Rinck, H. Nöth and K.L. Kompa, Chem. Phys. Lett. 45, 169 (1977).
51. R.V. Ambartzumian, N.V. Chekalin, V.S. Doljikov, V.S. Letokhov and E.A. Ryabov, Chem. Phys. Lett. 25, 515 (1974).
52. M.J. Coggiola, P.A. Schulz, Y.T. Lee and Y.R. Shen, Phys. Rev. Lett. 38, 17 (1977).
53. S. Mukamel and J. Jortner, J. Chem. Phys. 65, 5204 (1976).
54. J.G. Black, E. Yablonovitch, N. Bloemberger and S. Mukamel, Phys. Rev. Lett. 38, 1131 (1977).
55. R.V. Ambartzumian and V.S. Letokhov, Applied Optics 11, 354 (1972).
56. D. Popescu, C.B. Collins, B.W. Johnson and I. Popescu, Phys. Rev. A9, 1182 (1972).
57. H.T. Duong, P. Jaquinot, S. Liberman, J. Pinard and J.-L. Vialle, C.R. Acad. Sci. Paris, 276, Series B, 909 (1973).
58. E.H.A. Granneman and M.J. Van der Wiel, J. Phys. B, Atom. Molec. Phys. 8, 1617 (1975).
59. G.S. Hurst, M.H. Nayfeh and J.P. Young, Phys. Rev. A15, 2283 (1977).
60. B.B. Suavely, R.W. Solarz and S.A. Tuccio, Laser Spectroscopy, Springer-Verlag, p. 268 (1976).
61. P.E. Sherick, J.A. Armstrong, R.W. Dreyfus and J.J. Wynne, Phys. Rev. Lett. 36, 1296 (1976).
62. W.C. Lineberger and T.A. Patterson, Chem. Phys. Lett. 13, 40 (1972).
63. P.M. Johnson, J. Chem. Phys. 64, 4143 (1976).
64. P.M. Johnson, J. Chem. Phys. 64, 4638 (1976).
65. Studies of Atomic Collisions and Related Topics in Japan, Tokyo, 95 (1977), Progress Report No. 3; T. Arikawa, S. Shindo, paper 6A613 this congress.
66. G. Petty, C. Tai and F.W. Dalby, Phys. Rev. Lett. 34, 1207 (1977).
67. F.W. Dalby, G. Petty, M.H.L. Pryce and C. Tai, Can. J. Phys. 55, 1033 (1977).
68. R.V. Ambartzumian and V.S. Letokhov, Applied Optics, 11, 354 (1972).
69. S.V. Andreyev, V.S. Antonov, I.N. Kuyazev and V.S. Letokhov, Chem. Phys. Lett. 45, 166 (1977).
70. V.S. Letokhov, Uk. Fiz. Nauk. 118, 119 (1976).
71. T.W. Ducas, M.G. Lettman, R.R. Freeman and D. Kleppner, Phys. Rev. Lett. 35, 366 (1976).
72. L. Karlsson, L. Mattsson, R. Jadrny, T. Bergmark and K. Siegbahn, Physica Scripta 14, 230 (1976).
73. P. Pianetta and I. Lindau, J. Elect. Spectr. 11, 13 (1977).
74. H. Inokuchi, Discus. Faraday Soc. 51, 183 (1971).
75. A. Rosencwaig, G.D. Wertheim and H.J. Guggenheim, Phys. Rev. Lett. 27, 479 (1971).
76. D.C. Frost, A. Ishitani and C.A. McDowell, Mol. Phys. 24, 861 (1972).
77. S. Larrson, J. Elect. Spectr. 8, 171 (1976).
78. S. Svensson, N. Martensson, E. Basilier, P.A. Malmquist, U. Gelius and K. Siegbahn, Physica Scripta 14, 141 (1976).
79. R. Jadrny, L. Karlsson, L. Mattsson and K. Siegbahn, Chem. Phys. Lett. 49, 203 (1977).
80. L. Åsbrink, E. Lindholm and O. Edgwist, Chem. Phys. Lett. 5, 609 (1970).
81. C. Friedh and L. Åsbrink, J. Elect. Spectr. 7, 119 (1975).
82. M.S. Banna, D.C. Frost, C.A. McDowell and B. Wallbank, J. Chem. Phys. 66, 3509 (1977).
83. C.R. Brundle, N.A. Kuebler, M.R. Robin and H. Basch, Inorg. Chem. 11, 20 (1972).
84. W.R. Salaneck, J.W. Lin, A. Paton, C.B. Duke and G.P. Ceasar, Phys. Rev. B13, 4517 (1976).

85. D.W. Turner, C. Baker, A.D. Baker and C.R. Brundle, Molecular Photoelectron Spectroscopy, Wiley-Interscience, London (1970).
86. D.L. Ames and D.W. Turner, Proc. Roy. Soc. 348A, 175 (1976).
87. D.C. Frost, C.A. McDowell and N.P.C. Westwood, J. Elect. Spectr. 10, 293 (1977).
88. D.C. Frost, S.T. Lee, C.A. McDowell and N.P.C. Westwood, J. Chem. Phys. 64, 4719 (1976).
89. L.S. Cederbaum and W. Domcke, J. Chem. Phys. 60, 2878 (1974).
90. L.S. Cederbaum and W. von Niessen, Chem. Phys. Lett. 24, 263 (1974).
91. L.S. Cederbaum, G. Hohlneicher and W. von Niessen, Mol. Phys. 26, 1405 (1973).
92. L.S. Cederbaum, W. Domcke and W. von Niessen, Chem. Phys. 10, 459 (1975).
93. D.P. Chong, F.G. Herring and D. McWilliams, Chem. Phys. Lett. 25, 568 (1977); J. Chem. Phys. 61, 3567 (1974).
94. H. Hotop and W.C. Lineberger, J. Phys. Chem. Ref. Data 4, 539 (1975).
95. W.C. Lineberger and B.W. Woodward, Phys. Rev. Lett. 25, 424 (1970).
96. H. Hotop, T.A. Patterson and W.C. Lineberger, Phys. Rev. A8, 762 (1973).
97. A. Kasdan, E. Herbst and W.C. Lineberger, Chem. Phys. Lett. 31, 78 (1975).
98. C.E. Brion, A. Hamnett, G.R. Wight and M.J. Van der Wiel, J. Elect. Spec., submitted 1977.
99. S.T. Hood, A. Hamnett and C.E. Brion, Chem. Phys. Lett. 41, 428 (1976).
100. S.T. Hood, A. Hamnett and C.E. Brion, J. Elect. Spec. 11, 205 (1977).
101. J.S. Wells and K.M. Evenson, Rev. Sci. Instrum. 41, 226 (1970).
102. H.E. Radford, K.M. Evenson and C.J. Howard, J. Chem. Phys. 60, 3178 (1974).
103. P.D. Davies, D.K. Russell, B.A. Thrush and E.D. Wayne, J. Chem. Phys. 62, 3739 (1975).
104. P.D. Davies, D.K. Russell, B.A. Thrush and H.E. Radford, Proc. Roy. Soc. A353, 299 (1977).
105. C.J. Howard and K.M. Evenson, J. Chem. Phys. 61, 1943 (1977).
106. J.P. Burrows, G.W. Harris and B.A. Thrush, Nature 267, 233 (1977).

Pure & Appl. Chem., Vol. 50, pp. 759-769.
Pergamon Press Ltd.1978. Printed in Great Britain

0033-4545/78/0801-0759 $02.00/0

APPLICATIONS OF LASERS IN CHEMICAL SPECTROSCOPY AND DYNAMICS: HIGHER ORDER SUSCEPTIBILITY EFFECTS

Robin M. Hochstrasser and G. R. Meredith

Department of Chemistry and Laboratory for Research on the Structure of Matter, University of Pennsylvania, Philadelphia, Pennsylvania 19104

Abstract - A survey of recent experiments on molecular excited states will be presented. Many non-linear optical processes have now become extremely useful in chemical spectroscopy and dynamics. Laser E-fields induce a dipole moment μ in molecular systems which in turn acts as a source of additional fields in the medium. The polarization is generally a power series in the fields:

$$N\mu = \chi^{(1)}E + \chi^{(2)}EE + \chi^{(3)}EEE + \ldots.$$

Normally, centrosymmetric molecules have $\chi^{(2)} = 0$ and systems that are centrosymmetric will not generally exhibit second harmonic generation. Thus the study of $\chi^{(2)}$ in such cases has provided information on the magnetically induced SHG. This effect coupled with the two-photon absorption, a resonant part of $\chi^{(3)}$, was used to explore polariton effects in molecular crystals of anthracene and naphthalene. High resolution spectroscopy of gases and solids were also accomplished using three wave mixing brought about through two-photon and Raman resonances in $\chi^{(3)}$. These techniques allow accurate measurements of two-photon cross-sections. The various non-linear experiments yield new information on the relaxation and dephasing dynamics in molecular excited states.
Pulsed lasers permit the resolution in time of excited state relaxation in the condensed phase and experiments will be described in which non-linear phenomena were used to study vibrational relaxation in some simple diatomic solids at low temperature, and chemical reactions in the condensed phase.

1. INTRODUCTION:

During the sixties Bloembergen and his coworkers developed the ground work of the field of non-linear optics (1) and now those concepts are beginning to have impact on chemistry. Primarily the new found importance of non-linear responses in systems of chemical interest arises because of the availability of high powered tunable lasers. The power is needed in order that the higher order terms in the expansion of the dipole moments of the constituents contribute significantly to the polarization of the system; the tunability is required in order that the effects of specific molecular resonances can be explored.

The dipole moment per unit volume, or polarization, of a collection of molecules, ions or radicals may be expressed as:

$$N\mu_\alpha = P_\alpha = \chi^{(1)}_{\alpha\beta} E_\beta + \chi^{(2)}_{\alpha\beta\gamma} E_\beta E_\gamma + \chi^{(3)}_{\alpha\beta\gamma\delta} E_\beta E_\gamma E_\delta + \ldots \quad (1)$$

where the indices α, β, .. represent space fixed axis designations (repeated indices are summed over) and $\chi^{(n)}_{\alpha\beta..}$ is the $\alpha\beta..$ component of the n^{th}- order susceptibility tensor.

The literature contains many discussions of the macroscopic and microscopic origin of these tensors (1 to 5). A main point is that the existence of $\chi^{(n)}_{\alpha\beta..}$ and the presence of optical and/or static fields E_β, E_γ.. implies the existence of a polarization P_α. This polarization acts as a source term in generating a new optical field, the relations between

the polarization and the field being specified by the classical Maxwell's equations. Incoherent phenomena in the medium (e.g. fluorescence, phosphorescence, relaxations) occur only after the coherent polarization is damped. This article will be mainly concerned with measurements relating to the coherent effects and with the dissipative pathways or other types of scattering. The absorption of light corresponds to the formation of an incoherent population in which $N<\mu>$ is zero.

From the standpoint of spectroscopy it is important to recognize the effects of resonances on the various susceptibilities in equation (1). The purpose of the present paper is to describe some recent applications of non-linear optics to molecular spectroscopy and chemical dynamics. In each application a key feature will be that the process is resonance enhanced by a molecular transition. The relationship between the various induced spectroscopic processes and the susceptibility tensors in equation (1) is not really obvious. The chemical spectroscopist has usually been interested in the microscopic description of resonance phenomena in order that spectroscopic assignments may be used as a means of better understanding molecular structure. However the observed phenomena associated with the higher order susceptibilities require a more detailed consideration of the bulk material properties. If the susceptibilities are considered to be dipolar susceptibilities, in other words the various transition moments are all transition dipole moments, then important symmetry criteria can be readily deduced (5 and 6). For example $\chi^{(1)}$ exists for all materials regardless of their symmetry because it represents the constant of proportionality between two polar vectors (μ and E). The microscopic form of $\chi^{(1)}$, the usual polarizability, contains the transition dipole factor connecting the ground state (g) to and from all excited states (i), $\mu_{gi}\mu_{ig}$ and this factor exists for some i in all symmetry groups. The second-order susceptibility $\chi^{(2)}$ is clearly zero in centrosymmetric systems (suppose inversion through an origin transformed the system into itself, then the vector P would change sign, the product E^2 would remain unchanged so $\chi^{(2)}$ would equal $-\chi^{(2)}$) and this includes molecules belonging in centrosymmetric point groups, crystals in centrosymmetric space groups, as well as gases and liquids containing molecules of any symmetry. The observed coherent optical properties involve the square of the polarization. The absorption of energy is given by the cycle average $<P_\alpha E_\alpha>$. So it is easy to see that all incoherent non-linear properties (those dependent on a power of the light intensity greater than one must be described in the third or higher odd order susceptibility. The majority of the better known non-linear processes occur through $\chi^{(3)}$. The second order susceptibility while giving rise to frequency mixing (second harmonic generation, up and down conversion) does not describe absorption processes because $<\chi^{(2)} E_\alpha E_\beta E_\alpha> = 0$. Figure 1 summarizes the various processes that are discussed herein.

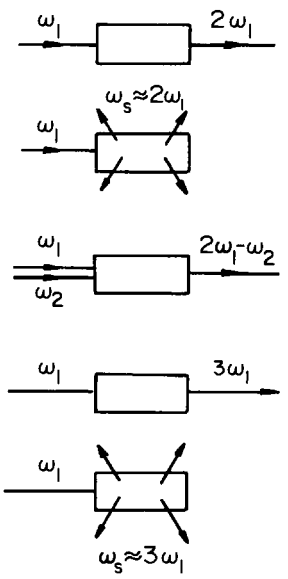

$\chi^{(2)}(-2\omega_1,\omega_1,\omega_1)$
SECOND HARMONIC GENERATION

$\mathrm{Im}\,\chi^{(3)}(-\omega_1,-\omega_1,\omega_1,\omega_1)$
TWO-PHOTON ABSORPTION

$\chi^{(3)}(\omega_2-2\omega_1,\omega_1,\omega_1,-\omega_2)$
CARS $\omega_1-\omega_2=\hbar\omega_v$
TWO-PHOTON RESONANCE $2\omega_1=\hbar\omega_i$

$\chi^{(3)}(-3\omega_1,\omega_1,\omega_1,\omega_1)$
THIRD HARMONIC GENERATION

$\mathrm{Im}\,\chi^{(5)}(-\omega_1,-\omega_1,-\omega_1,\omega_1,\omega_1,\omega_1)$
THREE PHOTON ABSORPTION

Figure 1. Schematic of various coherent and incoherent non-linear processes.

2. RESONANCE ENHANCED SECOND HARMONIC GENERATION:

In second harmonic generation coherent light at ω_1 is converted into coherent light at $2\omega_1$. Normally this process occurs only for non-centrosymmetric solids, liquids or gases (i.e. in the presence of applied electric fields in the case of isotropic systems). A number of molecular crystals are non-centrosymmetric and exhibit frequency doubling (4). The microscopic form for $\chi^{(2)}$ near a homogeneous resonance ($\omega_{oi} \approx \omega_1 + \omega_2$) is:

$$\frac{\epsilon_3 \cdot \mu_{oi} / \hbar^2}{\omega_{io} - \omega_1 - \omega_2 + i\Gamma} \sum_j \left[\frac{\epsilon_1 \cdot \mu_{ij} \mu_{jo} \cdot \epsilon_2}{\omega_{jo} - \omega_2} + \frac{\epsilon_2 \cdot \mu_{ij} \cdot \mu_{jo} \cdot \epsilon_1}{\omega_{jo} - \omega_1} \right] \tag{2}$$

The imaginary part or modulus squared of the first part is the one photon spectral profile of the $o \rightarrow i$ transition. The second term is a two-photon amplitude linking the ground state and the resonant state i. This amplitude is not sensitive in the usual case to small changes in the frequencies ω_1 and ω_2. The usual case is where $|i>$ is a low energy optically accessible state of the system and the two frequencies ω_1 and ω_2 have the same order of magnitude. Obviously (2) can then be written in the form:

$$\chi_i^{(2)} (-\omega_1 - \omega_2, \omega_1, \omega_2) = \frac{A_{SHG}}{\omega_{io} - (\omega_1 + \omega_2) + i\Gamma} \tag{3}$$

The electric field at $(\omega_1 + \omega_2)$ is obtained from Maxwell's equations and is proportional to $\chi^{(2)}$. The light intensity at $(\omega_1 + \omega_2)$ is then proportional to $|\chi^{(2)}|^2$. The damping parameter Γ is the homogeneous linewidth for the resonant transition. In crystals and gases there is also inhomogeneous broadening, so the polarization becomes:

$$P(\omega_1 + \omega_2) = \int P_i (\omega_1 + \omega_2)\, g(\omega_{io} - \omega)\, d\omega \tag{4}$$

where P_i is the polarization for the homogeneous system and $g(\omega_{io} - \omega)$ is the inhomogeneous distribution function peaking at ω_{io}. In most of our experiments $\omega_1 = \omega_2$, and $g(\omega_{io} - \omega)$ is a gaussian distribution having a width parameter σ so that the second harmonic light intensity near resonance is

$$I(2\omega_1) = K \left| A_{SHG} \int \frac{\exp[-(\omega_{io} - \omega)^2/\sigma^2]}{(\omega - 2\omega_1 + i\Gamma)}\, d\omega \right|^2 \tag{5}$$

where K depends on the phase matching (7). In most of our resonance experiments the system is perfectly phase matched at the peak signals. The resonance frequency ω_{io} corresponds to a polariton of particular wavevector, and in general the damping parameter is dependent on frequency for the case of polaritons (8). Apparently the factors in equation (3) or (5) will vanish unless the transition to the state i is both one and two photon electric dipole allowed, a situation that can prevail when the system is not centrosymmetric. For centrosymmetric systems (5) can exist if one of the three transition moments (μ_{oi}, μ_{ij} or μ_{jo}) is magnetic dipole (M) or electric quadrupole (9). The two situations that can arise are sketched in Figure 2. In Figure 2(a) the resonant state has the same parity as the ground state so the first factor in equation (3) is a magnetic dipole transition amplitude while the second is a normal two-photon amplitude involving intermediate states of u-parity. In Figure 2 (b) the resonant state has opposite parity from the ground state so the two-photon part of equation (3) contains the magnetic dipole transition moment. Both of these terms will be important in molecular spectroscopy. Case (a) will result in the production of coherent light at $\sim \omega_{oi}$ even in a conventional two-photon absorption experiment. Thus if the crystal has other transitions of the appropriate parity near ω_{oi} this beam may become absorbed in a secondary process, thereby resulting in a two-photon fluorescence signal. The anisotropy of two-photon transitions in crystals may therefore be subject to errors, since the two-photon absorption through Im $\{\chi^{(3)}\}$ does not have the same anisotropy as the effect discussed here. Case (b) gives rise to a coherent beam at $\sim \omega_{oi}$, and this beam can certainly be absorbed in a one photon process, since the $o \rightarrow i$ transition is allowed. If the two-photon transition is being detected by fluorescence or attenuation of the beams at ω_1 or ω_2 we see that the magnetic part of $|\chi^{(2)}|^2$ will contribute always in case (b) and also in case (a) if other u-states lie in the region of the state i. For the case (b) the

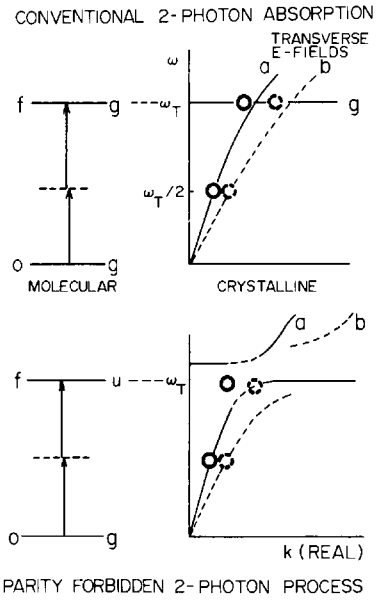

Figure 2. (a) Conventional allowed 2-photon processes.
(b) Unconventional forbidden 2-photon-process.
In (a) phase matching to produce excitons is non-critical; in (b) the phase matching is onto polariton states and it is critical.

separation of the second harmonic generation from two-photon absorption is not so simple to achieve experimentally. Far off resonance, where the attenuation of the second harmonic beam is small one may readily study the resonance enhanced SHG, but it is more difficult to separate the effects of SHG from two-photon absorption when an indirect method, such as fluorescence, is used to detect the two-photon transition. Ovbiously the same considerations will hold for systems having no center of symmetry. For example in a molecular crystal where the unit cell has no inversion center, the relaxed fluorescence resulting from two-photon resonances with vibronic states will contain resonant parts due to $|\chi^{(2)}|^2$ as well as Im $\{\chi^{(3)}\}$. One can therefore expect that two-photon induced fluorescence spectra would resemble closely the one-photon spectra of the same transitions, at least in the condensed phase. In general, molecules have states of different symmetry in the same spectral region because of the various vibrational or phonon symmetries. Thus radiation having a frequency larger than the 0-0 transition of a particular electronic state is always partially absorbed regardless of its polarization.

3. $\chi^{(2)}$ AND Im $\chi^{(3)}$ SPECTROSCOPY IN ORGANIC CRYSTALS:

In conventional induced two-photon processes connecting two stationary states of a crystal there is no phase matching difficulty. The situation, depicted in Figure 2(a), for a centrosymmetric system is that the Im $\{\chi^{(3)}\}$ describes two-photon absorption from the g - ground state to g - excited states of the crystal. Since electromagnetic fields at ca. 2ω do not couple significantly to the system via the g → g transition the phase matching is entirely non-critical. For example (see Figure 2(a)) light having wavevector k and frequency ω matches to an exciton at 2ω and 2k for all k. On the other hand (see Figure 2(b)) if the two-photon absorption is unconventional such as between a g and a u level of the crystal the "light" at 2ω does interact with the crystal through the resonantly enhanced $\chi^{(1)}$ at 2ω. In that case the two-photon absorption is the fusion of two photon-polaritons to produce a polariton at ca. 2ω. Now the phase matching is critical since photons at ω phase match only for k=k'. Furthermore for optically nonisotropic crystals the observed spectrum will depend on the direction of propagation and polarization of the light at ω, whereas in the conventional situation the spectral line position is the same for all directions of propagation. These same phase matching conditions should persist for two-photon absorption and second harmonic generation.

These features are illustrated by our recent work on the naphthalene crystal at low temperatures. Light at ω (region of <6200 Å) incident on the crystal produces many sharp transitions at 2ω (region of <3100 Å) that were detected (10) by means of the fluorescence (incoherent emission) of the crystal. These two-photon spectra were independent of propagation direction in the crystal and the transitions were identified as $g \rightarrow g$ vibronic transitions corresponding to upper states involving the various ungerade vibrations of the naphthalene B_{2u} state. In the region of $2\hbar\omega$ equal to the energy of the 0-0 band of this transition the situation is quite different (11). Here the two-photon absorption is dependent on the direction of propagation as shown in Figure 3. In addition to two-photon absorption in this experiment the second harmonic generation is observed for 2ω both at lower and at higher energy than the region of two-photon absorption.

The spectrum of Figure 3 exposes the main features of the polariton dispersion curve. Of special interest is the knee region where the lower and upper branches come closest. When the phase matching is appropriate to reach the knee there should arise the possibility of widening the range of frequencies (2ω) that can be reached with a given incident beam direction and laser divergence. In other words the phase matching curve at some direction of incidence will run parallel to the polariton dispersion curve. This appears to be a likely interpretation of the narrow angular region (marked near $-5°$ in Figure 3) where the two photon induced signal is considerably broadened.

These spectra through their widths and the comparisons of second harmonic generation and two-photon absorption provide valuable information on the damping of polaritons in molecular crystals. The concepts involved in the dynamical aspects of excited states of crystals are illustrated in Figure 4.

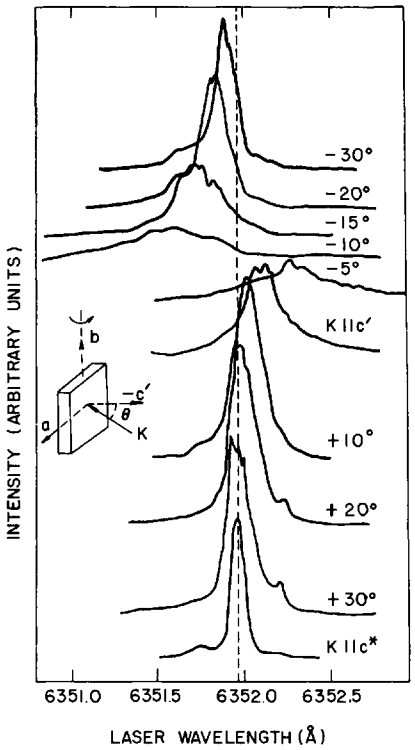

Figure 3. Two-photon excitation spectrum of naphthalene at 1.6K using colinear Geometry (11).

The distinction between coherent optical events in Figure 4 is quite analogous to the more conventional problem of distinguishing coherent scattering from incoherent fluorescence of molecular excited states (12). The field at ω if far from a crystal resonance propagates in the crystal as a photon-polariton. For weak fields in a perfect crystal this coherent polarization can only be diminished by conventional Raman scattering, creating new photon-

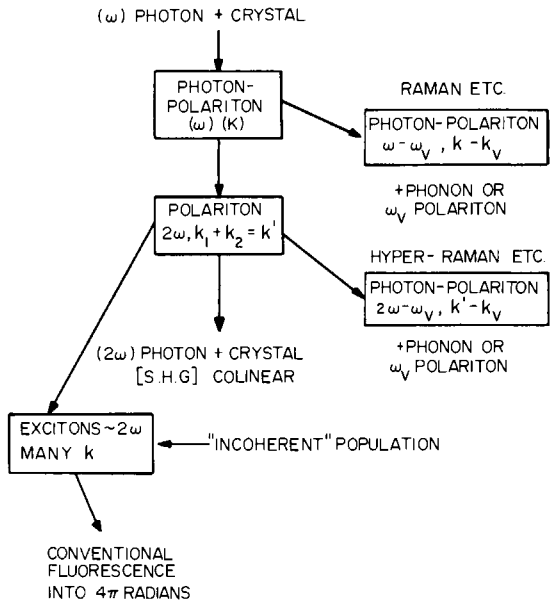

Figure 4. Dynamical events in light absorption by a crystal.

polaritons. The non-linear susceptibility allows polariton fusion to occur resulting in a coherent polarization at 2ω and thus an electromagnetic field at 2ω will be observed outside the crystal. When 2ω is near a crystal resonance an exciton-polariton (or simply a polariton) is generated in the crystal. This polariton, which if undamped will result in the second harmonic wave, may be damped by various spontaneous processes. One way is the spontaneous production of a polariton and a phonon corresponding to different frequencies and wavevectors. This is hyper-Raman scattering. Another cause of damping is the exciton-phonon interaction which generates an incoherent population of excitons in the crystal. Clearly this damping depends on the exciton density of states at the polariton frequency. The population of excitons thus produced may radiate light in the region of 2ω (or less) corresponding to conventional fluorescence of the crystal. This fluorescence is emitted into 4π radians with a spectral distribution given by the dephasing of the dipoles created in the crystal.

4. THREE-WAVE MIXING SPECTROSCOPY: GENERAL

In general two laser beams having frequencies ω_1 and ω_2 interact with a sample to produce a third beam, nearly colinear with the incident sources, that has a frequency $\omega_3 = 2\omega_1 - \omega_2$. It is very well known that the generation of the ω_3 beam is strongly enhanced when $[\omega_1 - \omega_2]$ is also a vibrational (or electronic) frequency of the medium - this process being CARS. If the medium has a resonance at $2\omega_1$, an enhancement of the ω_3 beam due to the two-photon resonance is also expected. Diagrams for these two resonances in $\chi^{(3)}$ are given in Figure 5.

Originally demonstrated (13) for excitons in CuCl the two-photon resonance has very recently been studied in organic liquids (14, 15). An advantage of the two-photon resonances in $\chi^{(3)}$ in studies of optical spectra is that comparisons of the CARS and two-photon resonant signals are readily achieved. The ratio of the two signals can be arranged in favorable circumstances to be independent of the power and mode structure of the lasers. The CARS portion involves only the Raman cross-section and linewidths.

If the ω_1 beam is scanned and ω_2 fixed, the intensity of the ω_3 beam as a function of ω_1 yields the spectrum of the resonances that occur at $2\omega_1$ when $(\omega_1 - \omega_2)$ is far from CARS resonances. The three wave mixing technique has great advantages over indirect methods of detecting two-photon absorption because no special properties of the resonant state are needed other than that a conventional two-photon matrix element exist between that state and the ground state. For example, two-photon resonances in three wave mixing could be studied for dissociative states and nonfluorescent systems whose lifetimes would preclude the use of the fluorescence methods of studying two-photon absorption. The spectral inten-

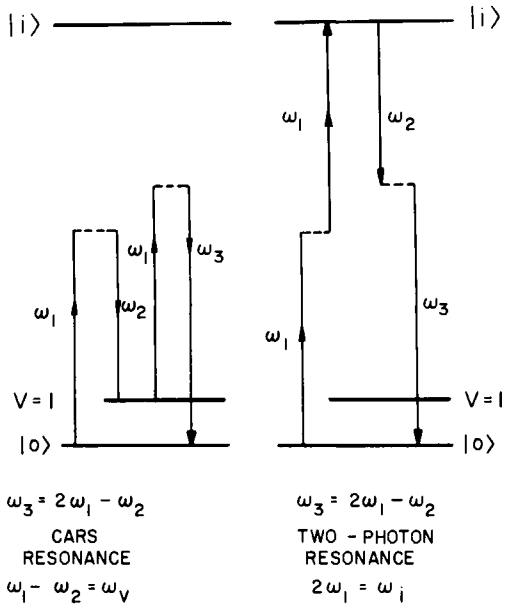

Figure 5. Two of the resonance processes involved in the generation of coherent light at ω_3 due to the interaction of light at ω_1 and ω_2 with any medium.

sity profiles obtained are not influenced in a first approximation by higher order processes or by quantum yields of incoherent relaxations and so provide an unperturbed intensity distribution.

4. (a) TWO-PHOTON RESONANCES IN GASES (16):

Two-photon resonances in $\chi^{(3)}$ can be readily obtained for molecular gases and used for moderately high resolution spectroscopy. The well-known two-photon absorption spectrum of nitric oxide (17) was used in order to demonstrate the effects.

The experimental apparatus consisted of a Molectron UV1000 nitrogen laser used to pump two Hansch type dye lasers both of which produced 50 to 100 μj. The beams were rendered colinear through a 60° prism and focused into a 10 cm gas cell. Lenses were used after both lasers to partially compensate for divergence and to assure that both beams focused simultaneously in the same region. A prism monochromator and double 3/4m monochromator were used to select the $\omega_3 = 2\omega_1 - \omega_2$ beam, which was monitored by a Hamamatsu 213 photomultiplier tube. Signals were viewed on an oscilloscope in order to optimize detection, to confirm $\chi^{(3)}$ behavior that demands the signal intensity is proportional to $I_1^2 I_2$, and to remove scattered light problems. A Boxcar integrator was used as a linearly gated amplifier. Spectra were obtained by fixing ω_2 at some desired frequency and scanning ω_1 while the double monochromator was scanned at twice the ω_1 rate. Monochromator bandpasses were kept as large as possible to minimize synchronization errors.

The two-photon resonances observed in NO (Figure 6) were easily identifiable by their invariance to the value of ω_2, by their linewidths which were laser limited (the ω_1 laser was narrower than the ω_2 laser by at least a factor of 2), and by reference to known spectra.

The CARS resonance signals were observed for NO, and for N_2 in air after lifting the sample from the beam focus region. The latter signal was useful for maximizing detection optics before inserting the gas cell and searching for two-photon signals. Besides this helpful maximization, a calibration of the two-photon signal can be achieved since the cell alters the collection optics only minimally, and the CARS (Raman) resonance susceptibility for N_2 is known.

For a gas the damping parameter used in the expressions for the contribution of a

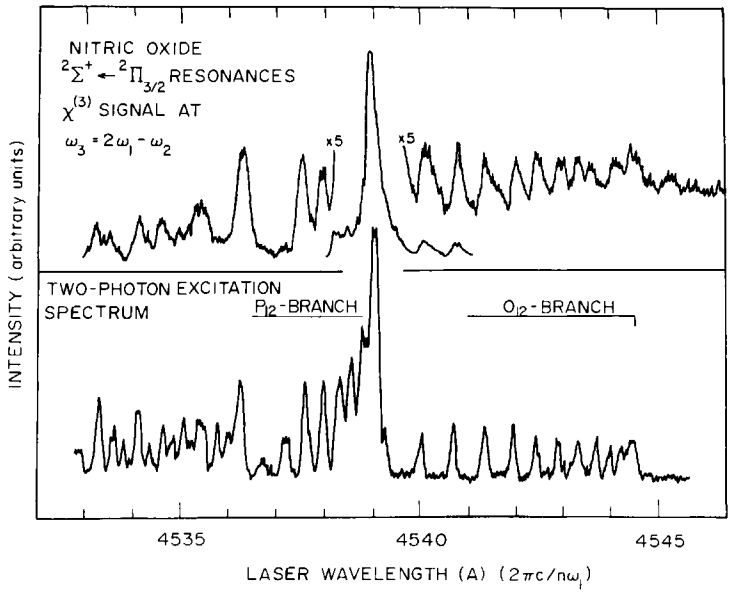

Figure 6. Two-photon resonances in NO gas.

resonance to $\chi^{(3)}$ is determined by the collisional and natural damping, and the Doppler broadening creates an inhomogeneous distribution of resonances. The nonlinear polarization at frequency ω is generated by the effect of the electric field amplitudes of all lasers operating through the bulk susceptibility function. That due to the i^{th} resonance is

$$P_i(\omega) = \iiint d\omega_1' d\omega_1'' d\omega_2' \, \delta(\omega + \omega_2' - \omega_1' - \omega_1'') \, E_1(\omega_1') \, E_1(\omega_1'') \, E_2(\omega_2') \int d\omega_i'' [\pi\sigma^2]^{-\frac{1}{2}} e^{-(\omega_i' - \omega_i)^2/\sigma^2} [2 - \delta_{\omega_i' \omega_j''}] \, 3 \, \chi_i^{(3)}(\omega_i', \Gamma_i) \tag{6}$$

where $\chi_i^{(3)}(\omega_1', \Gamma_i)$ is the susceptibility appropriate to a resonance at ω_i' with damping constant Γ_i, and σ is the appropriate Doppler width. For the closely spaced J components of the nitrogen Raman Q-branch, the sum of these terms effectively yields the total polarization. The light intensity generated at ω is then proportional to the total polarization modulus squared.

The determination of two-photon cross sections relative to Raman cross sections have recently appeared in the literature (14, 15). Our laser widths were appreciably wider than the resonance widths, so the spectra must be deconvoluted. In addition, the homogeneous and inhomogeneous widths need to be known since the former enters the expression for $\chi^{(3)}$ at resonance and the latter describes the distribution of the resonances. The comparison to N_2 CARS in air is nevertheless a convenient way to calibrate the two-photon signal. The two-photon hyperpolarizability determined via this method, $|\alpha_{xx}^T \alpha_{yy}^T|$ for $E_1 \perp E_2, E_3$, is not that for two photons at ω_1, but is the geometric mean of this cross section with that for absorption of two photons at frequencies ω_2 and ω_3 where $\omega_2 + \omega_3 = 2\omega_1$. In general $|\alpha_{xx}^T \alpha_{yy}^T|$ is different from the comparable quantity needed for two-photon cross-sections, say $|\alpha_{xx}^T|^2$, but in certain cases these averages are related.

By appropriate averaging we find for the 0_{12} branch of the γ bands of NO that $|\alpha_{xx}^T \alpha_{yy}^T| = \frac{1}{2}|\alpha_{xx}^T|^2$. Our measurements yielded for $0_{12}(6\frac{1}{2})$, $|\alpha_{xx}^T|^2 = 3.0 \times 10^{-52}$ cm^6. The commonly quoted quantity δ for single beam two photon absorption in a single rotational transition is then

$$\delta = \frac{8\pi^3}{c^2} \omega^2 g(2\omega) \{|\alpha_{xx}^T|^2 / f[0_{12}(6\tfrac{1}{2})]\} f[J]$$

where g (2ω) is a normalized lineshape function, and the f [J] are line strengths from Table 2 of reference 18. Specifically for 0_{12} $(6\frac{1}{2})$ this yields

$$\delta = 7.5 \times 10^{-51} \; g\,(2\bar{\nu})\ \text{cm}^4\ \text{s/photon-molecule with}\ \bar{\nu}\ \text{in cm}^{-1}.$$

4. (b) TWO-PHOTON $\chi^{(3)}$ RESONANCES IN MOLECULAR SOLIDS (19):

In molecular crystals at low temperatures it is easily possible to separate spectrally transitions to the many different vibronic states. We have recently shown that $\chi^{(3)}$ spectroscopy can be used with great effect to study gerade resonant states in the ultraviolet by means of visible lasers (19).

One example we have studied is the biphenyl crystal. The first excited electronic state having the same spin as the ground state is $^1B_{3g}$, to which a two-photon transition from the ground state is fully allowed. The Raman spectrum of the biphenyl crystal is also well-known, and one of the strongest lines is at 1277 cm^{-1}. The demonstration of the $\chi^{(3)}$ spectroscopy of these two states ($^1B_{3g}$ electronic state and an ^1A_g vibrational state, the ground vibrational state being ^1A_g) is shown in Figure 7.

In this experiment $\lambda_2 = 2\pi c/\omega_2$ was kept fixed at 6548 Å while ω_1 was scanned through the regions where $\omega_1 - \omega_2$ equalled the vibrational frequency and $2\omega_1$ equalled the electronic resonance frequency. The general form of $\chi^{(3)}$ is

$$\chi^{(3)} = \frac{A_V}{\omega_V - (\omega_1 - \omega_2) + i\Gamma_V} + \frac{A_T}{\omega_E - 2\omega_1 + i\Gamma_E} + \chi^{NR} \qquad (7)$$

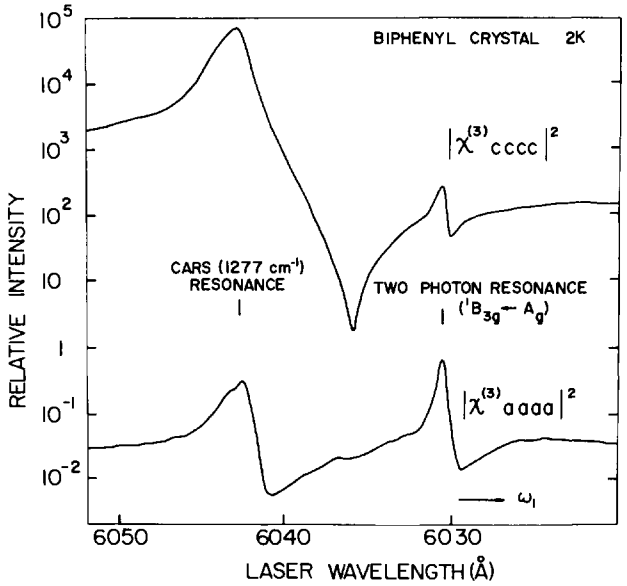

Figure 7. Two-photon and CARS resonances in the biphenyl crystal at 1.6K.

The ω_3 signal shown in Figure 7, on scanning ω_1 first goes through the vibrational (CARS) resonance, $(\omega_1 - \omega_2) = \omega_V$, and then the electronic resonance when $2\omega_1 = \omega_E$. The fact that the electronic state has different symmetry from the vibrational state is strongly manifested in Figure 7 by the entirely different anisotropies for three-wave mixing via the CARS and two-photon resonances.

5. THREE-PHOTON ABSORPTION:

The simultaneous absorption of three-photons to produce an incoherent population of excited states occurs through Im $\chi^{(5)}$ (see Figure 1). Whereas with many centrosymmetric organic crystals the two-photon absorption is an electronically forbidden process that requires the intervention of nuclear motion, those g → u transitions are allowed in three-photon ab-

sorption. Three-photon absorption is a useful adjunct to one-photon spectra in cases where XYZ belongs in a different irreducible representation than any of the three coordinates X, Y or Z. Such is the case with D_{2h} where XYZ transforms as A_u. The benzene crystal factor group has symmetry D_{2h} so that the molecular states are each split into four crystal states one of which has A_u symmetry. Our preliminary study of the three-photon absorption is shown in Figure 8 (20).

This spectrum was seen by detecting fluorescence in the ultraviolet arising from absorption of three red photons from a single laser beam focused into a single crystal of benzene at 1.6K. The A_u transition does not show up in this case because the electric vector is not projecting simultaneously onto all three crystal axes. The signal varies as I_1^3

6. TIME RESOLVED $\chi^{(3)}$ SPECTRA:

The various coherent spectroscopies described here are useful in studies of dynamics. For example in the nitric oxide experiments described above a 2ns laser pulse is used to probe the rotational temperature of NO. We have also used picosecond pulses to study the CARS resonance in nitrogen gas (21).

In gases the interval between hard sphere collisions is very long (ca 10^{-7} sec torr) compared with the duration of a picosecond pulse (say, 5 to 50 ps depending on the laser system used) even for relatively high pressures. Thus for vibrational effects, isolated molecule conditions might prevail up to many hundreds of torr when the experimental observations are made in the picosecond time regime. Rotational relaxation effects are known to have

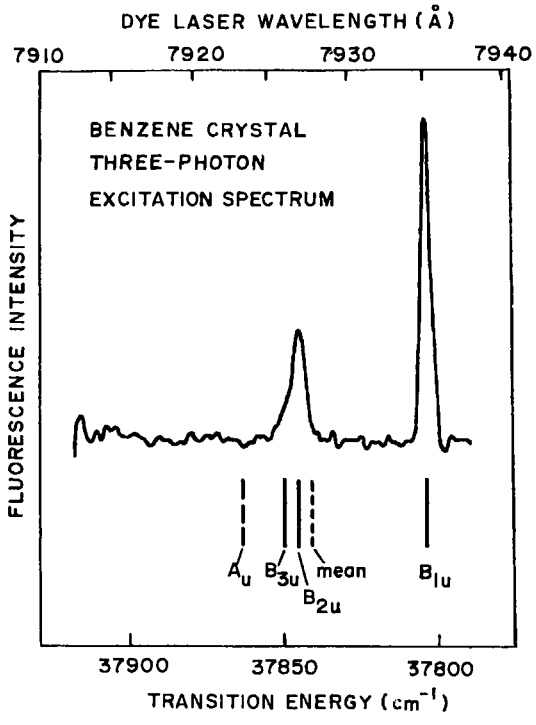

Figure 8. Three-photon excitation spectrum of crystalline benzene.

cross-sections often many times gas-kinetic, so the collision-free pressure limit relevant to picosecond experiments is not expected to be so high. Of course, except for rather light molecules the rotational spacings are in any case narrower than the transform frequency bandwidth of a picosecond pulse.

These experiments show the feasibility of using picosecond laser pulses to study ultrafast chemical reactions under essentially isolated molecule conditions at moderately high pressures. In many respects these non-linear phenomena are extremely convenient adjuncts to picosecond spectroscopy because they expand the range of wavelengths that can be used to study fast processes.

7. CONCLUSIONS:

The purpose of this presentation was to summarize some recent developments from this laboratory on applications of non-linear optical techniques in chemical spectroscopy. This field is very young and these early results suggest that non-linear optical spectroscopy at moderately high resolution will be a fruitful approach for the study of molecular excitons, mixed crystals and gases.

Acknowledgement - This research was supported by a PHS grant GM 12592, the Army Research Office (Durham), and the National Science Foundation, MRL Program under Grant No. DMR 76-00678.

REFERENCES:

1. N. Bloembergen, Nonlinear Optics, Benjamin, New York, 1965.
2. Y. R. Shen, Rev. Mod. Phys. 48, 1 (1976) and references contained therein.
3. D. Bedeaux and N. Bloembergen, Physica 69, 57 (1973).
4. C. Flytzanis, "Theory of Nonlinear Optical Susceptibilities" in Quantum Electronics: A Treatise, ed. H. Rabin and C. L. Tang, Academic, New York, 1975, Vol. I.
5. P. N. Butcher, Nonlinear Optical Phenomena, Ohio State University Engineering Publications, Columbus, 1965.
6. R. R. Birss, Symmetry and Magnetism, Selected Topics in Solid State Physics, Volume III; North-Holland 1966.
7. S. H. Kurtz, "Measurement of Nonlinear Optical Optical Susceptibilities" in Quantum Electronics: A Treatise, ed. H. Rabin and C. L. Tang, Academic, New York, 1975, Vol. I.
8. D. Frohlich, E. Mohler and Ch. Uihlein, Phys. Stat. Sol. 55, 175 (1973); D. Boggett and R. Loudon, J. Phys. C. 6, 1763 (1973).
9. S. Kielich, Acta Phys. Polon, 29, 875 (1965); P. S. Pershan, Phys. Rev. 130, 919 (1963).
10. R. M. Hochstrasser and H. N. Sung, J. Chem. Phys. 66, 3276 (1977).
11. R. M. Hochstrasser and G. R. Meredith, J. Chem. Phys. 67, 1273 (1977).
12. R. M. Hochstrasser and F. A. Novak, Chem. Phys. Lett., in Press.
13. S. D. Kramer, F. G. Parsons and N. Bloembergen, Phys. Rev. B 9, 1853 (1973); S D. Kramer and N. Bloembergen, Phys. Rev. B 14, 4654 (1976).
14. R. T. Lynch, Jr. and H. Lotem, J. Chem. Phys. 66, 1905 (1977).
15. R. J. M. Anderson, G. R. Holtom and Wm. M. McClain, J. Chem. Phys. 66, 3332 (1977).
16. R. M. Hochstrasser, G. R. Meredith and H. P. Trommsdorff, submitted to Chem. Phys. Lett.
17. R. G. Bray, R. M. Hochstrasser and J. E. Wessel, Chem. Phys. Lett., 27, 167 (1974); R. G. Bray, R. M. Hochstrasser and H. N. Sung, Chem. Phys. Lett. 33, 1 (1975).
18. R. G. Bray and R. M. Hochstrasser, Mol. Phys. 31, 1199 (1975).
19. R. M. Hochstrasser, G. R. Meredith and H. P. Trommsdorff, in preparation.
20. R. G. Bray, C. M. Klimcak and R. M. Hochstrasser, unpublished research from this laboratory.
21. B. Greene, R. M. Hochstrasser and R. B. Weisman (results illustrating picosecond CARS presented at the IUPAC symposium are in preparation for publication elsewhere.)

Pure & Appl. Chem., Vol. 50, pp. 1231-1238.
Pergamon Press Ltd. 1978. Printed in Great Britain.

0033-4545/78/1201-1231 $02.00/0

PICOSECOND TIME-RESOLVED MEASUREMENTS OF VIBRATIONAL ENERGY TRANSFER AND RELAXATION PHENOMENA IN LARGE POLYATOMIC MOLECULES

W. Kaiser and A. Laubereau

Physik Department der Technischen Universität München, Germany

Abstract - Vibrational modes in the electronic ground state are investigated by recently developed ultrashort measuring techniques. Using tunable infrared pulses well defined vibrational states are first excited far above the thermal equilibrium value, and with delayed probe pulses the instantaneous population of various vibrational states is monitored. Rapid redistribution (1×10^{-12} sec) between neighboring energy states is seen in various molecules while the decay to lower vibrational levels is found to depend very strongly on the mode structure of the individual molecule. Population lifetimes of 1 psec and 40 psec are measured for CH_3 modes in CH_3I and ethanol, respectively.

In this short review, experimental studies are described which allow quite directly the investigation of a series of very rapid vibrational processes. Here we restrict ourselves to vibrational modes in the electronic ground state.

Fig. 1 gives somewhat schematically an outline of several experimental techniques which had to be developed in order to measure various new molecular parameters. Well-defined vibrational modes are excited by a first intense ultrashort laser pulse via stimulated Raman scattering or via direct resonance infrared absorption (left column of Fig. 1). A second interrogating pulse which is properly delayed with respect to the first exciting pulse monitors the instantaneous state of the excited vibrational system. Three different ways of probing (center of Fig. 1) give a variety of information (right column of Fig. 1).

(i) With coherent probing we measure the state of phase correlation within the excited volume. Time does not allow to discuss this topic here since it is not the main subject of the present talk. We briefly note that an important molecular parameter, the dephasing time of a specific vibrational mode, can be directly obtained by a coherent probing experiment.

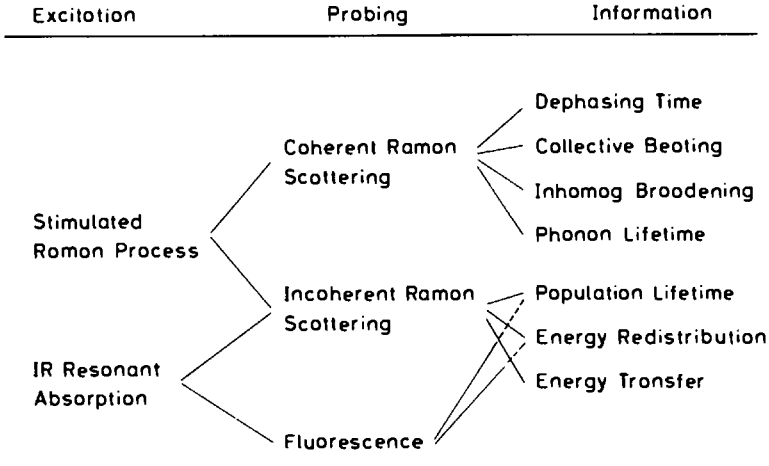

Fig. 1 Short outline of the paper. Two excitation processes allow to excite a specific vibrational mode. Three different probing techniques provide time resolved data on a variety of subjects listed on the right.

(ii) Of special interest for the present topic is the observation of the (spontaneous) anti-Stokes Raman signal of the interrogating probe pulse. This signal is a direct measure of the momentary degree of population of a specific vibrational state. With this technique it was possible for the first time to observe population lifetimes, energy transfer and vibrational redistribution of polyatomic molecules in the liquid state. We note that such data are - in most cases - not available from other experimental methods.

(iii) In highly diluted systems, it is possible to investigate the momentary occupation of a vibrational state by a recently developed fluorescence technique. The time delayed probe pulse promotes the excited molecules close to the bottom of the first excited singlet state. The degree of fluorescence from this latter state is directly proportional to the momentary occupation of the excited vibrational state in S_o.

Before we present various experimental results, several short remarks should be made concerning the experimental system. We work with a Nd-glass laser system consisting of an oscillator and an amplifier. We know from various investigations that we have single pulses of 6 psec duration and a frequency bandwidth of 3 cm^{-1}, i.e., our pulses are very nearly bandwidth limited. Starting with these pulses we prepare new frequencies by second harmonic generation or - more interesting - by the three-photon parametric process. The latter technique allows to generate ultrashort infrared pulses over a substantial frequency range. With $LiNbO_3$ crystals and a pumping frequency of 9455 cm^{-1} a tuning range up to 2500 cm^{-1} is possible ($LiNbO_3$ absorbs at longer wavelengths).

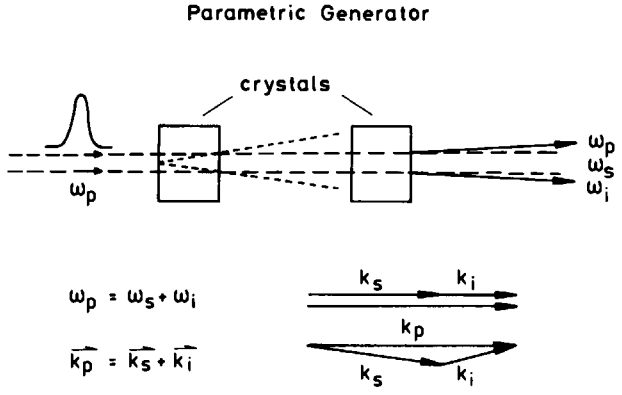

Fig. 2 Schematic diagram of parametric generator set-up. The incident pump pulse generates a parametric emission in the first crystal which is used as an input signal for the amplification process in the second specimen.

Picosecond Pulses in the Infrared

Tunability	2500 to 7000 cm^{-1}
Frequency Width	8 cm^{-1}
Pulse Duration	3 psec
$I_p \times \Delta V$ =	0.7
Divergence	3×10^{-3} rad
Intensity	~ 10^9 W/cm^2
Energy Conversion	~ 5 %

Fig. 3 Table of pulse properties generated by the parametric generator scheme.

We have spent considerable effort to obtain a small bandwidth of the infrared pulses in the parametric process. The two-crystal technique depicted in Fig.2 produces infrared pulses which come close to the Fourier transform limit. As indicated in Fig. 2, the first crystal acts as a frequency generator of large divergence and correspondingly large bandwidth while the second crystal, placed at a distance of approximately 40 cm from the first crystal, amplifies only the small frequency band in the center of the pump beam. The experimental data of our IR-pulses are summarized in Fig. 3. The parametric process shortens somewhat the pulse duration and, more important, steepens the wings of the pulse on account of the nonlinear parametric generation process. In Fig. 4, our experimental system is depicted schematically. The powerful laser pulse

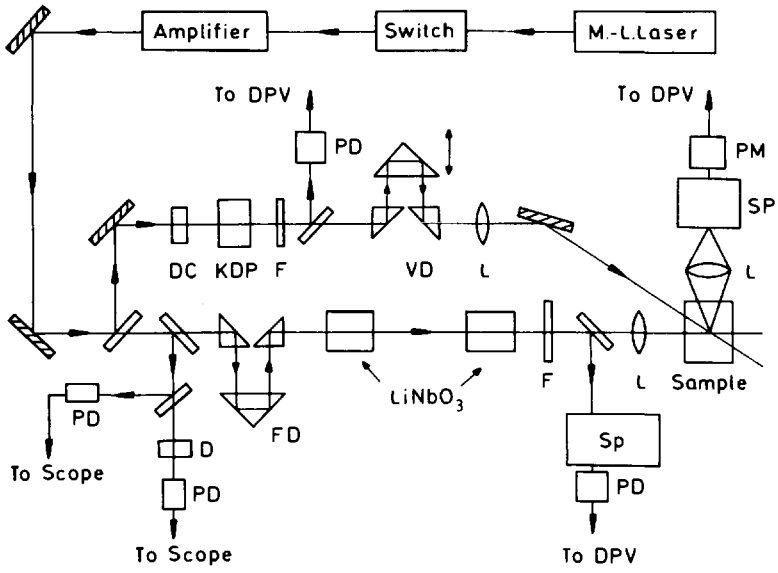

Fig. 4 Experimental system used to measure energy relaxation times. A single picosecond laser pulse generates either stimulated Raman scattering in the sample or produces ultrashort infrared pulses when the two nonlinear crystals (broken line) are inserted. The infrared frequency is tuned by crystal rotation. The probe pulse travels through the upper delay system and interrogates the excited volume. With spectrometer (SP) and photomultiplier (PM) a spontaneous anti-Stokes signal or a fluorescence signal can be measured. The input intensity is determined by two fast photodiodes (PD) in conjunction with a nonlinear absorber (D).

enters the two parametric crystals from the left and the generated infrared light excites the sample located at the lower right of the Figure. A beam splitter in the input beam produces the second interrogating pulse which is transformed to the second harmonic frequency in a KDP crystal. After a proper delay, both pulses meet in the same volume of the specimen. The anti-Stokes Raman signal or the generated fluorescence is monitored by a spectrometer in conjunction with a photomultiplier. We have studied a variety of molecules and vibrational modes and found a wide range of population lifetimes. Two examples should be discussed here.

First we present experimental data on ethanol. A CH-stretching mode of the molecule was excited by an infrared pulse of $\nu = 2930\ cm^{-1}$ and the anti-Stokes Raman signal with the same frequency shift was measured. The experimental curve of Fig. 5 suggests two time constants. The first rapid decay of the primary scattered signal is interpreted as being due to a redistribution of vibrational energy between neighboring energy states, while the following slow decay corresponds to the decay to lower energy states. In fact, the subsequent occupation of the bending modes at $\sim 1500\ cm^{-1}$ has been observed in an earlier experiment. Fig. 6 shows the energy levels of ethanol and the energy states which are involved in the excitation and decay processes of our experiment. Note the numerous energy states around $3000\ cm^{-1}$ which have smaller effective

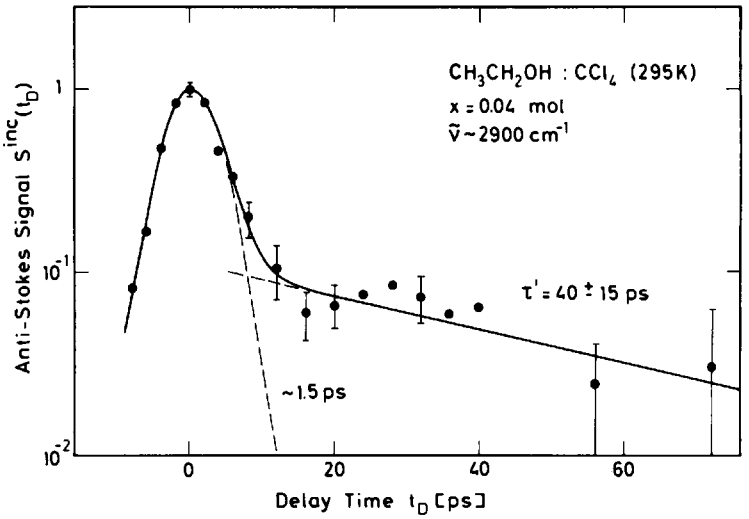

Fig. 5 Incoherent anti-Stokes probe signals with frequency shift of ~ 2900 cm^{-1} versus delay time. Sample: 4 mol per cent CH_3CH_2OH in CCl_4. The CH_3-stretching mode was excited by an infrared pulse. The first fast signal decay is related to rapid energy redistribution between neighboring energy states. The slower decay corresponds to energy relaxation to lower bending modes.

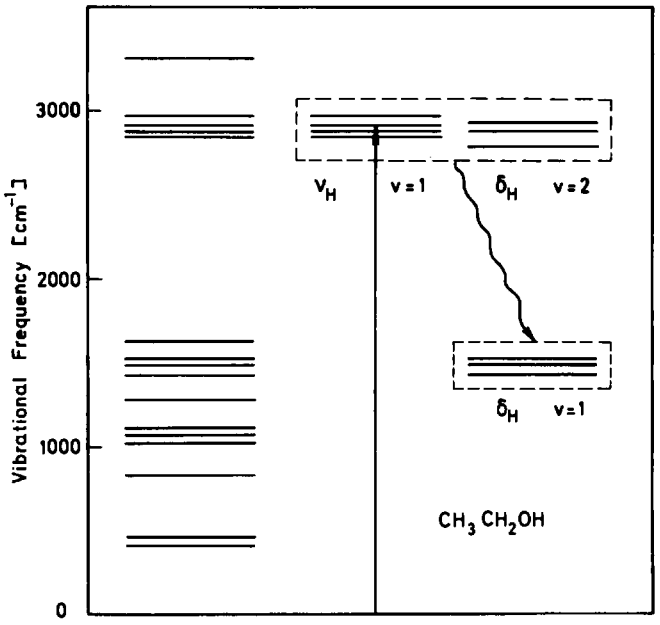

Fig. 6 Schematic diagram of vibrational states of ethanol. A CH stretching mode is excited by the infrared pump pulse after energy redistribution among the neighboring overtones of the CH bending modes (time constant 1.5 psec). A much slower decay was observed to the bending modes around 1400cm^{-1}.

Raman cross sections than the primary excited mode. The subsequent decay to the lower bending modes is indicated. Quite different from the preceeding case is the vibrational energy decay in a relatively small molecule CH_3I. Two experiments were performed (see Fig. 7). First, the symmetric CH_3 stretching mode (ν_1) was measured; then the asymmetric CH_3 stretching mode (ν_4) was ex-

cited at 3050 cm^{-1} and the instantaneous occupation of the lower ν_1 level was measured as a function of time. In both cases we find an energy decay of approximately 1 psec indicating rapid depopulation of the excited vibrational states. We emphasize that in the second experiment the position of the excitation maximum is only slightly shifted by approximately 1 psec indicating very rapid energy exchange between the ν_1 and ν_4 levels. Recent calculations by

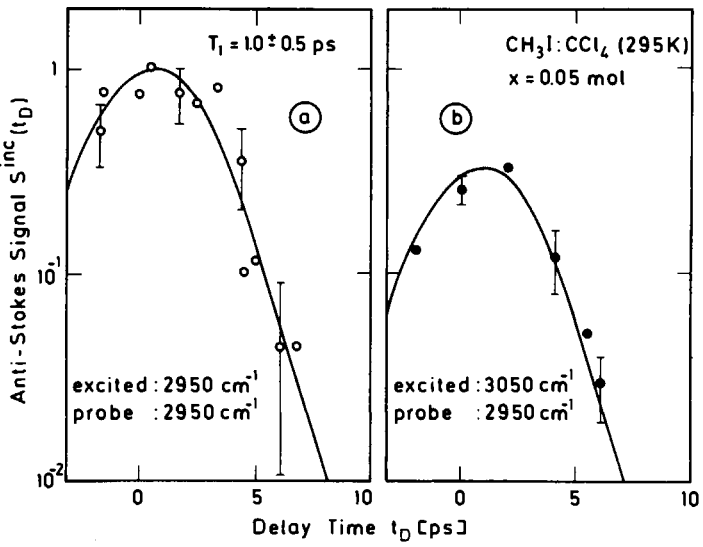

Fig. 7 Incoherent anti-Stokes signals of CH_3I measured at a frequency shift of 2950 cm^{-1}. (a) The molecule is excited by an infrared pulse of ν = 2950 cm^{-1} (open circles). (b) The infrared pumping pulse has a frequency of ν = 3050 cm^{-1} exciting the highest vibrational mode of CH_3I. Note the small time delay necessary for energy exchange.

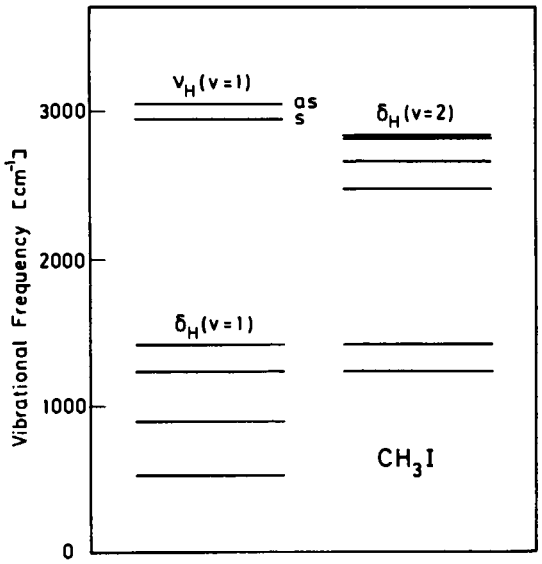

Fig. 8 Vibrational energy states of CH_3I. In our investigations (see Fig. 7), the symmetric or asymmetric CH_3 stretching mode was excited by the infrared pump pulse and the excess population of the symmetric mode was monitored as a function of time. We observe energy redistribution between the two levels with a time constant of 1.5 psec.

S. Fischer et al. of our Department suggest strong coupling between the ν_1 and ν_4 levels and strong mixing between the two CH_3 levels and the $2\nu_5$ state. The theoretical results are in good agreement with the short time constants reported here. Fig. 8 shows the energy states of CH_3I related to our investigations. The most important levels, the two CH_3 modes and the overtone of the bending mode ν_5, are indicated.

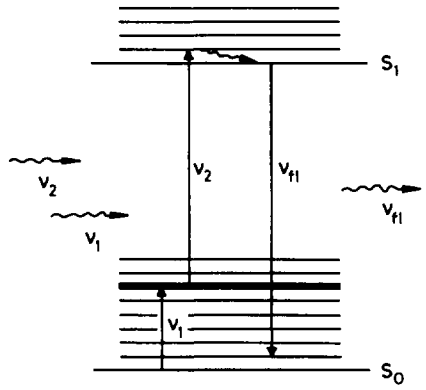

Fig. 9 Double-resonance fluorescence probing technique. Schematic diagram of the relevant molecular energy states. Vibrational level (2) is excited by an infrared pulse of frequency ν_1. The time dependence of the population of level (2) is monitored with a second delayed pulse of frequency ν_2. The (integrated) fluorescence at ν_{fl} is a measure of the population lifetime T_1 of level (2).

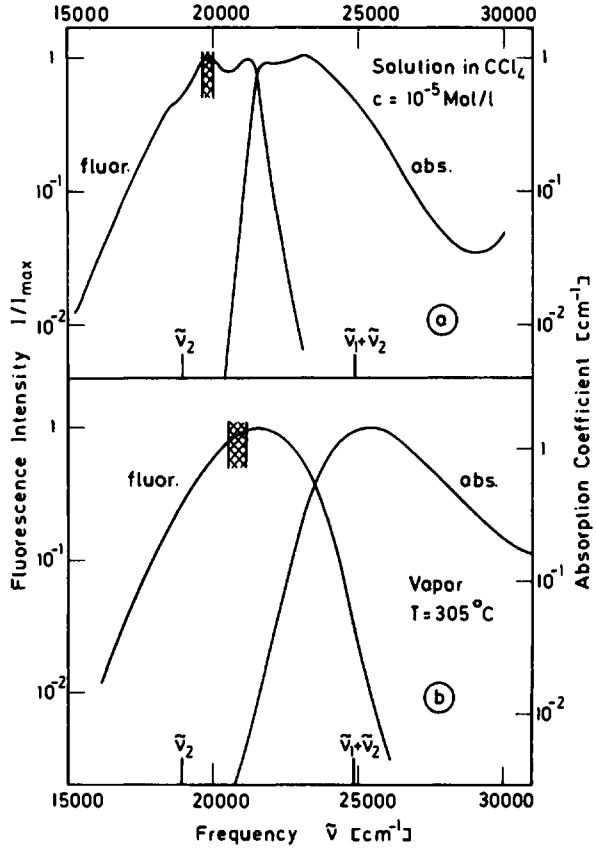

Fig. 10 Absorption and fluorescence of coumarin 6 molecules: (a) Liquid solution of 10^{-5} mol/liter in CCl_4 and (b) vapor phase at 305°C (1 torr). The frequency $\tilde{\nu}_1 + \tilde{\nu}_2$ (infrared pulse + green pulse) is indicated at the abscissa.

Now we turn to the two-step frequency excitation with observation of the generated fluorescence. Fig. 9 shows very schematically the energy levels involved in this technique. The infrared pulse of frequency ν_1 excites a vibrational level in the S_o state above its thermal equilibrium value. A second pulse at a (visible) frequency ν_2 pumps the excited molecules to the fluorescent S_1 state. The fluorescence is observed as a function of delay time between the two pulses. In Fig. 10 we show the absorption and fluorescence spectra of coumarin 6, a relatively large molecule consisting of 42 atoms (see top of Fig. 11). In the upper part of Fig. 10 we see results of a 10^{-5} molar solution of coumarin 6 in CCl_4. The broad bands are typical for dye molecules of the size investigated here. In the lower part of Fig. 10, the spectra of coumarin 6 vapor at 300°C are depicted. The corresponding vapor pressure was measured to be one torr. A similar shift of absorption at higher temperature has been reported for similar molecules. In a first experiment, we measured the relaxation time of coumarin 6 in CCl_4 solutions after excitation of vibrational states at 2970 cm^{-1}. We found a very short time constant of close to 1 psec. Subsequently, we excited a vibrational overtone at 6000 cm^{-1} in a coumarin vapor at 305°C and observed a time constant of 4 psec only (see Fig. 11). There are two

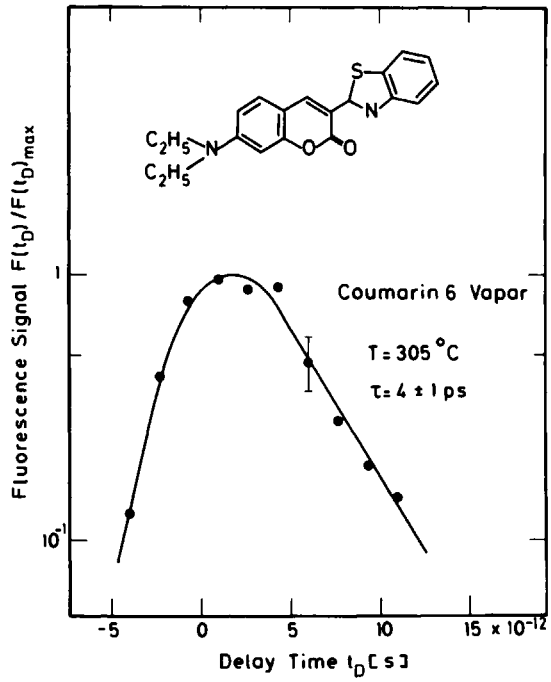

Fig. 11 Vibrational relaxation time of coumarin 6 in the vapor at 305°C. An overtone at 5950 cm^{-1} is primarily excited by an infrared pulse. The fluorescence, produced by the probe pulse, is plotted versus delay time between the excited infrared and probing green pulse. The exponential decay of the signal gives a population lifetime of 4 ± 1 psec. Top: The coumarin 6 molecule.

possibilities for the rapid decay of our signal: Fast redistribution between neighboring energy states with smaller effective Franck-Condon factors and quick vibrational energy decay to lower vibrational states. In any case, the fast time constant in a collission-free gas system is an interesting observation which has not been reported previously.

In summary, we wish to say that we are very much at the beginning. Nevertheless, our measurements indicate quite clearly the potential of determining ultrafast vibrational processes with picosecond infrared light pulses.

For details the reader is referred to the following papers:

A. Laubereau, D. von der Linde and W. Kaiser, Phys. Rev. Lett. 28, 1162 (1972)
A. Laubereau, L. Greiter and W. Kaiser, Appl. Phys. Lett. 25, 87 (1974)
A. Laubereau, A. Seilmeier and W. Kaiser, Chem. Phys. Lett. 36, 232 (1975)
K. Spanner, A. Laubereau and W. Kaiser, Chem. Phys. Lett. 44, 88 (1976)
J.P. Maier, A. Seilmeier, A. Laubereau and W. Kaiser, Chem. Phys.Lett. 46, 527 (1977)

Pure & Appl. Chem., Vol.50, pp. 771-779.
Pergamon Press Ltd. 1978, Printed in Great Britain.

0033-4545/78/0801-0771 $02.00/0

MICROWAVE SPECTRAL STUDIES OF INTERSTELLAR MOLECULES

R. D. Brown

Department of Chemistry, Monash University, Clayton, Victoria, Australia

Abstract - Although the study of the rotational spectra of molecules considerably predates the discovery of interstellar molecules, the radioastronomical applications make three special demands. The first of these is that large radiotelescopes often have been designed for work at lower frequencies than the frequency ranges popularly studied by microwave spectroscopists. A second problem is that some potentially interesting interstellar species are short-lived and rapidly destroyed under normal laboratory conditions. A third problem is that other interesting substances especially those of biological importance are not volatile under normal laboratory conditions. Much of the activity of the Monash University Microwave Group has been directed towards tackling these problems. For the first problem a large L-band cell suitable for Stark modulation has been built. Its performance is illustrated by some recent results on a low frequency line of deuteromethanol.
For the second problem several special purpose spectrometers have been constructed at Monash. Among other successful studies of unstable species we have recently detected HNC and its various isotopic variants. This molecule was simultaneously detected by two other groups using rather different experimental procedures. The Monash work alone led to a determination of the dipole moment of HNC.
To overcome the problem of molecules of low volatility other special spectrometers have been constructed. With these the spectrum of urea was analysed then, more recently, a number of lines in the spectrum of the simplest amino acid - glycine - have been detected. A partial analysis of the spectrum has already been achieved and the complete assignment is expected shortly.

The first interstellar molecules discovered-CH, CH^+ and CN - were identified in the 1930's from the presence of certain lines in the optical spectra of some distant hot stars such as ζ Oph (1). They remained something of an astronomical curiosity until, with the use of radioastronomy, first OH (2) and then, from 1969 on, a pharmacopoeia of chemical compounds were identified. A current list of known interstellar molecules is given in Table 1.

TABLE 1. Interstellar Molecules

Interstellar Molecules

H_2		NH_3	$HC\equiv C-CN$
CH		H_2O	$CH_3-C\equiv CH$
CH^+		H_2CO	CH_3CN
CN		H_2CS	$HCONH_2$
CO		OCS	CH_3OH
CS		HCN	CH_3CHO
SiO		HNCO	CH_3OCH_3
SiS		H_2S	C_2H_5OH
SO		SO_2	$CH_2=CH-CN$
NS		HNC	HCO_2CH_3
OH		C_2H	NH_2CN
	HCO^+	HNO	$CH\equiv C-C\equiv C-CN$
	N_2H^+	HCO_2H	$CH_3-C\equiv C-CN$
	HCO	CH_2NH	$H-C\equiv C-C\equiv C-C\equiv C-CN$
			C_2H_5-CN
		CH_2-CH_2 (O)	$CH_2=C=O$

The molecules have been found, in the main, in dark nebulae-massive clouds of dust and gas that occur in various places in the Milky Way Galaxy and other galaxies. The discoveries have attracted great interest, not only because they provide valuable spectroscopic "tools" that enable astronomers and astrophysicists to elucidate the physical nature and composition of these, the coldest objects in the universe, but because dark nebulae are considered to be the sites of formation of new stars and new planetary systems. The chemical evolution of dark nebulae may be a significant first step along the tortuous path of evolution of life on suitable planets.

Microwave spectroscopy has played a crucial role in the discovery of interstellar molecules because it is the rotational transitions occurring in the microwave region that have been detected by radiotelescopes trained on dark nebulae. It was in a sense fortunate that this branch of molecular spectroscopy had been extensively developed in advance of the radioastronomical studies. In nearly all cases the interstellar molecular lines are so weak that there is no chance of scanning through a wide frequency range in the hope of detecting a molecular line. The telescope is used in multichannel mode in which a very tiny frequency range, usually just encompassing a single line, is observed over a very long integration time. Long integrations are usually needed in order to achieve acceptable signal/noise ratios. For example Fig. 1 illustrates the multiplet that was first detected by us on the Parkes radiotelescope and identified with the laboratory multiplet of the $1_{10} \rightarrow 1_{11}$ transition of methanimine ($CH_2 = NH$). It required integration over four days to achieve the modest S/N ratio exhibited in Fig. 1.

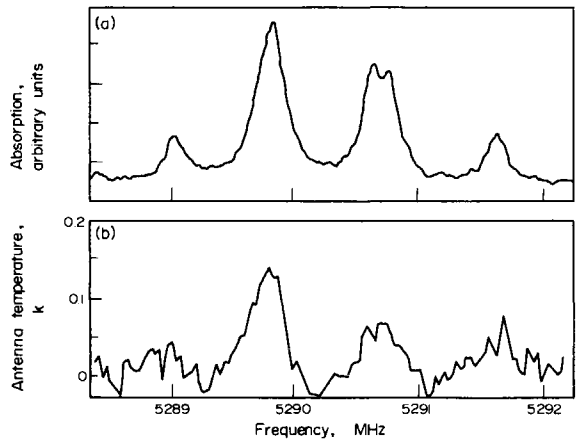

Fig. 1. The $1_{10} \leftarrow 1_{11}$ interstellar line of methanimine in Sgr. B2 (from P. D. Godfrey and R. D. Brown et. al., Astrop. Letters 13, 119-121 (1973)).
(a) laboratory spectrum
(b) telescope signal

From the spectroscopist's point of view there are several kinds of challenges associated with the study of interstellar molecules. Firstly some of the interesting molecular transitions involving the lowest rotational energy states fall at frequencies below those normally studied by microwave spectroscopists (i.e. below 8 GHz). At Monash University we have risen to the challenge by building a very large (L - band 15 cm × 71/2 cm cross-section) waveguide cell suitable for Stark modulation (Fig. 2) which, with suitable BWO sources, enables us to scan the frequency range down to 1 GHz.

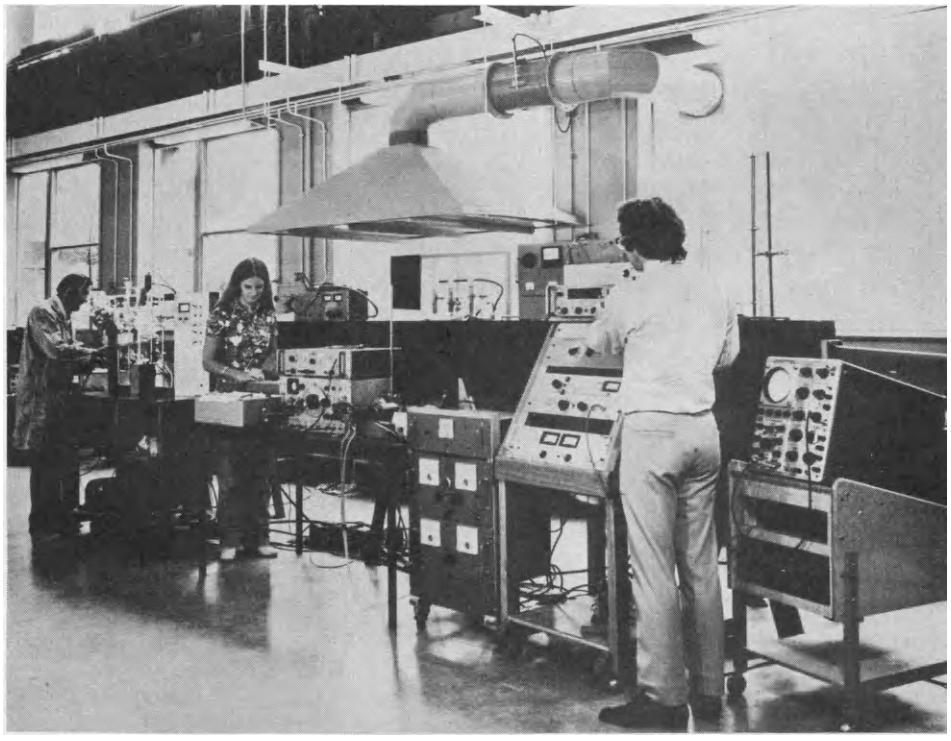

Fig. 2. Microwave spectrometer for measuring molecular absorptions in the microwave region down to frequencies of 1 GHz.

At these low frequencies the strengths of absorption lines are very low and so repetitive scanning with computer controlled sampling and processing of data is often essential if adequate signals are to be obtained.

Fig. 3 shows a block diagram of the spectrometer/computer combination and Fig. 4 shows the $1_{10} \leftarrow 1_{11}$ transition of CH_3OD at 1.3603 GHz that we recently observed before starting a search on the 140' radiotelescope at Greenbank, W. Virginia. Incidentally, the quadrupole hyperfine structure arising from the deuterium is reasonably well resolved, this being feasible with such low-frequency lines in the L-band spectrometer.

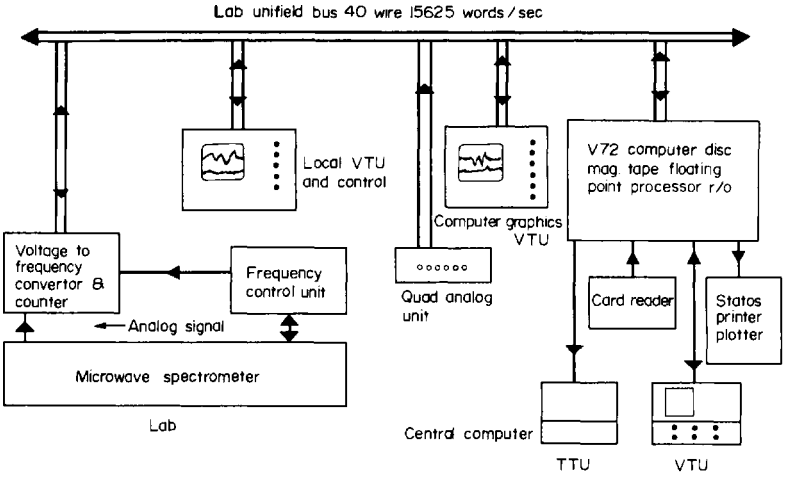

Fig. 3. Block diagram of spectrometer/computer combination used at Monash University.

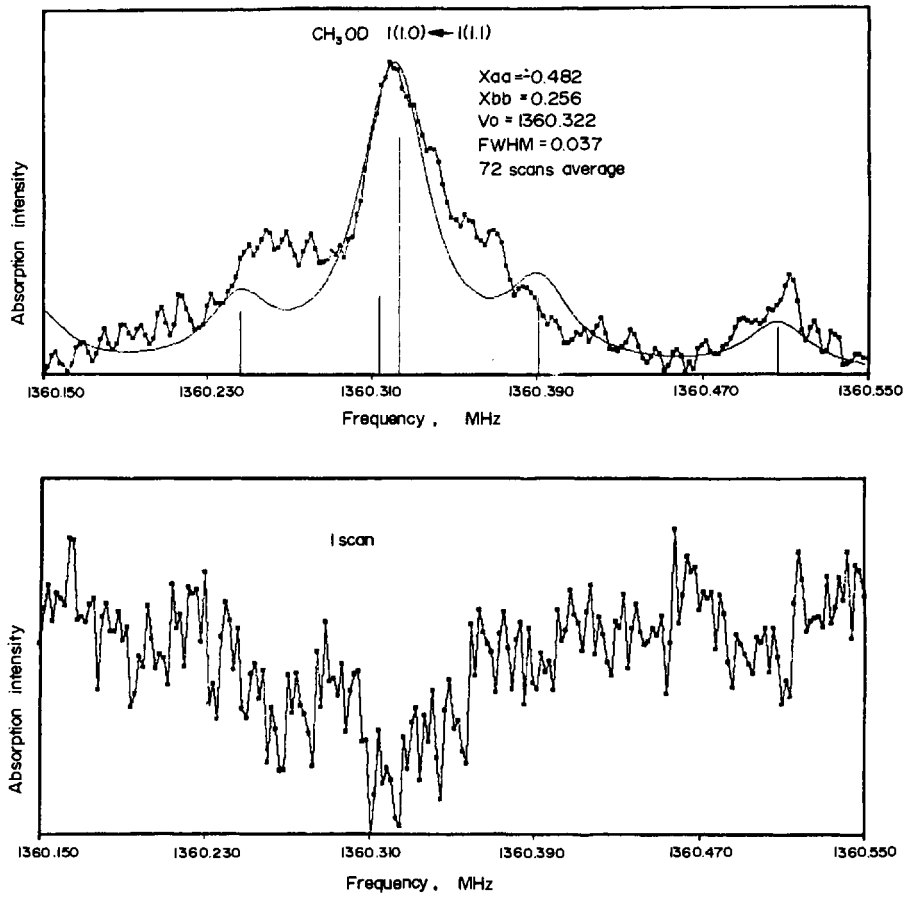

Fig. 4. Deuteromethanol line at 1.3603 GHz observed in L-band microwave spectrometer: (lower) single scan, (upper) computer averaged 72 scans and computer-filted multiplet superimposed.

A second problem is that some potentially interesting interstellar species are short-lived radicals or other highly reactive molecules that are rapidly destroyed under normal laboratory conditions. This was the case for the first molecular species detected by radioastronomy - the OH radical. Its detection depended on a pioneering study in the laboratory by C. H. Townes and co-workers using a free-space glass cell and a discharge in a side arm to produce the OH which was steadily pumped through te cell. We have used a similar cell at Monash University to study other radicals like NO_2 and NF_2 (Fig. 5).

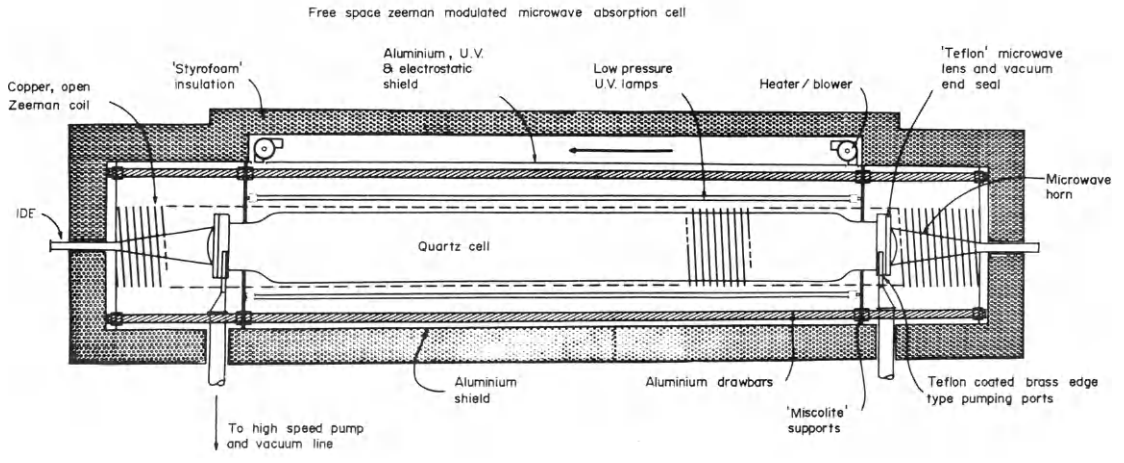

Fig. 5. Free space Zeeman-modulated quartz cell used for study of radicals.

A number of other short-lived species of astronomical interest have been studied by the expedient of generating them in the side-arm of a spectrometer cell, a microwave discharge or pyrolysis being used to disrupt a suitable precursor molecule and the species so generated being pumped through the spectrometer cell. Here in Japan Dr. Saito has been particularly successful with this technique. Table 2 summarises the species so far studied. Special mention must be made of the success of R. Claude Woods and his colleagues in observing for the first time the rotational spectra of the ions CO^+ (3) HCO^+ (4) and N_2H^+ (5). The novel technique of generating these ions in a plasma tube and detecting microwave absorptions through the plasma was used.

TABLE 2. SHORT-LIVED SPECIES

SHORT-LIVED SPECIES			
OH	Sanders, Schawlow, Dousmanis, Townes	1953	free space cell, Zeeman mod., discharge in H_2O vap.
CS	Mockler & Bird	1955	X-band cell, Stark mod., 60Hz discharge in CS_2.
SO	Powell & Lide	1964	split wave guide cell, RF discharge: O + OCS.
SiS	Hoeft	1965	high temperature cell, FeS + Si at 1050° - 1300°.
SiO	Törring	1968	high temperature cell, Si + SiO_2 at 1800°.
NS	Amano, Saito, Hirota	1969	parallel plate cell, Stark mod., RF discharge N_2 + SCl_2
HCO	Saito	1972	parallel plate cell, Stark mod., H_2CO + product of discharge on CF_4.
H_2CNH	Johnson & Lovas	1972	parallel plate, Stark mod., pyrolysis of CH_3NH_2.
HNO	Saito, Takagi	1973	parallel plate, Stark mod., H atom +NO.
HCO^+	Woods, Dixon, Saykally, Szanto	1975	plasma cell, video det., CO + H_2.
HNC	Blackman, Brown, Godfrey, Gunn	1976	parallel plate, Stark mod., pyrolysis of HCN.
	Saykally, Szanto, Anderson, Woods		plasma cell, source mod.
	Creswell, Pearson, Winnewisser, Winnewisser		free space cell, video det., active N + CH_3Br.
N_2H^+	Saykally, Dixon, Anderson, Szanto, Woods	1976	plasma cell, source mod., N_2 + H_2.

Another species first detected by the accidental discovery of its J = 1 → 0 transition among radiotelescope signals and for which we had searched for some years at Monash is HNC. We tried to produce this molecule in a variety of ways, including seeking it in equilibrium with its more stable isomer HCN. We finally succeeded by using a sufficiently high temperature, rapidly expanding HCN through a row of tiny holes in a long stainless steel tube heated to about 1000°C. The issuing gas streams passed between parallel plates of a microwave spectrometer cell. By this means we succeeded (6)(7) in observing the J = 1 ← 0 absorptions of HNC, DNC, $HN^{13}C$ and $H^{15}NC$ (Table 2). The technique that we used enabled us to determine the dipole moment of HNC as 3.05D from the Stark effect. It is symptomatic of the way in which science evolves that simultaneously and independently R. Claude Woods and colleagues (8) and Creswell et. al. in Germany (9) succeeded in detecting HNC but generated it by means of a plasma discharge through a suitable mixture of precursor gases.

The third kind of challenge that is associated with the study of interstellar molecules is that one would like to search the dark nebulae for molecules of particular biological interest, such as urea or simple aminoacids. Such compounds are normally encountered in the laboratory as involatile solids that decompose chemically on heating. However by using carefully designed heated cells it has proved possible to observe and analyse the microwave spectrum of urea (10). In this case the optimun conditions within the cell were determined by continuous direct monitoring of the cell contents with a mass spectrometer while the spectrum was being scanned (Fig. 6).

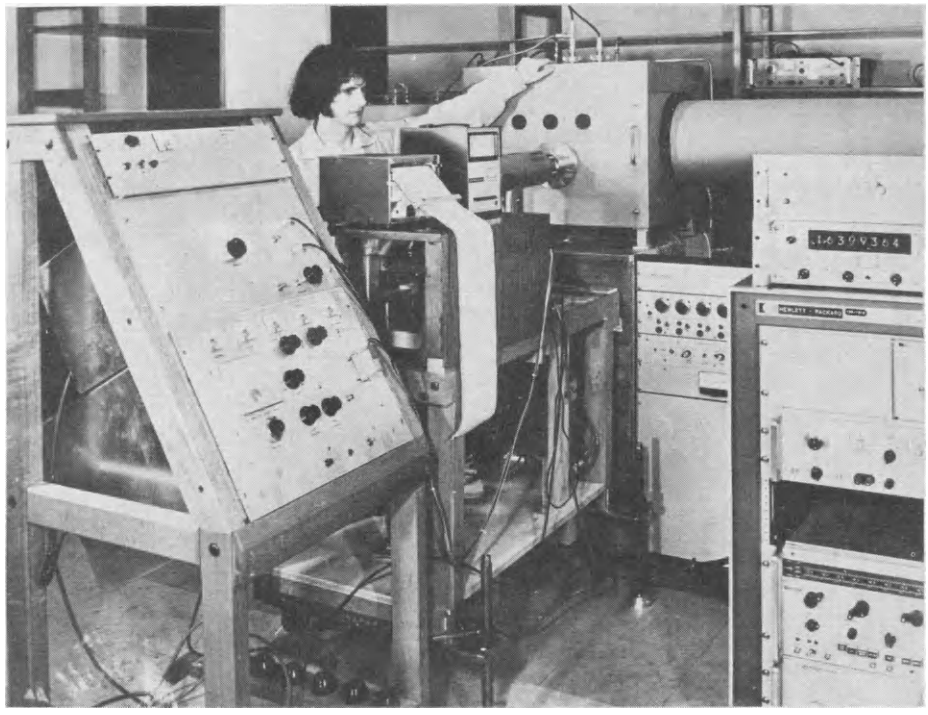

Fig. 6. Combination of heated waveguide cell and quadrupole mass spectrometer for optimising conditions for observing microwave spectra of species of low volatility.

More recently we have detected a number of lines in the microwave spectrum of glycine using a still more elaborate heated cell (Fig. 7). The lines are so weak that the analysis has taken some time and is not yet complete but it seems clear that, if sufficient time and effort are devoted to it, it will be possible to study many of the smaller biologically significant molecules by this technique.

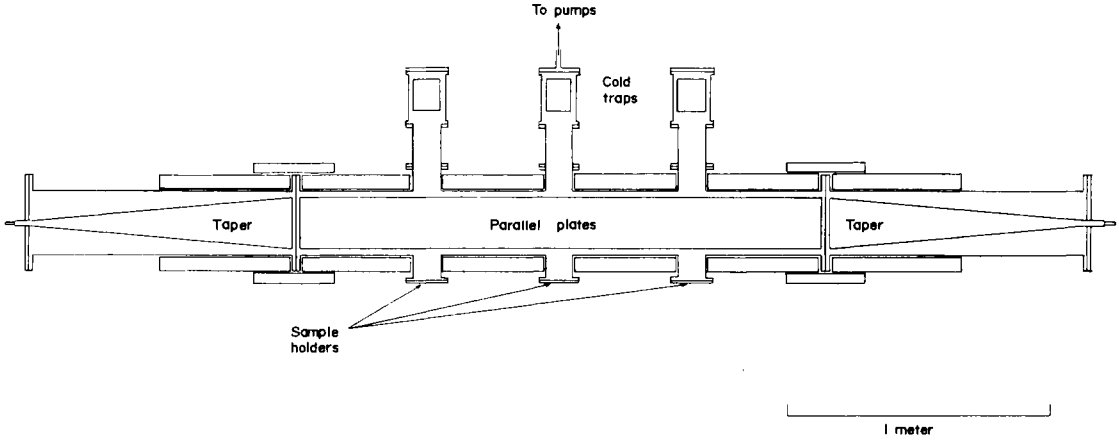

Fig. 7 (a). Heated parallel-plate cell used for studying the microwave spectrum of glycine.

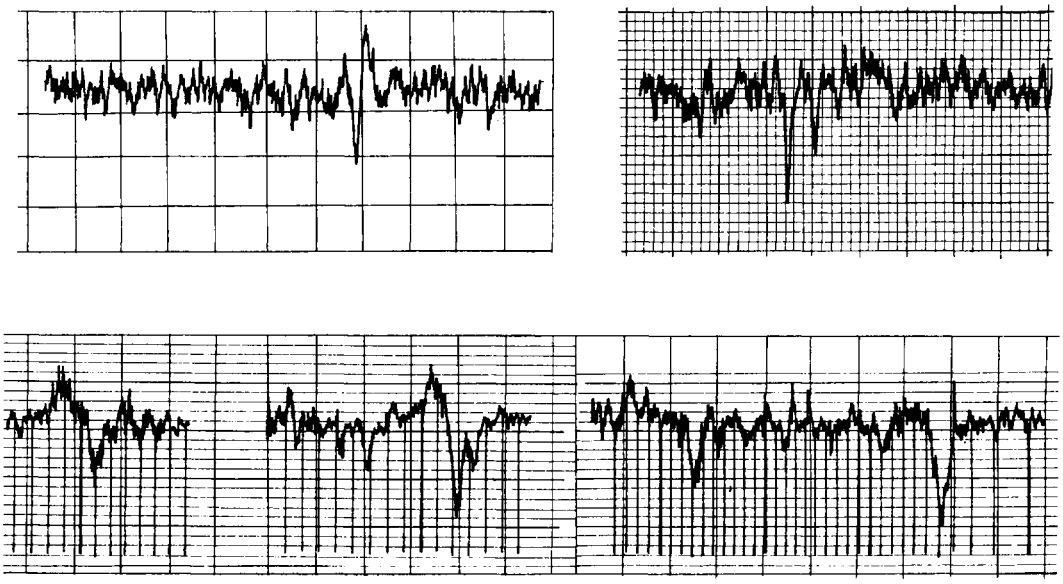

Fig. 7 (b). Some lines of glycine detected in the heated cell.

In the next few years we can expect to see a steady stream of accomplishments in microwave spectroscopy for small transient species of shorter and shorter lifetimes while the study of molecular ions, now in its infancy, will surely rapidly blossom. This will not only provide astronomers and astrophysicists with more extensive data for elucidating the chemistry and physics of dark nebulae but will of course greatly enrich our knowledge of the structural chemistry of hitherto elusive species.

REFERENCES

(1) T. Dunham and W. S. Adams, Publ. Astron. Soc. Proc. 49, 26 (1937).
P. Swings and L. Rosenfeld, Astrophys. J., 86, 483 (1937).
A. E. Douglas and G. Herzberg, Astrophys. J., 94, 381 (1941).
A. McKellar, Publ. Dominion Astrophys. Obs. Victoria B. C., No. 15, 7, 251 (1942).
(2) S. Weinreb, A. H. Barrett, M. L. Meeks and J. C. Henry, Nature, 200, 829 (1963).
(3) T. A. Dixon and R. C. Woods, Phys. Rev. Let., 34, 61 (1975).
(4) R. C. Woods, T. A. Dixon, R. J. Saykally and P. G. Syanto, Phys. Rev. Let., 35, 1269 (1975).
(5) R. J. Saykelly, T. A. Dixon, T. G. Anderson, P. G. Syanto and R. C. Woods, Ap. J. Let., 205, L101 (1976).
(6) G. L. Blackman, R. D. Brown, P. D. Godfrey and H. I. Gunn, Nature, 261, 395 (1976).
(7) R. D. Brown, P. D. Godfrey, H. I. Gunn, G. L. Blackman and J. W. V. Storey, MNRAS, 180, 87P (1977).
(8) R. J. Saykally, P. G. Syanto, T. G. Anderson and R. C. Woods, Astrophys. J., 204, L143 (1976).
(9) R. A. Creswell, E. F. Pearson, M. Winnewisser and G. Winnewisser, Z. Naturforsch, 319, 221 (1976).

LEGEND TO FIGURES.

Fig. 1. The $1_{10} \leftarrow 1_{11}$ interstellar line of methanimine in Sgr. B2 (from P. D. Godfrey and R. D. Brown et. al., Astrop. Letters 13, 119-121 (1973)).
(a) laboratory spectrum
(b) telescope signal.

Fig. 2. Microwave spectrometer for measuring molecular absorptions in the microwave region down to frequencies of 1 GHz.

Fig. 3. Block diagram of spectrometer/computer combination used at Monash University.

Fig. 4. Deuteromethanol line at 1.3603 GHz observed in L-band microwave spectrometer: (lower) single scan, (upper) computer averaged 72 scans and computer-filted multiplet superimposed.

Fig. 5. Free space Zeeman-modulated quartz cell used for study of radicals.

Fig. 6. Combination of heated waveguide cell and quadrupole mass spectrometer for optimising conditions for observing microwave spectra of species of low volatility.

Fig. 7. (a) Heated parallel-plate cell used for studying the microwave spectrum of glycine.
(b) Some lines of glycine detected in the heated cell.

Pergamon Press Ltd. 1979. Printed in Great Britain.

CHEMICAL APPLICATIONS OF IONIZING EXCITED ATOM-MOLECULE COLLISIONS

Arend Niehaus

Fakultät für Physik, Universität Freiburg/Br., 78 Freiburg, Germany

Abstract - The different types of ionizing excited atom-molecule collisions are discussed, emphasizing those aspects which are most important for the role these collisions play for the chemistry of systems in which they occur as one of the initial elementary steps. Where possible, the ionization and reaction mechanisms are explained and general rules derived which allow to qualitatively estimate the importance, and the effect, of ionization by excited species in cases where no experimental data are available.

INTRODUCTION

If some excited atom or molecule A^* carries sufficient electronic energy into a collision with some molecule M, as a result chemically highly reactive ions and radicals are created, with probabilities of the order of unity per gas kinetic collision. In general, different reaction paths can be taken by a collision system and sometimes competition between the different possibilities exists. Qualitatively this is indicated by the following scheme:

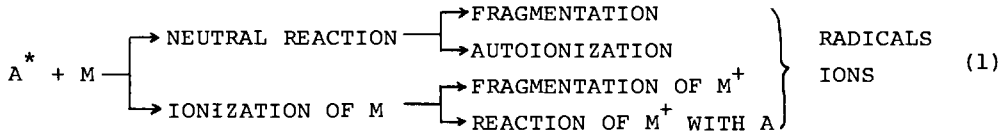

(1)

Whether collisions of the described type can become chemically important depends - since the formed ions and radicals are stable - only on the lifetime (τ) of the excited species A^* as compared to the mean time between collisions (t), i.e., the time spent by A^* for traversing the mean free path λ. For a given lifetime τ, and a given collision cross section (σ), therefore, a lower limit of the density of the considered matter may be derived, above which the collisions become important. At room temperature, and for a typical cross section for reaction (1) of $\sigma \sim 3 \times 10^{-15}$ cm^2, the corresponding lower limit of pressure, $P_{min}(\tau)$, is plotted in Fig. 1 as a function of lifetime τ. The condition $t = \tau$ was taken to derive $P_{min}(\tau)$, so that in the shaded region for a given τ the time between collisions is smaller than the lifetime τ. Lifetimes of outer shell electronically excited states range from 10^{-9} - ca. 10^2 s. One may distinguish between (i) states coupled to lower states by allowed dipole transitions with lifetimes 10^{-9} s to 10^{-6} s, (ii) metastable states with lifetimes 10^{-3} s to 10^2 s, and (iii) Rydberg states with lifetimes $\gtrsim 10^{-6}$ s. For Rydberg states with high principle quantum numbers (n), and correspondingly large geometrical sizes, the cross sections are larger than the assumed 3×10^{-15} cm^2, leading to a lower limit of pressure, $P_{min}(\tau)$, as indicated in Fig. 1 by the curved dashed line.

Excited species are formed in the three most important atomic processes, namely by electron, photon, and heavy particle impact. In addition, under certain conditions a large part of initially created ions may recombine to give excited species. Therefore, the chemical changes induced by the primary atomic processes are often dominated by reactions of type (1). As a consequence, the investigation of these processes is part of the research of many branches of Chemistry: for instance, Photochemistry, Radiochemistry, Plasma Chemistry, and the Chemistry of our atmosphere. The study of reaction mechanisms in these fields is usually very difficult, due to the great variety of possible elementary steps, however, it is clear that progress depends crucially on a

thorough understanding of the initial steps, an important one of which is reaction (1). The goal of this lecture is to present our present knowledge on this reaction for the various types of collision systems. The more general features will be emphasized rather than reporting too many details. The main questions to be

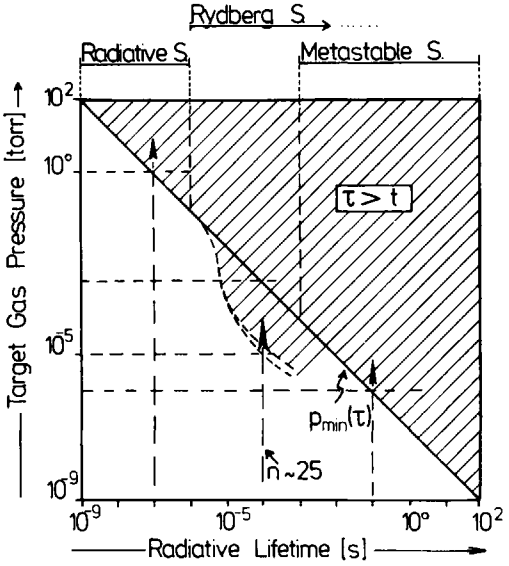

Fig. 1. Lower limit of pressure $P_{min}(\tau)$, above which reactions with excited species of lifetime τ may become important, plotted against lifetime τ. The assumed cross section is $\sigma = 3 \times 10^{-15}$ cm^2.

answered with regard to the chemical consequences are, (i) what kind of reaction occurs, (ii) how large is the cross section, and (iii), in which states are the products formed.

A. PENNING IONIZATION BY METASTABLES

Penning ionization of a molecule M in collisions with an excited species A^* can occur if the excitation energy $E_*(A)$ is greater than the lowest ionization potential of M, IP(M). By far the most detailed knowledge on this process is available for the case that A is a rare gas metastable atom. It is reviewed in a number of articles (Ref. 1-8). Schematically, Penning ionization of a molecule may be written as

$$A^* + M \longrightarrow A + M^{+**\#} + e^-(P(\varepsilon)) \qquad (2)$$

$$\longrightarrow \text{fragmentation, reaction with A}$$

At distances between A^* and M which are somewhat larger than average chemical bond distances, the molecule is ionized into certain vibronic states (* = electronic, # vibrational) in the first step, and reacts then further in the second step depending on its preparation. In the following the different aspects of this rather complex reaction will be discussed.

A.1. Cross sections

For $A^* \equiv He^*(2^1S)$, $He^*(2^3S)$, and M being small molecules, the situation was found to be especially simple. Cross sections obtained in flowing afterglow measurements for the destruction of the metastables (Ref. 9, 10, 11) are equal to total ionization cross sections obtained in beam experiments (Ref. 12), if the comparison is made at the same temperature (Ref. 11, 13). From this it follows that for these systems neutral reactions, which as shown by the general scheme (1) compete with ionization, are not occurring to a measurable extent. The reason probably is that, due to the high value of $E_*(A)$ - IP(M), the internal energy of the system A^* - M lies in a range where there are no

other states of the type A - $M^{*\#}$ which at small internuclear distances could provide potential surface crossings, necessary for excitation transfer, or neutral reactions, to occur. This is suggested by the fact that, in the case of $Ar^*(^3P_{2,0})$ - M collision systems, for which in most cases $E^*(A)$ - IP(M) is small, the neutral path in reaction (1) plays an important role (see Ref. 7). In the absence of neutral reactions the ionization cross section and its variation with collision energy is determined by two quantities the interaction potential $V^*(\underline{R})$ between A and M, and the transition probability $W(\underline{R})$ (autoionization probability) at a certain distance and relative orientation $\underline{R}$. In reality these are of course complicated functions, depending on the vector $\underline{R}$, about which we have no exact knowledge. However, for a description of the main features of the total ionization in thermal collisions, where there is no strong penetration of A^* and M, it suffices to use orientation averaged functions $V^*(R)$ and $W(R)$. The case of the Penning ionization of a molecule is in this way reduced to the case of Penning ionization of an atom. For atoms as targets and metastable atoms as projectiles it is found experimentally (Ref. 14, 15) as well as in ab initio calculations (Ref. 16) that, within the distance range accessible in thermal collisions, the transition probability decreases with distance exponentially as $W(R) = \text{const.} \exp(-\alpha R)$. This is a consequence of Penning ionization being an electron exchange process (Ref. 14) whose probability at a certain distance during the collision is approximately proportional to the square of the overlap between the target electron orbital to be ionized and that orbital of the projectile, which is unoccupied due to the excitation. Since this latter orbital is rather concentrated, one may also say that the transition probability decreases with distance approximately as the electron density of the target electron orbital to be ionized. For molecules as targets the situation is in principle the same, and therefore it is very probable that also here the ionization probability decreases approximately exponentially with distance. This is also supported by experimental evidence as will be discussed below.

The description of the total ionization cross section by $V^*(R)$, and $W(R) = \text{const.} \exp(-\alpha R)$, implies that, for all systems A^*/M belonging to the here considered type, one may distinguish three characteristic collision energy regions:

(i) the region in which the collision energy E_K is considerably larger than the well depth (D) of $V^*(R)$ the attractive forces between the particles can then be neglected and $V^*(R)$ be approximated by an exponential $V^*(R) \approx \text{const.} \exp(-\beta R)$. Under the assumption that the transition probability per collision is considerably smaller than unity one can then derive a simple approximate expression for the cross section (Ref. 7) which varies with collision energy as

$$\sigma(E_K) \quad \propto E_K^{\alpha/\beta - 1/2}. \tag{3}$$

Since the repulsion of $V^*(R)$ is mainly determined by the density of the excited electron of A, one may estimate the ratio α/β by

$$\alpha/\beta \approx [IP(M) \; / \; IP(A^*)]^{1/2} \tag{4}$$

(ii) the region in which E_K is considerably smaller than the well depth (D) of $V^*(R)$ the attractive forces determine the cross section. In this case the ionization cross section is proportional to the cross section for close collisions with turning points at the repulsive wall of $V^*(R)$. If the attractive part of $V^*(R)$ is approximated as $V^*(R) \propto R^{-s}$, again a simple approximate expression for $\sigma(E_K)$ can be derived (Ref. 5) which decreases with collision energy as

$$\sigma(E_K) \quad \propto E_K^{-2/s} \tag{5}$$

(iii) the region where E_K is approximately equal to the well depth (D) of $V^*(R)$ neither (3) nor (5) can be applied. However, since α/β, according to (3), is always greater than 0.5, the cross section increases in the range $E_K \gg D$, so that in the range $E_K \sim D$ there should arise a minimum.

The measured collision energy dependence of the total ionization cross section for ionization of several atoms and N_2 by $He(2^3S)$ and $He(2^1S)$ in the thermal energy range (Ref. 13), as well as the measured temperature dependence of the destruction rate constants of $He(2^3S)$ by several atoms and simple molecules, are in accord with the above discussion. The small molecules H_2 and N_2 have

small values of D so that in the thermal range $E_K > D$ (Ref. 17). Consequently the cross section rises with E_K as predicted by (3). The slope of this rise in a log-log plot is even quantitatively predicted by (4). This is demonstrated in Fig. 2 for the variation of cross section with collision energy of the systems $He(2^3S)/N_2$, $He(2^1S)/N_2$, and in Fig. 3 for the temperature dependence of the rate constant of the system $He(2^3S)/H_2$. The other three molecules for which the temperature dependence of the destruction rate constant by $He(2^3S)$ has been measured are, O_2, CO_2, and NH_3. Whereas for O_2 and CO_2 the temperature dependence indicates that, within the range 300 - 900 K, we have $D \sim E_K$, the rate for $He(2^3S)/NH_3$ increases in this range approximately as $\alpha T^{1/6}$, as predicted by (5) for the case s = 6, indicating that $E_K \lesssim D$, and that $V_* \alpha R^{-6}$. For other molecules with similar, or larger, polarizabilities than the one of NH_3 one would

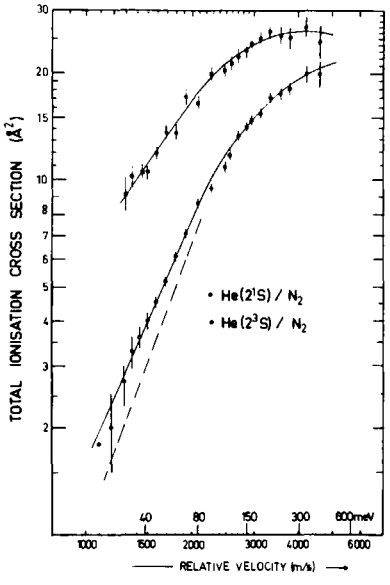

Fig. 2. Variation of total ionization cross section with relative collision velocity for the systems $He(2^3S)/N_2$, and $He(2^1S)/N_2$. Also indicated (---) the slope calculated from relations (3) and (4).

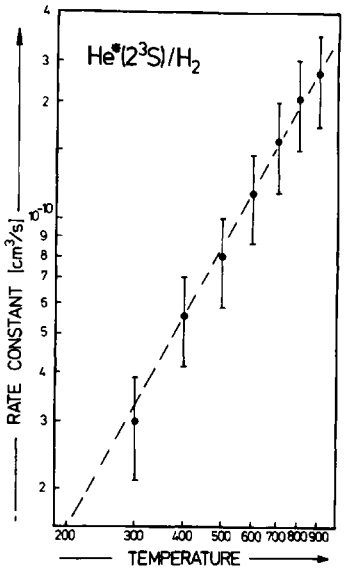

Fig. 3. Temperature dependence of the rate constant for destruction of $He(2^3S)$ by H_2. Also indicated the variation predicted by relations (3) and (4)(---).

therefore expect also a $T^{1/6}$ dependence of the ionization rate. This then allows one to obtain good estimates on ionization rate constants in a certain temperature range from extrapolation of the values obtained at room temperature for a rather large number of molecules ionized by He^* (Ref. 18).

A.2. Vibrational population of molecular ions

The Penning ionization step is an electronic change. In case of ionization by metastables a sudden electron transfer from M to A^*, and a simultaneous ejection of the excited electron from A^*. Such an electronic process is always fast compared to nuclear vibrations in the molecule. As a consequence, the $M \rightarrow M^{+**}$ transition in the Penning ionization is a "vertical" process for which the vibrational population into the different electronic states can be calculated from the molecular potential curve of the ground state V_{mg}, and the respective molecular potential curve of the ionic state V_{m+}, as the square of the overlap of the vibrational wavefunctions. In this respect, Penning ionization equals photoionization or ionization by fast electron impact. The vibrational population of molecular ions from Penning ionization can, however, still be different from the population resulting from photoionization, because of three reasons.

(i) The potential curves V_{mg} and V_{m+} may be distorted at the instant of the

ionization;

(ii) the population may, after the ionization, change due to collisions with the projectile particle in the second half of the collision;

(iii) the ionization may be an autoionization $V_{m*} \rightarrow V_{m+}$, following an excitation transfer $A^* + M \rightarrow A + M^*$, which in general will lead to a completely different vibrational population due to the different molecular potential (V_{m*}) involved.

The "initial" vibrational population can be measured by the method of "Penning electron spectroscopy" (PES) (Ref. 5, 6, 19 - 23), and the "final" population - after the completed collision - by "Penning optical spectroscopy" (POS) (Ref. 4, 8, 24). Differences between results obtained with the two methods are due to reason (ii) mentioned above. As expected, it is found that in collision systems with weak interaction between the colliding particles - where the molecular potentials are only slightly perturbed during the collision - vibrational population of the molecular ion in the different electronic states is nearly the same as in photoionization. An example is shown in Fig. 4 where the photoelectron spectrum of N_2 obtained with the 584 Å-line

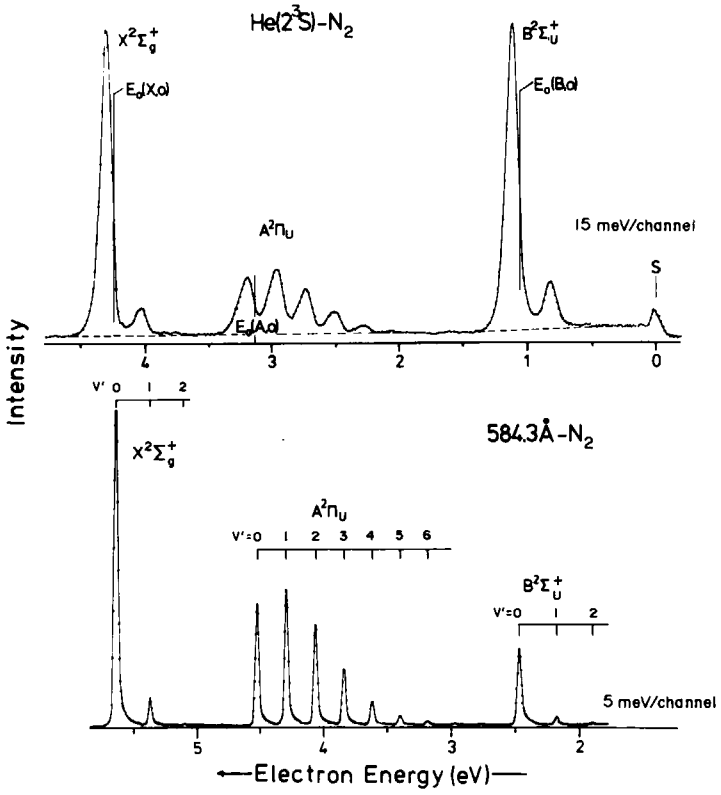

Fig. 4. Comparison of Penning electron for $He(2^3S)/N_2$ with photo electron spectrum for $h\nu$ (584 Å)/N_2.

of He is compared to the Penning electron spectrum from ionization with $He(2^3S)$ (Ref. 25). Differences between the populations measured by (POS) and (PES) - which are evidence of interactions in the second half of the collision (reason (ii) above) - have been observed for the collision systems $He(2^3S)$/HBr, HCl, O_2 (Ref. 24). The strength of the interaction between the colliding particles - before and after the ionization step - shows up in the width of the individual vibrational lines of the Penning electron spectra (Ref. 17, 21), strong interaction leading to broad lines. For the case of strong interaction, therefore, the individual lines cannot be resolved any more, and the exact vibrational populations can not be determined. This is found to be true for

most larger molecules (Ref. 22, 23), although the spectra indicate that probably the vibrational population for Penning ionization is still similar to the one for photoionization. By the method of (POS) it is not possible to decide due to which of the causes (i) - (iii) an observed deviation of the vibrational population from the one for photoionization arises. By (PES) this is possible in principle, however, up until the present only in one collision system, $Ne^*(^3p_{2,0})/O_2$, has it been reported that gives clear evidence of exitation transfer followed by autoionization (cause (iii) Ref. 26).

A.3. Population of electronic states

If the condition $E^*(A) > IP(M)$ holds not only for the lowest ionization potential but also for higher ones, then the corresponding excited ion states may be populated in the Penning process. The total ionization probability then branches into the individual ionization probabilities as $W(R) = \Sigma_i W_i(R)$. The branching ratios defined by $a_i(R) = W_i(R)/W(R)$ are reflected by the corresponding relative ionization cross sections σ_i. If the dependence of the branching ratios on the distance is not strong, we have approximately $a_i \approx \sigma_i/\sigma_{tot}$. These cross section ratios can directly be obtained from Penning electron spectra as the area below the vibrational lines belonging to a certain electronic state, devided by the total area. An example is the N_2-Penning spectrum shown in Fig. 4. It is seen that the branching ratios are different for photoionization and Penning ionization. This is a general result for Penning ionization by metastables, which has its origin in the different types of electronic processes involved. Whereas photoionization is governed by the dipole matrix element with the corresponding selection rules, Penning ionization is dominated by an exchange (monopole) matrix element which, except for spin conservation, leads to no strict selection rules. The available experimental data on branching ratios in Penning ionization are in accord with the following simple rules:

(i) Only ionic states can be populated which can be reached without violating the total spin conservation selection rules;

(ii) states which can be reached by single electron transitions are strongly preferred;

(iii) a rough relative order of the values of branching ratios into states which involve only a single electron rupture is given by the relative overlap during the collision, of the orbital to be ionized, with the unfilled orbital in the excited atom, times the number of electrons in the respective target particle orbital (Ref. 5, 14). The observed feature that Penning ionizations involving the rupture of a "lone pair" electron are relatively enhanced (Ref. 22) can be explained by this rule.

A.4. Fragmentation of a Penning ionized molecule

In the case of small molecular ions, where electronic energy is not converted in radiationless transitions to internal vibrations and rotations, the fragmentation pattern depends strongly on the electronic branching ratios of the ionizing process, and should therefore in general be different for photoionization and Penning ionization, even if the same energy is used for photons and metastables. In the case of "large" molecules - here CH_4, e.g., should already be considered large - the statistical theory of unimolecular decomposition (for references see Ref. 27) predicts that the breakdown only depends on the amount of energy put into the molecular ion in the ionization process. As a consequence differences in the fragmentation follwoing photoionization, and Penning ionization, should be due only to differences in the respective internal energy spectra, and not to different breakdown patterns. Since the Penning electron spectrum is the mirror image of the internal energy spectrum of the molecular Penning ion, it would in this way be possible to calculate the fragmentation from theoretical breakdown patterns and the measured electron spectra. No systematic studies of the Penning electron spectra of large molecules or of their fragmentation in the Penning process have been made. A list of most of the observed Penning ionization reactions, including fragmentations of large molecules, are given in (Ref. 3). In our laboratory we have found that the fragmentations of $C_4H_{10}^{+\ddagger}$ and $C_4H_6^{+\ddagger}$ (1,3-Butadiene) are rather similar when formed by 584 Å (21.22 eV) photoionization, and by Penning ionization using $He^*(2^1S)$ (20.6 eV) and $He^*(2^3S)$(19.8 eV), respectively (Ref. 28). There are however significant differences observed. Whether such differences are due to different internal energy spectra or also to different breakdown patterns can be tested by measuring electron spectra in coincidence with the fragment ion spectra for the two processes. Such studies are under way in

our laboratory.

A.5. Reactions

As indicated by (2), there may occur reactions between the Penning ionized molecule and the projectile in the "second half" of the collision. Since most experimental studies on Penning ionization have been performed with metastable rare gas atoms, which are not very reactive in their ground states, such reactions were not very important in most of the investigated systems. But, in general, this might not be true. A good example of a system where reactions occur after the ionization step is $He^*(2^3S)/H_2$ (Ref. 29). The evidence showing that the whole process may in this case be viewed as a two step process, as

$$\begin{array}{l} He(2^3S) + H_2 \longrightarrow (H_2^{+\#} + He) + e^-(P_{(\varepsilon)}) \\ \qquad\qquad\qquad\qquad\qquad\qquad \longrightarrow He + H_2^{+\#} \\ \qquad\qquad\qquad\qquad\qquad\qquad \longrightarrow HeH_2^+ \\ \qquad\qquad\qquad\qquad\qquad\qquad \longrightarrow HeH^+ + H\ , \end{array} \tag{6}$$

is given by the electron spectrum, which shows narrow vibrational lines, and a vibrational population almost identical with the one measured for photoionization (Ref. 30). As discussed in A.2., this means that, at the instant of ionization, there is only little perturbation of H_2, and therefore also no reaction which could account for the observed ions HeH^+, and HeH_2^+ (relative abundances, HeH^+: 11%; HeH_2^+: 2%). Electron-fragment-ion coincidence measurements performed in our laboratory (Ref. 31) have now shown that HeH_2^+ is only formed in those cases where the initial ionization led to population of the ($v = 0$) vibrational state of H_2^+, and HeH^+ only in cases where ($v \geq 4$). From these details, and from the measured initial vibrational populations, a rather detailed reaction scheme leading to the observed abundances can be constructed.

Reactions of the Penning ion with the deexcited projectile particle have also been observed for collision systems $H_2^{*\#}/RH_2$ (Ref. 32), with $H_2^{*\#}$ being the hydrogen molecule in a long lived excited state of energy $11.75 \leq E_*(H_2^{*\#}) \leq 12.2$ eV, and RH_2 being hydrocarbons, and NH_3, which have ionization potentials $IP(RH_2) < E_*(H_2^{*\#})$. When D_2 was used, ions with masses M + 1, M + 2, and M + 3 were observed, with M being the mass of the target molecule. From this result the occurrance of the following reactions can be concluded:

$$\begin{array}{l} D_2^{*\#} + RH_2 \longrightarrow (D_2 + RH_2^{+\#}) + e^-(P(\varepsilon)) \\ \qquad\qquad\qquad\qquad\qquad\qquad \longrightarrow RHD^+ + HD \\ \qquad\qquad\qquad\qquad\qquad\qquad \longrightarrow RH_2D^+ + D \\ \qquad\qquad\qquad\qquad\qquad\qquad \longrightarrow RH_2^+ + H_2 \\ \qquad\qquad\qquad\qquad\qquad\qquad \longrightarrow RD_2H^+ + H \end{array} \tag{7}$$

It was noted that, with increasing number of atoms in the target molecule, the relative importance of reactions of the type (7), as compared to simple ionization and fragmentation, decreased.

A.6. Competition with excitation transfer

Whereas in collision systems with He^* the Penning ionization seems in most cases to be the dominant process, this is not true any more for collision systems with Ar-metastables, which have an excitation energy of $E_*(Ar^*) \approx 11.7$ eV. In this energy region many molecules have neutral excited states - for instance Rydberg states leading to higher ionization limits - so that excitation transfer at potential surface crossings become more general. Measurements of the quenching cross sections of Ar^* by molecules with ionization potentials below and above $E_*(Ar^*)$ do not give systematically larger cross sections for systems with $IP(M) < E_*$, which are capable of Penning ionization (Ref. 33). Although it has not been shown experimentally, there is little doubt that the quenching is effected by excitation transfer followed by neutral

fragmentation. This fragmentation should be very similar to the fragmentation caused by absorption of a photon of energy E_*.

B. PENNING IONIZATION BY NON-METASTABLES

This process cannot be studied in beam type experiments, and therefore experimental information until present has been restricted to total cross sections for ionization or quenching. For projectiles A^* in states which are coupled to the ground state by dipole transition matrix elements, μ_A, a simple approximate expression for the ionization of an atom or molecule M has been derived (Ref. 34):

$$\sigma = 13.9\ (\mu_A^2 \cdot \mu_M^2/hv)^{2/5}$$

Here μ_M is the dipole matrix element for transitions $M \rightarrow M^+ + e^-$, and v the relative collision velocity. The ionization process described by (8) may be viewed as a photo-ionization by a photon of energy $E_*(A^*)$ which is, in the collision between A^* and M, transferred to M with a probability proportional to the probability for the radiative transition $A^* \rightarrow A$. The approximate validity of this resonance theory was verified for a large number of molecules for which the sensitized ionization cross sections by $Ar^*(^1P_1)$ and $Ar^*(^3P_1)$, were measured, and compared with the predictions by (8), using dipole matrix elements determined in separate absorption experiments (Ref. 35). An important prediction of the resonance mechanism is that, the chemical consequences are the same when a molecule absorbs a photon of a certain energy directly, or when it is ionized in a collision with a particle in a radiative state of excitation energy equal to the photon energy. On the other hand, for atoms in excited states which are not metastable, but also are not directly coupled to the ground state by dipole matrix elements, relation (8) yields a vanishing cross section. Therefore, for all such atoms the dominant ionization mechanism should be the exchange mechanism discussed in section (A). Indeed, cross sections measured for the quenching of $He^*(3^1S)$ and $He(3^3P)$ by Ne, Ar, Kr, and Xe are approximately equal to the cross sections for $He^*(2^3S)$ and $He(2^1S)$ (Ref. 36), while the cross sections for the resonance state $He^*(3^1P)$ are approximately twice as large (Ref. 37). The fact that the cross sections predicted by (8), although somewhat larger than the measured cross sections arising from the exchange mechanism, are not larger by an order of magnitude, suggests that there might be an effective competition between the two mechanisms in the case of radiative states. An important point to be made is that ionization cross sections due to both mechanisms should decrease with principal quantum number (n) because of the types of matrix elements involved. This has not been verified experimentally in the region of low values of (n), however, for highly excited Rydberg states it was found (Ref. 29, 32, 38) that still other mechanisms, to be discussed below, are dominant.

C. IONIZATION IN COLLISIONS WITH HIGH-N-RYDBERG ATOMS

The very loosely bound electron in a Rydberg atom A^{**} may, during a collision of A^{**} with a molecule M, gain enough energy by superelastic scattering from M to become ionized (Ref. 39), thus leading to the process

$$A^{**} + M^{\#} \rightarrow A^+ + M^{\#'} + e^- . \qquad (9)$$

In this collisional ionization process it is the small change of internal energy $\Delta E = E^{\#} - E^{\#'}$ of M, caused by the scattering process $e^- + M^{\#} \rightarrow e^- + M^{\#'}$, which leads to ionization, rather than the large electronic excitation energy E_{**}. Cross sections of reactions of type (9) for $A^{**} \equiv He^{**}, Kr^{**}$, in states with n in the range $15 \lesssim n \lesssim 50$, and M being the polar molecules H_2O, NH_3, SO_2, C_2H_5OH, were found to be very large, of the order 10^{-12} cm^2 (Ref. 38), whereas cross sections for $M = H_2, N_2, O_2, NO, CH_4$ are by orders of magnitude smaller (Ref. 6, 38). Cross section of the order of 10^{-12} cm^2 are also found for molecules having a positive electron affinity (Ref. 38, 40, 41), for the cases $M = SF_6, CCl_4, CCl_3F, CH_3I, C_7F_{14}$. Here the initial step is the transfer of an electron

$$A^{**} + M^{\#} \rightarrow A^+ + M^{-\#} . \qquad (10)$$

The negative ion may in some cases decompose (Ref. 40). For both, reactions of type (9) and (10), the cross sections increase with n but seem to "saturate" in a range $n \sim 30$ (Ref. 7, 41).

If the Rydberg atom is not ionized at large distance from the collision partner - as is the case for nonpolar small molecules with negative electron affinity - it may be ionized at smaller separation by diabatic coupling, by which the loosely bound electron can gain energy from the relative motion of the colliding particles. Such ionization processes have been observed in collisions of Ar^{**} and Kr^{**} with H_2. These ionizations at smaller distances may with considerable probability be followed by ion molecule reactions in the second half of the collision (Ref. 29).

D. TRUE ASSOCIATIVE IONIZATION

In contrast to the associative ionization process arising in the Penning process when the ejected electron carries away so much energy that the collision partners cannot separate, we deal in this section with ionization processes which can, energetically, only occur because energy is gained by formation of a bond between the collision partners, or by any other ion-molecule reaction, after ionization. Denoting by D_+ the energy which can be gained - in the simplest case of pure association D_+ is the binding energy between the deexcited projectile and the ionized molecule - the energy condition for true associative ionization to be possible is

$$E_*(A) + E_K > IP(M) - D_+ \quad . \tag{11}$$

Condition (11) can also be fulfilled if $E_*(A) = 0$, i.e. for collisions between particles in their ground states. Then it is necessary that $D_+ > IP(M)$. Many systems exist for which this condition holds, but unique identification of the reactions - which play an important role, e.g. in hydrocarbon-oxygen flames - has been difficult. Unique identification was reported for several metal-oxygen systems (Ref. 42, 43). Examples are:

$$\begin{aligned} U + O_2 &\rightarrow UO_2^+ + e^- \\ U + NO &\rightarrow UNO^+ + e^- . \end{aligned} \tag{12}$$

Preliminary results of measurements of the electron spectra from these reactions indicate that most electrons have low kinetic energy which suggests that the ions formed are vibrationally highly excited (Ref. 43). The exoergicity for reaction (12) between U and O_2 is 4.1 eV.

Systems for which condition (11) usually is met are systems of the type

$$M^* + M \rightarrow M_2^+ + e^- \tag{13}$$

where one of the particles is excited to a state not too far below the ionization limit. Special examples are the well known Hornbeck-Molnar processes (Ref. 44), where M is an atom, which have been studied in some detail (for references see Ref. 3). Cross sections are of the order of 10^{-15} cm^2. In the case of large molecules the process (13) will in most cases be followed by fragmentation of the associatively formed molecular ion. No experimental knowledge seems to be available for such homo-molecular true associative ionization processes, but it is very probable that they are possible in most cases, and probably have cross sections of the order of the corresponding homo-atomic processes. There exists, of course, always the competition of neutral fragmentation.

Little information exists on the normal type of true associative ionization for molecules. Some of the few examples are the reactions of metastable D_2^* molecules - with E* between 11.75 and 12.2 eV - and the molecules O_2, H_2O, HCl, CO_2, CO (Ref. 32). It was observed that the main reactions occurring are

$$D_2^* + M \rightarrow MD^+ + D + e^- \quad . \tag{14}$$

No details on the mechanisms of such complicated reactions are available. However, it is very probable that they proceed analogously to true associative atom-atom reactions. In a study of the collision systems A^*/H with $A^* \equiv Ar(^3P_{2,0})$, $Xe(^3P_{2,0})$, it was found - by electron spectroscopy - that the associative ionization may be viewed as a Penning ionization at small distances $R < R_c$. Where after crossing from the A^*/H-potential curve $V_*(R)$ into the continuum of the A_*/H^+-potential curve $V_+(R)$, the system ejects spontaneously an electron with a certain probability W(R), populating vibrational states of

the ion $AH^{+\#}$ with probabilities in accord with the assumption of "vertical" transitions $V_*(R) \rightarrow V_+(R)$ (Ref. 45). For molecules one would have similar conditions with only the potential curves replaced by corresponding potential hypersurfaces. Due to the larger number of paths along which such a system can "escape" from that region of coordinate space where V_* lies in the continuum, it is to be expected that conversion of the electronic excitation will, in the case of large molecules, compete effectively with ionization, enhancing reactions along neutral channels.

REFERENCES

1. A. Fontijn, Progress React.Kin. 6, 75 - 142 (1972)
2. A. Fontijn, Pure and Applied Chemistry 39, 287 - 306 (1974)
3. F.W. Lampe, Ion Molecule Reactions, Vol. 2, Ch. 13, J.L. Franklin, Ed. Plenum: New York (1972)
4. D.H. Stedman, D.W. Setser, Progress React.Kin. 6, 193 - 238 (1972)
5. A. Niehaus, Ber.Bunsenges.Phys.Chem. 77, 632 - 640 (1973)
6. H. Hotop, Radiat.Res. 59, 379 - 404 (1974)
7. A. Niehaus, Radiation Research, Biomedical, Chemical, and Physical Perspectives, p. 227, Academic Press: New York (1975)
8. D.L. King, D.W. Setser, Annual Rev.Phys.Chem. 27, 407 - 19 (1976)
9. A.L. Schmeltekopf, F.C. Fehsenfeld, J. Chem.Phys. 53, 3173 - 77 (1970)
10. R.C. Bolden, R.S. Hemsworth, M.J. Shaw, N.D. Twiddy, J.Phys.B3, 61 - 71 (1970)
11. W. Lindinger, A.L. Schmeltekopf, F.C. Fehsenfeld, J.Chem.Phys. 61, 2890 - 95 (1974)
12. J.P. Riola, J.S. Howard, R.D. Rundel, R.F. Stebbings, J.Phys. B7, 376 - 85 (1974)
13. E. Illenberger, A. Niehaus, Z.Physik B20, 33 - 41 (1975)
14. H. Hotop, A. Niehaus, Z.Physik 228, 68 - 88 (1969)
15. H. Hotop, A. Niehaus, Z.Physik 238, 452 - 465 (1970)
16. W.H. Miller, C.H. Slocomb, H.F. Schäfer III, J.Chem.Phys. 56, 1347 - 58 (1972)
17. H. Hotop, A. Niehaus, Intern.J.Mass.Spectr.Ion Phys. 5, 415 - 41 (1970)
18. A.L. Schmeltekopf, F.C. Fehsenfeld, J.Chem.Phys. 53, 3173 - 77 (1970)
19. V. Cermák, Collection Czech.Chem.Commun. 33, 2739 - 64 (1968)
20. H. Hotop, A. Niehaus, Intern.J. Mass Spectrom.Ion Phys. 5, 415 - 41 (1970)
21. A. Niehaus, The Physics of Electronic and Atomic Collisions, p. 649, B.C. Cobic, M.V. Curepa, Ed., Beograd (1973)
22. V. Cermák, A.J. Yencha, J.Electr.Spectrosc.Rel.Phenom. 8, 109 - 21 (1976); 9, 419 - 39 (1976); 11, 67 - 73 (1977)
23. D.S.C. Yee, C.E. Brion, J.Electr.Spectrosc.Rel.Phenom. 8, 377 - 88 (1976);
24. W.C. Richardson, D.W. Setser, J.Chem.Phys. 58, 1809 - 25 (1972)
25. H. Hotop, G. Hübler, J.Electr.Spectrosc.Rel.Phenom. 11, 101 - 21 (1977)
26. H. Hotop, A. Zastrow, Book of Abstracts, X ICPEAC, Paris (1977), p. 306
27. R. Stockbauer, M.G. Inghram, J.Chem.Phys. 65, 4081 - 92 (1976)
28. B. Brutschy, Diplomarbeit, Freiburg (1973)
29. H. Hotop, A. Niehaus, Z.Physik 215, 395 - 407 (1968)
30. H. Hotop, A. Niehaus, Chem.Phys.Lett. 9, 687 - 90 (1969)
31. M. Mack, A. Münzer, A. Niehaus (to be published)
32. H. Hotop, F.W. Lampe, A. Niehaus, J.Chem.Phys. 51, 593 - 97 (1968)
33. L.G. Piper, J.E. Velazeo, D.W. Setser, J.Chem.Phys. 59, 3323 - 40 (1973)
34. T. Watanabe, K. Katsuura, J.Chem.Phys. 47, 800 - 11 (1967)
35. C.E. Klots, J.Chem.Phys. 56, 124 - 31 (1971)
36. S. Kubota, C. Davis, T.A. King, J.Phys. B8, 1220 - 27 (1975)
37. S. Kubota, C. Davis, T.A. King, Phys.Rev. A II, 1200 - 04 (1975)
38. H. Hotop, A. Niehaus, J.Chem.Phys. 47, 2506 - 7 (1967)
39. M. Matsuzawa, J.Chem.Phys. 55, 2685 - 89 (1971)
40. F.B. Dunning, G.F. Hildebrand, F.G. Kellert, G.W. Foltz, K.A. Smith, R.F. Stebbings, Book of Abstracts, X ICPEAC, Paris (1977), p. 172
41. W.P. West, G.W. Foltz, F.B. Dunning, C.J. Latimer, R.F. Stebbings, Phys.Rev.Lett. 15, 854 - 58 (1976)
42. W.L. Fite, P. Irving, J.Chem.Phys. 56, 4227 - 28 (1972)
43. P. Vasu, H.H. Lo, W.L. Fite, Book of Abstracts, X ICPEAC, Paris (1977), p. 1160
44. J.A. Hornbeck, J.P. Molnar, Phys.Rev. 84, 621 - 25 (1951)
45. A. Niehaus, Physics of Ionized Gases, p. 143, B. Navinsek, Ed. J. Stefan Institute: Ljubljana (1976)

Pure & Appl. Chem., Vol. 50, pp. 1239-1250. 0033-4545/78/1201-1239 $02.00/0
Pergamon Press Ltd. 1978. Printed in Great Britain.

MICROWAVE SPECTROSCOPY OF SHORT-LIVED MOLECULES

Shuji Saito

Institute for Molecular Science, Okazaki 444, and
Sagami Chemical Research Centre, Sagamihara 229, Japan

Abstract - Microwave spectroscopy is discussed from a viewpoint of detecting short-lived molecules, especially free radicals. Greater stress is laid on sensitivity of spectrometer, production of molecules and prediction of their transitional frequencies. Some typical examples of the observed short-lived molecules are given in detail with their significance in the related fields such as chemical kinetics, photochemistry and radioastronomy.

INTRODUCTION

Short-lived molecules are produced as intermediates in chemical reactions. They are in some cases the keystones determining how the chemical reactions proceed and how they are affected by physical and chemical factors. A confirmation of the existence of the intermediates in a real process is especially desirable for a deeper understanding of the chemical reaction. The intermediate having one or more unpaired electrons, that is, the free radical, is important in the field of the molecular structural study. The unpaired electron has electromagnetic interactions with the electrons and nuclei of the molecule and acts as a probe revealing the detailed molecular structure which is not obtained in the study of non-paramagnetic molecules. The free radical presents the most interesting and exciting problems to modern high resolution spectroscopy.
The first example of the free radical was prepared accidentally by Gomberg (1) in 1900. It was a stable but complicated molecule, triphenyl methyl radical. However, most of simple and fundamental free radicals are very active and have short lifetimes. The production, trapping and detection of the short-lived molecules have been extremely difficult problems (Ref. 2). A great variety of chemical and physical methods has been used to overcome these difficulties. Among them the flash-photolysis combined with high-resolution ultraviolet and visible spectroscopy has been one of the methods achieving the most fruitful results pertinent to molecular structures and chemical kinetics. This method has made clear the existence of many diatomic and polyatomic short-lived molecules and has given information about their molecular constants (Ref. 3-5).
The results accumulated by optical spectroscopy have made possible more detailed studies of short-lived molecules by means of recently developed spectroscopic techniques such as molecular beam method, EPR, microwave spectroscopy and LMR. Microwave spectroscopy is one of the most productive methods of observing free radicals. Microwave spectroscopy of free radicals is not straight-forward, but it gives accurate and unique information about the molecules.

THE ESSENTIAL FEATURES OF MICROWAVE SPECTROSCOPY FOR SHORT-LIVED MOLECULES

Generally, the concentrations of short-lived molecules are so low in the absorption cell that it is a rather hard task to detect them. The essential points in microwave spectroscopy of free radicals are sensitivity of the spectrometer, production of molecules and prediction of their transition frequencies.

Sensitivity of the Spectrometer

A high sensitivity is indispensable for detection of short-lived molecules of low concentration. The sensitivity was improved by stabilization of

microwave sources as well as careful selection of detector crystals (Ref. 6). Fig. 1 shows a recorder tracing of the J = 1 ← 0 transition at 11.12 GHz of the $^{18}O^{12}C^{34}S$ molecules in natural abundance. The concentration of this species is about 0.009 %.

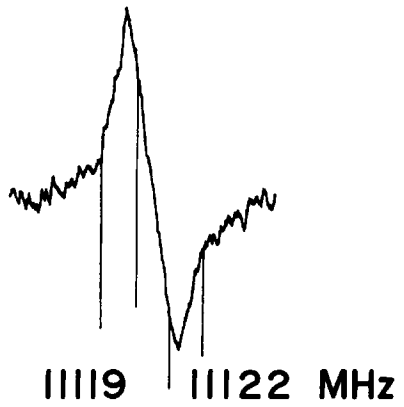

Fig. 1. A recorder tracing of the J = 1 ← 0 transition at 11.12 GHz of the $^{18}O^{12}C^{34}S$ molecules in natural abundance. Experimental conditions: room temperature, 0.07 torr pressure, 1N23G detector, 430 V/cm Stark modulation, 16 sec time constant.

The absorption cell used was made of an X-band waveguide of 3 m in length. The signal to noise ratio of the spectral line is about 25 and its maximum absorption coefficient is $5X10^{-10}$ cm^{-1}. The sensitivity of our spectrometer, given by the minimum detectable absorption coefficient, $(\gamma_{max})_{min}$, is about $2X10^{-11}$ cm^{-1} at the X band. This means that the minimum detectable total number of molecules, N_t, is about $5X10^{12}$. When the parallel plate type absorption cell designed for observations of short-lived molecules, as is given later (Fig. 2), is used at 60 GHz, $(\gamma_{max})_{min}$ is $8X10^{-10}$ cm^{-1} and N_t $8X10^{12}$. At 120 GHz, $(\gamma_{max})_{min}$ is $3X10^{-9}$ cm^{-1} and N_t $8X10^{12}$. As the peak intensity of a line is proportional to the square of the transition frequency, it becomes stronger in higher frequency. However, the efficiency of microwave detectors decreases in millimeter wave region so that the minimum detectable total number of molecules is not reduced remarkably.
If we want to observe the spectrum of a short-lived molecule, we should produce at least 10^{13} molecules in the absorption cell.

Production of short-lived molecules

For production of such a large amount of molecules in the cell, we should use the best chemical reaction suitable for the molecule to be studied. The best method of production differs widely for each molecule. It depends on the lifetime of the molecule.
In the production of molecules of rather long lifetime, 100 msec or more, the parent molecule was discharged or pyrolyzed at about 20 cm upstream of the absorption cell (Fig. 2) and the reaction products were pumped through the cell.
When the lifetime of the molecule becomes shorter, the molecule cannot survive through the full length of the cell or cannot reach to the cell. The molecule of shorter lifetime has to be generated just inside the parallel plates. The parent gas was discharged in the reaction tube. The second reacting gas was mixed with the discharged products through the shower nozzle just between the edges of the parallel plates (Fig. 2). It is important to use a large linear velocity of gas flow. The gas mixture was pumped out from the absorption cell with the linear velocity of 10 m/sec.

This means that a molecule having the lifetime of 10 msec can survive a path of 10 cm. The molecule of a lifetime as short as 10 msec can be observed by the use of our spectrometer described below.

Prediction of the transitions

When a short-lived molecule has no unpaired electrons, its rotational levels are the same as those of the stable molecule (Ref. 7). The problem is how a resonable geometrical structure can be estimated for the molecule.

The rotational levels of the free radical having unpaired electrons vary greatly with its electronic state. The rotational levels split and shift in a complicated way according to the electromagnetic interactions among the angular momenta due to the electron orbital motion, electron spin, rotation and nuclear spin.

If we want to try to detect a new free radical, it is important to look over its predicted spectrum and pick up the transitions most suitable for spectroscopy. The intensity of each transition, the sensitivity of the spectrometer, the optimum voltages of Stark modulation and dc bias, and reliability of predicted transition frequencies have to be considered.

For example, the spectra of the molecule in the $^2\Pi_{3/2}$ or $^1\Delta$ electronic state show the first-order Stark effect because of its Λ-type degeneracy. Small Stark modulations do not give serious leakage of modulation power to the amplifier. Small dc biases do not bring about an electric breakdown between the parallel electrodes so that the sensitivity of the spectrometer can be maintained at higher levels. The NCO($^2\Pi_i$) (Ref. 8), SO($^1\Delta$) (Ref. 9) and IO($^2\Pi_{3/2}$) (Ref. 10) radicals were observed under these conditions. When the molecule in the $^3\Sigma$ state has a large spin-spin interaction, its spectrum deviates greatly from the well-known rotational spectral pattern. The linear molecule in the $^2\Sigma$ state or the nonlinear molecule in the doublet state having a large spin-rotation interaction shows a similar deviated spectrum. The rotational levels of the light molecules in the $^2\Pi_{1/2}$ state generally split into large Λ-type doublets. It is rather difficult to predict these spectra precisely.

Information from other spectroscopic methods is indispensable for a good prediction of the transition frequencies of short-lived molecules. In some cases, the rotational constants have been determined by studies of high-resolution optical spectroscopy (Ref. 3-5). However, the parameters of fine and hyperfine structures have been rarely reported by these methods. Gas-phase EPR spectroscopy which also sees the rotational levels of paramagnetic molecules has succeeeded in detecting many diatomic and triatomic free radicals. (Ref. 11.). It uses the high-Q cavity resonator of small volume which is advantageous to detection of short-lived free radicals. Furthermore, the magnetic fields to be searched for are predictable on the basis of the quantum state of the molecule. Recently developed laser magnetic resonance (LMR) is bringing about the more reliable molecular constants of short-lived free radicals because it is extremely sensitive and its accuracy is high.

MICROWAVE SPECTROMETER FOR SHORT-LIVED MOLECULES

The microwave spectrometer used was a conventional 100 kHz Stark modulated system of high sensitivity (Ref. 6) with some modifications required for spectroscopy of short-lived molecules. The schematic diagram of a typical absorption cell is shown in Fig. 2.

It was made of a pair of gold plated parallel plates 40 cm long. Microwave discharge was made in the quartz tube by a modified Evenson-Broida 2450 MHz cavity (Ref. 12.). The microwave power dissipated in the cavity was within 100 W. The gas mixture was pumped out from the cell by a mechanical booster pump with a pumping speed of 3300 l/ min followed by two liquid nitrogen traps and by a rotary pump of 600 l/ min.

Microwave power sources up to 138 GHz were mainly the OKI klystrons. In the frequency region above 130 GHz, a harmonic generator, T5707, was employed as the power source. The output frequency of the klystrons was determined with accuracy of about 10^{-6} - 10^{-7} by monitoring a beat of their output with the X-band output of a Hewlett-Packard K10-8400B phase-locked microwave sweep oscillator. The beat was generated by a mixer equipped with an 1N78 and was

detected with an all-wave receiver.
The detector crystals used were carefully selected as described above. Above 80 GHz, a GaAs Schottky barrier diode mixer, W3420A, was used. The microwave spectrometer using these power sources and detectors combined with the parallel-plate absorption cell is satisfactorily usable up to 170 GHz (Ref. 13)

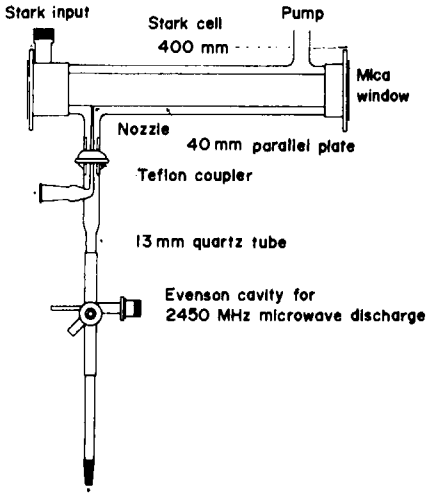

Fig. 2. The schematic diagram of the absorption cell and the microwave-discharge quartz tube.

MICROWAVE SPECTRUM OF SHORT-LIVED MOLECULES

We observed the microwave spectra of several free radicals and unstable molecules by using the method and principle discussed above. The results obtained are typical examples of the rotational spectra of the molecules in the various electronic states. Some results have considerable significance in related fields such as chemical kinetics, photochemistry and radioastronomy. The main features of each molecule observed are as follows:

- $IO(^2\Pi_{3/2})$. The last homologue of the halogen monoxide radical. Short lifetime (~10 msec). Large hyperfine interactions.
- $SO(^1\Delta)$. The first example of the electronically excited molecule studied by microwave spectroscopy. Significant to chemical reactions analogous to those of $O_2(X^3\Sigma_g^-)$ and $O_2(^1\Delta_g)$.
- $NCO(^2\Pi_1)$. The first example of the linear triatomic radical having Renner effect. One of the rare cases where all the hyperfine coupling constants were determined with high accuracy.
- $HCO(^2A')$. $1_{01} \leftarrow 0_{00}$ was observed. Identified as an interstellar molecule. Signigicant to the kinetics in hydrocarbon flame.
- $HO_2(^2A'')$. Most of the transitions up to 140 GHz were observed. The off-diagonal component of the spin-rotation interaction tensor was obtained. Highly important to many fundamental chemical reactions.
- $HNO(^1A')$. The spin multiplicity of the ground electronic state was derived from the microwave spectrum.
- CH_2=CHOH. The stable existence of vinyl monomer was confirmed for the first time by means of microwave spectroscopy. Long lifetime.

The detailed results for some of these molecules will be discussed below.

$SO(^1\Delta)$ (Ref. 9)

It is well known that the oxygen molecule in the first electronically excited state, the so-called singlet oxygen, can be easily produced in a large amount by microwave or rf discharge of gaseous oxygen (Ref. 14), and has a long lifetime. The $^1\Delta_g$ state of oxygen is metastable at 7918 cm^{-1} above the $^3\Sigma_g^-$ ground state (Ref. 15). This is because the transition between the $^1\Delta_g$ state and the $^3\Sigma_g^-$ ground state is triply forbidden. The SO radical,

analogous to the molecular oxygen, has a low-lying metastable excited state, $^1\Delta$, located at about 6350 cm^{-1} above the $^3\Sigma^-$ ground state (Ref. 16). Since the population of the molecules in the electronically excited states is nearly zero due to the Boltzmann distribution law, the molecule in the excited state could be hardly observed by conventional microwave spectroscopy. Carrington, Levy, and Miller (Ref. 17) observed the EPR stectrum of the $^1\Delta$ SO and obtained the molecular constants of the $^1\Delta$ SO (Ref. 18).
We have observed the lowest rotational transition of the SO radical in the $^1\Delta$ state. This is the first observation of the rotational transition for a molecule in an electronically excited state. The SO radical in the $^1\Delta$ state was produced by mixing OCS with the product of microwave discharge in molecular oxygen(Ref. 19). A line observed at 127770.47 ± 0.15 MHz showed a paramagnetic behavior, indicated the first-order Stark effect which is a characteristic of the Λ degeneracy and was resolved into four well-separated components at higher Stark dc bias, as shown in Fig. 3.

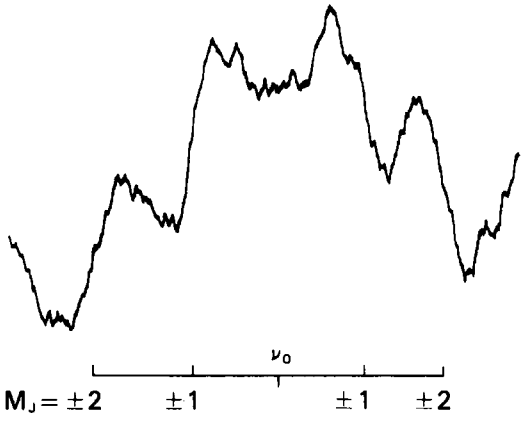

Fig. 3. The J = 3 ← 2 transition of the SO radical in the $^1\Delta$ electronic state: Stark dc bias = 55.3 V/cm; Stark ac modulation = 2.3 V/cm, ν_o = 127770.47 MHz.

This is just expected from the J = 3 ← 2 transition of the $^1\Delta$ molecule composed of the nuclei of zero spins. The rotational constants, the SO bond length and the dipole moment determined are listed in Table 1 where the molecular constants of the SO molecule in the ground state are given for comparison. It should be noted that the SO distance of the $^1\Delta$ state is slightly longer than that of the $^3\Sigma^-$ state whereas the situation is reverse for the dipole moments of both states. These features present interesting information for molecular orbital calculation.
Now that both the spectra of the triplet and singlet SO are known, it would be interesting (Ref. 20-23) to discuss the chemical reactions of the SO radical from the viewpoint of spin multiplicity of the reactants as has been done for many important reactions of O_2.

The lifetime of the free radical becomes shorter as the number of the atoms constituting it increases. This hampers observations of polyatomic free radicals by microwave spectroscopy. Only a few polyatomic free radicals have been studied so far. We observed three of such radicals. One is a linear triatomic radical, NCO(Ref. 8). The others are bent unsymmetrical triatomic molecules, HCO(Ref. 24) and HO_2(Ref. 13).

HCO(^{2}A') (Ref. 24)
HCO is one of the most fundamental molecules to molecular spectroscopy, chemical kinetics and radioastronomy. It has been frequently postulated and is known as an important intermediate in many chemical reactions such as

hydrocarbon flame (Ref. 25). HCO has been expected to exist in appreciable amount in interstellar space because hydrogen, oxygen and carbon have relatively high cosmic abundances.

Table 1. Molecular Constants of the SO molecule

Constant	$X^3\Sigma^-$	$a^1\Delta$
T_e (cm^{-1})	0	~6350[a]
ω_e (cm^{-1})	1148.19[b]	
B (MHz)	21609.5$_5$±0.15[c]	21295.1±0.7[d]
r (A)	1.48108±0.00005[c]	1.49198±0.00002[d]
μ (D)	1.55±0.02[e]	1.336±0.045[d]

a. Ref. 21. b.R. G. Norrish and C. A. Oldershaw, Proc. Roy. Soc. Lond. A, 249, 498 (1959). c. B_e and r_e: T. Amano, E. Hirota, and Y. Morino, J. Phys. Soc. Japan, 22, 399 (1967). d. This work. e. F. X. Powell and D. R. Lide, Jr., J. Chem. Phys. 41, 1413 (1964).

Its related molecules, H_2CO and CO, were found to be widely distributed in interstellar space (Ref. 26). Jefferts et al. (Ref. 27) searched for the $1_{01} \leftarrow 0_{00}$ transition of the interstellar formyl radical on the basis of the rotational constants determined from optical absorption spectra (Ref. 28), but they could not detect it in molecular clouds showing strong lines of H_2CO and CO. Some low-J K-type doubling transitions of HCO were first observed in laboratory by Carrington and his group (Ref. 29-31) using EPR spectroscopy and then by Austin et al. (Ref. 32). The formyl radical was produced by a reaction of H_2CO with the product of a microwave discharge in CF_4. The strongest component of the $1_{01} \leftarrow 0_{00}$ transition of HCO is shown in Fig. 4.

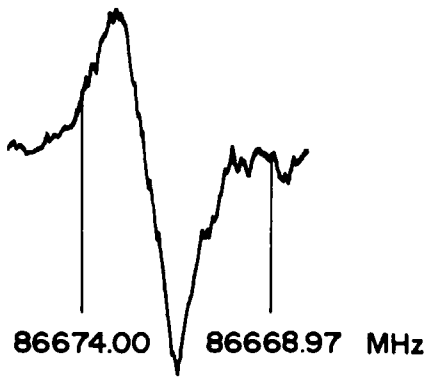

Fig. 4. The F= 2 ← 1 component of the J = 3/2 ← 1/2, $1_{01} \leftarrow 0_{00}$ transition of the HCO radical.

The deuterated species DCO was produced by the reaction of D_2CO.

As the formyl radical has an odd number of electrons and resultant electronic spin, each rotational level is split in two by the interaction of the electron spin with molecular rotation. Each split level is further split by the interaction of the electron spin with the nuclear spin of the hydrogen or

deuterium, such as Fermi interaction and magnetic dipole-dipole interaction. As a result, there may be six hyperfine components for the $1_{01} \leftarrow 0_{00}$ transition of HCO and nine for that of DCO corresponding to $\Delta J = 0, \pm 1$, and $\Delta F = 0, \pm 1$ selection rules. We observed four components for HCO and seven for DCO. The observed spectra were analyzed with consideration for spin-rotation, Fermi and dipole-dipole interactions (Ref. 33). The molecular constants obtained are shown in Table 2,

Table 2. The Molecular Constants of HCO and DCO (MHz)

Constants	HCO	DCO
$B_o + C_o$	86718.07 ± 0.10	73533.9 ± 0.2
	(86796)[a]	(73521)[a]
$\epsilon_{bb} + \epsilon_{cc}$	-187.3 ± 0.40	-168.4 ± 0.4
a_F	393 ± 8	58.7 ± 0.2
	(±303.9)[b]	(±58.0)[b]
$T_{bb} + T_{cc}$	-11.8 ± 0.5	-1.4 ± 0.4

a. Ref. 28. b. F. J. Adrian, E. L. Cochran, and V. A. Bowers, J. Chem. Phys. 36, 1661 (1962).

where ϵ, a_F and T are the coupling constants of spin-rotation, Fermi contact and magnetic dipole-dipole interactions, respectively.
It is noted that there is a discrepancy of about 78 MHz between the $B_o + C_o$ values of HCO obtained by this study (Ref. 24) and by optical spectroscopy (Ref. 28). On the basis of the observed frequencies for the component shown in Fig. 4, Snyder et al. (Ref. 34) detected the interstellar HCO in some particular moderate-density molecular clouds containing ionized carbon.

$HO_2(^2A'')$ (Ref. 12)

The hydroperoxyl radical HO_2 is also fundamental to chemical kinetics. It is an often quoted intermediate in reactions containing oxygen and hydrogen atoms (Ref. 35) or in hydrocarbon oxidation (Ref. 25). Recently it turns out that HO_2 takes part in main photochemical reactions in the upper atmosphere. However, because of its short lifetime, accurate spectroscopic studies of this radical have become possible only very recently. Radford et al. (Ref.36) succeeded in detecting the LMR spectra of several rotational transitions of HO_2 in the far infrared region. Based on the molecular constants determined by LMR (Ref. 37), Beers and Howard observed all of the fine and hyperfine structures of the $1_{01} \leftarrow 0_{00}$ transition for HO_2 (Ref. 38) and DO_2 (Ref. 39) by using a Zeeman modulated cavity microwave spectrometer.
The HO_2 radicals were produced by a reaction of allyl alcohol with the product of a microwave discharge in the oxygen. All the a-type $N = 2 \leftarrow 1$ transitions and four b-type transitions were observed with rather good signal-to-noise ratios. The observed spectra were analyzed on the basis of the following Hamiltonian:

$$\mathcal{H} = \mathcal{H}_r + \mathcal{H}_{sr} + \mathcal{H}_{hfs} \quad (1)$$

where $\mathcal{H}_r$ is the ordinary rotational Hamiltonian, $\mathcal{H}_{sr}$ the electron spin-rotation interaction, and $\mathcal{H}_{hfs}$ the magnetic hyperfine interaction. The effective expressions for $\mathcal{H}_{sr}$ and $\mathcal{H}_{hfs}$ are as follows:

$$\mathcal{H}_{sr} = \epsilon_{aa}N_aS_a + \epsilon_{bb}N_bS_b + \epsilon_{cc}N_cS_c + (\epsilon_{ab} + \epsilon_{ba})(N_aS_b + S_aN_b)/2 \quad (2)$$

$$\mathcal{H}_{hfs} = a_F \mathbf{S}\cdot\mathbf{I} + \mathbf{S}\cdot\mathbf{T}\cdot\mathbf{I}. \quad (3)$$

The matrix elements of $\mathcal{H}_{sr}$ and $\mathcal{H}_{hfs}$ were discussed in detail by Curl and Kinsey (Ref. 33), by Raynes (Ref. 40), and more recently Bowater et al. (Ref. 30).
In the analysis of the observed spectra the off-diagonal component of the spin-rotation coupling tensor, $\epsilon_{ab} + \epsilon_{ba}$, was included though its contributions to transition frequencies are small. This was carried out by

taking into account the second-order perturbation terms of $\epsilon_{ab} + \epsilon_{ba}$ in the analysis of the spin doublings. Since the energy differences between the rotational levels of N_{ON} and $(N-1)_{1,(N-2)}$ are minimum and change their sings around N = 9 and 10 as shown in Fig.5, the second-order contributions to the $9_{09} \leftarrow 8_{18}$, J = 17/2 ← 15/2 and $10_{0,10} \leftarrow 9_{19}$, J = 19/2 ← 17/2 transitions are especially large and opposite in signs.

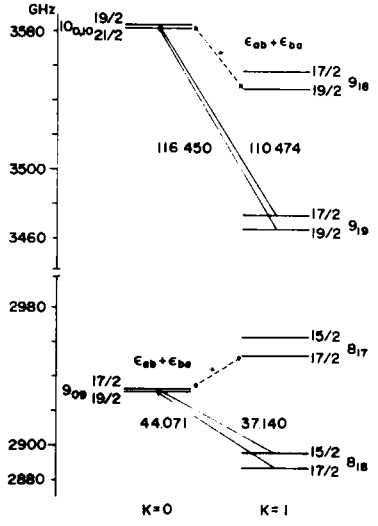

Fig. 5. The energy levels of HO_2, concerned with the remarkable second-order perturbation of $\epsilon_{ab} + \epsilon_{ba}$. Observed transitions are shown by solid arrows and their frequencies are given in GHz.

In fact, if the second-order terms are not included in the analysis of the spin doublings, the spin doublings calculated for the $9_{09} \leftarrow 8_{18}$ and $10_{0,10} \leftarrow 9_{19}$ transitions deviate from the observed values by -19 and 13 MHz, respectively. However, when the second-order terms are taken into account in the analysis, the agreement between the observed and calculated values of the spin doublings is satisfactory. The molecular constants obtained are listed in Table 3 where those determined from the LMR spectra are also given for comparison. The agreement is good.

All the hyperfine constants of HO_2 were obtained for the first time. The magnitude of the Fermi contact parameter is small, -28 MHz. This leads to the conclusion that the unpaired electron of the HO_2 radical occupies a π-type orbital. Adrian, Cochran, and Bowers (41) observed the ESR spectrum of HO_2 in argon matrix and concluded that the isotropic hyperfine constant, , a_F, is -10.2 Oe (-28.6 MHz) and the out-of-plane component of the anisotropic part of the hyperfine tensor, T_{cc}, is -4.4 Oe (-12.3 MHz). These are in good agreement with the corresponding values obtained in this study. Also all the principal components of the tensor were determined separately in this study. This result will be useful for the detailed studies of the Zeeman effect of HO_2 because the principal components of the spin g tensor can be calculated from the principal components of the ϵ tensor through Curl's relation(Ref. 42). The observed transitional frequencies as well as the molecular constants given above have now been used for the study of HO_2 in other related fields. Astronomical searches for the b-type transitions were made in some molecular clouds with the 6 m telescope at the Tokyo Astronimical Observatory (Ref. 43). Radford of Harvard College Observatory (Ref. 44) also made searches for the N = 2 ← 1 transitions at 130 GHz in likely astronomical sources. Both the results were negative. HO_2 is of paticular interest to stratospheric chemistry and its atmospheric searches are now in progress (Ref. 45 & 46).

The molecules so far given are paramagnetic. There have been known many non-paramagnetic molecules of short lifetime, which play an important role in the

fundamental chemical reactions. Some of them may be considered as free radicals after the definition by Herzberg (Ref. 5). We have studied two of such unstable molecules, HNO (Ref. 47-49) and CH_2=CHOH (Ref. 50).

Table 3. Molecular Constants of HO_2 (MHz)[a]

Constants	Mw[b]	LMR[c]
A	610257±35	610318±225
B	33511.95±0.60	33514±38
C	31673.46±0.60	31679±38
D_N	0.112±0.068	0.126±0.060
D_{NK}	3.47±0.48	3.6±0.75
D_K	123[e]	123±23
ϵ_{aa}	-49546.1±5.8[f]	-49292±650
ϵ_{bb}	-431.9±3.3	-486±200
ϵ_{cc}	17.6±3.3	54±200
$\lvert\epsilon_{ab}+\epsilon_{ba}\rvert/2$	189±30	
a_F	-27.6±1.4	
T_{aa}	-8.1±1.1	
T_{bb}	19.5±1.1	
T_{cc}	-11.4±1.1	

a. The error quoted for each molecular constant is 2.5 times the standard deviation. b. This work. c. Ref. 36. d. An effective ϵ_{bb}(b) obtained from the b-type transitions is -417.9±1.5 MHz. e. Assumed. d. The value for the K=1 levels.

HNO(^{1}A') (Ref. 47-49)

HNO is isoelectronic with molecular oxygen so that the linear HNO should have an electronic structure similar to O_2. However, as the HNO angle becomes smaller, the $^1\Delta$ state splits into two states, ^{1}A' and ^{1}A", and the ^{1}A' state goes down energetically according to Walsh diagram (Ref. 51). Hence, there had been some discussions (Ref. 4.) on the ground electronic state of HNO: which is the ground electronic state of HNO, singlet or triplet. The electronic absorption spectrum of HNO was first observed by Dalby (Ref. 52) using the flash photolysis method. He assigned the transition to ^{1}A" - ^{1}A' and determined the molecular constants in both states, but there is a possibility that the triplet state must lie very low and might even be the true ground state. Triplet states of HNO have not been observed.
DNO was produced by the reaction of NO with the D atom generated by a microwave discharge in the deuterium gas. The a-type $1_{01} \leftarrow 0_{00}$ and three K-type doubling transitions, and two b-type R and P branch transitions were observed. Some of the transitions showed the hyperfine structure due to the quadrupole interaction of the nitrogen nucleus. They were not due to stable molecules such as DNO_2, DNO_3, NH_2D, NHD_2, D_2O, and N_2O nor to paramagnetic molecules such as NO_2. The rotational constants determined agreed with those of DNO in the lower electronic state ^{1}A' determined by Dalby (Ref. 52) within the error limits as shown in Table 4. Subsequently the microwave spectrum of the H species was observed by the use of reactions of NO with the H atom. The molecular constants obtained are also given in Table 4.
Moreover, the lifetime of the molecule giving the spectra was found to range from 1 to 40 sec depending upon the conditions. This long lifetime can be understood from the fact that all the halogen derivatives of nitroxyl are rather stable compounds. Thus the molecular species observed was assigned to the HNO molecule, and its ground electronic state was determined to be ^{1}A'.
HNO has been also expected to exist in inerstellar spece. After many unsuccessful searches (Ref. 53&54), the $1_{01} \leftarrow 0_{00}$ transition of HNO was detected in emission from the directions of Sagitarius B2 and NGC2024

(Ref. 55). The most significant aspect of this result is that HNO is the first interstellar molecule containing the NO bond. This will inevitably lead to an improvement or and extension of the ion-molecule reaction theory explaining the formation of various interstellar molecules.

Table 4. Molecular Constants of HNO and DNO (MHz)

Constant	HNO	DNO
A	553903.0±2.7	315496.5±2.3
	(553994 ±15)[a]	(315449 ±21)[a]
B	42308.52±0.10	38732.16±0.10
	(42316 ±6)[a]	(38734 ±12)[a]
C	39169.46±0.10	34353.68±0.10
	(39187 ±6)[a]	(34364 ±12)[a]
Δ_o^b	0.04489±0.00006	0.06116±0.00008
χ_{aa}	0.36±0.40	1.03±0.40
χ_{bb}	-5.46±0.40	-6.13±0.26
χ_{cc}	5.10±0.26[c]	5.10±0.26
μ_a	1.03±0.01 D	1.18±0.04 D
μ_b	1.31±0.02 D	1.22±0.04 D
μ_{total}	1.67±0.03 D	1.70±0.05 D

a. Ref. 52. b. amuA^2. c. Assumed.

Vinyl Alcohol, CH_2=CHOH (Ref. 50)

Vinyl alcohol, a tautomer of acetaldehyde, has been suggested to be an intermediate of reactions leading to the formation of acetaldehyde (Ref. 56-59). In 1973, Blank and Fisher (Ref. 60) observed the NMR spectrum of presumable vinyl alcohol, highly enhanced by CIDNP during photolysis of acetaldehyde and of 2- hydroxybutane-3one (acetoin). The observation has, however, been carried out only in the liquid phase, and the existence of vinyl alcohol in the gas phase has never been recognized

On the other hand, it is well known that various derivatives of vinyl alcohol such as methyl vinyl ether, vinyl acetate, and especially poly(vinyl alcohol) are very stable. This may be explained from the equilibrium of the keto-enol tautomerization, favourable to the existence of acetaldehyde (Ref. 61). Vinyl alcohol was produced by a dehydration reaction of ethylene glycol. Ethylene glycol was introduced into a 6 mm quartz tube, heated to 700 - 1000 degree centigrade. Pyrolyzed sample was pumped through the parallel plate absorption cell. An appreciable amount of acetaldehyde and a small amount of ethylene oxide as well as unreacted ethylene glycol were identified in the reaction products by monitoring their microwave spectra. In addition to the spectra of known stable molecules, a series of strong and sharp lines were observed at 50 to 70 GHz with the optimum intensity at about 900°C. The lines were assigned to a series of the b-type Q branch transitions by means of well-resolved Stark patterns. The rotational constants preliminarily obtained were consistent with a structure of vinyl alcohol in the syn form. The inertia defect derived from the rotational constants was positive and small. This strongly supported that the molecule is planar. The conclusion was definitely confirmed by the observation of the spectrum of CH_2=CHOD, which was produced by the dehydration of CH_2ODCH_2OD.

The lifetime of vinyl alcohol was measured by monitoring its lines on CRO. The reaction products were stored in a conventional absorption cell of an X-band waveguide 3 m long at room temperature. The halflife was found to be about 4 sec. On the other hand, the halflife of vinyl alcohol was about 30 minutes, when stored in a Pyrex flask of 500 cm^3 equipped with a hydrocarbon-greased stopcock. Vinyl alcohol is nearly stable in the glass ware. It is

Acknowledgement - The author would like to thank Professor Yonezo Morino for his valuable discussions and encouragement throughout this study. He also expresses his sincere thanks to Professor Eizi Hirota for critical reading of the manuscript.

REFERENCES

1. M. Gomberg, J. Am. Chem. Soc. 22, 757 (1900).
2. A. M. Bass and H. P. Broida, eds., "Formation and Trapping of Free Radicals", Academic Press, New York, 1960.
3. G. Herzberg, "Spectra of Diatomic Molecules", Van Nostrand Company, Princeton, N. J. (1950).
4. G. Herzberg, "Electronic Spectra and Electronic Structure of Polyatomic Molecules", Van Nostrand Reinhold Company, New York (1966).
5. G. Herzberg, "The Spectra and Structures of Simple Free Radicals", Cornell University Press, Ithaca (1971).
6. S. Saito, J. Mol. Spectrosc. 30, 1 (1969).
7. C. H. Townes and A. L. Schawlow, "Microwave Spectroscopy", McGraw-Hill, New York, 1955.
8. S. Saito and T. Amano, J. Mol. Spectrosc. 34, 383 (1970).
9. S. Saito, J. Chem. Phys. 53, 2544 (1970).
10. S. Saito, J. Mol. Spectrosc. 48, 530 (1973).
11. A. Carrington, "Microwave Spectroscopy of Free Radicals", Academic Press, New York, 1974.
12. F. C. Fehsenfeld, K. M. Evenson, and H. P. Broida, Rev. Sci. Instr. 36, 294 (1965).
13. S. Saito, J. Mol. Spectrosc. 65, 229 (1977).
14. D. R. Kearns, Chem. Rev. 71, 395 (1971).
15. L. Herzberg and G. Herzberg, Astrophys. J. 105, 353 (1947).
16. R. Colin, Can. J. Phys. 46, 1539 (1968).
17. A. Carrington, D. H. Levy, and T. A. Miller, Proc. Roy. Soc. London, A293, 108 (1966).
18. A. Carrington, D. H. Levy, and T. A. Miller, J. Chem. Phys. 47, 3801 (1967).
19. A. Carrington, D. H. Levy, and T. A. Miller, Trans. Faraday Soc. 62, 2994 (1966).
20. S. Saito, Tetrahedron Letters, 48, 4961 (1968).
21. S. Saito, Bull. Chem. Soc. Japan, 42, 667 (1969).
22. W. H. Breckenridge and T. A. Miller, J. Chem. Phys. 56, 465 (1972).
23. D. M. Lemal and P. Chao, J. Am. Chem. Soc. 95, 922 (1973).
24. S. Saito, Astrophys. J. 178, L95 (1972).
25. N. N. Semenov, "Photochemistry and Reaction Kinetics", (P. G. Ashmore, F. S. Dainton, and T. M. Sugden, Ed.), 229, Cambrige Univ. Press, London, 1967.
26. D. M. Rank, C. H. Townes, and W. J. Welch, Science, 174, 1083 (1971).
27. K. B. Jefferts, A. A. Penzias, R. W. Wilson, M. Kutner, and P. Thaddeus, Astrophys. Letters, 8, 43 (1971).
28. G. Herzberg and D. A. Ramsay, Proc. Roy. Soc. London, A, 233, 34 (1955).
29. I. C. Bowater, J. M. Brown, and A. Carrington, J. Chem. Phys. 54, 4957 (1971).
30. I. C. Bowater, J. M. Brown, and A. Carrington, Proc. Roy. Soc. London, A, 333, 265 (1973).
31. P. H. S. Bolman, J. M. Brown, and A. Carrington, Proc. Roy. Soc. London, A, 335, 113 (1973).
32. J. A. Austin, D. H. Levy, C. A. Gottlieb, and H. E. Radford, J. Chem. Phys. 60, 207 (1974).
33. R. F. Curl, Jr. and J. L. Kinsey, J. Chem. Phys. 35, 1758 (1961).
34. L. E. Snyder, J. M. Hollis, and B. L. Ulich, Astrophys. J. 208, L91 (1976).
35. A. C. Lloyd, Int. J. Chem. Kinet. 6, 169 (1974).
36. H. E. Radford, K. M. Evenson, and C. J. Howard, J. Chem. Phys. 60, 3178 (1974).
37. J. T. Hougen, H. E. Radford, K. M. Evenson, and C. J. Howard, J. Mol. Spectrosc. 56, 210 (1975).
38. Y. Beers and C. J. Howard, J. Chem. Phys. 63, 4212 (1975).
39. Y. Beers and C. J. Howard, J. Chem. Phys. 64, 1541 (1976).
40. W. T. Raynes, J. Chem. Phys. 41, 3020 (1964).

41. F. J. Adrian, E. L. Cochran, and V. A. Bowers, J. Chem. Phys. 47, 5441 (1967).
42. R. F. Curl, Jr., J. Chem. Phys. 37, 779 (1962).
43. M. Morimoto, private communication, 1975.
44. H. R. Radford, private communication, 1975.
45. H. R. Radford, private communication, 1976.
46. R. H. Gammon, private communication, 1976.
47. K. Takagi and S. Saito, J. Mol. Spectrosc. 44, 81 (1972).
48. S. Saito and K. Takagi, Astrophys. J. 175, L47 (1972).
49. S. Saito and K. Takagi, J. Mol. Spectrosc. 47, 99 (1973).
50. S. Saito, Chem. Phys. Letters, 42, 399 (1976).
51. A. D. Walsh, J. Chem. Soc. 2288 (1953).
52. F. W. Dalby, Can. J. Phys. 36, 1336 (1958).
53. N. Fourikis, M. W. Sinclair, R. D. Brown, J. G. Crofts, and P. D. Godfrey, Astrophys. J. 194, 41 (1974).
54. T. Oka, private communication, 1975.
55. B. L. Ulich, J. M. Hollis, and L. E. Snyder, preprint.
56. E. Erlenmeyer, Chem. Ber. 14, 320 (1881).
57. L. I. Avramenko and R. V. Kolensnikova, Advan. Photochem. 2, 25 (1964).
58. G. C. Bond, "Heterogenious Catalysis", 91, Clarendon Press, Oxford, 1974.
59. J. M. Hay and D. Lyon, Nature 216, 790 (1967).
60. B. Blank and H. Fischer, Helv. Chim. Acta 56, 506 (1973).
61. A. Gero, J. Org. Chem. 19, 469 (1954).

Pure & Appl. Chem., Vol. 50, pp. 1251-1259.
Pergamon Press Ltd. 1978. Printed in Great Britain.

0033-4545/78/1201-1251 $02.00/0

ELECTRONIC STRUCTURES OF AROMATIC HYDROCARBONS WITH HIGH SPIN MULTIPLICITIES IN THE ELECTRONIC GROUND STATE

Koichi Itoh

Department of Chemistry, Faculty of Science, Osaka City University, Sugimoto-cho, Sumiyoshi-ku, Osaka 558, Japan

Abstract - It has been established experimentally that there are alternant hydrocarbons (AH) with high spin multiplicities in the electronic ground state, the highest multiplicity known up to date being septet. Such electronic structures are rationalized by utilizing the degeneracy of non-bonding pi molecular orbitals (NBMO) predictable from the theory of Longuet-Higgins in conjunction with the non-bonding orbitals of divalent carbon atoms which are perpendicular to p_π orbitals and are nearly degenerate with NBMO. The degeneracy of NBMO is determined by the topological nature of molecules which permits the ground state with high spin multiplicities according to Hund's rule in spite of their low molecular symmetries. The nature of AH having high spin multiplicities in the ground state reported so far is understood in this manner. It was found, however, that for some AH the high spin multiplet states are unexpectedly not the ground states although they lie very close to the singlet ground state. The difference between these two types of AH with high spin multiplicities is associated with the fact that the spin distribution of NBMO is alternant in the former AH, but not in the latter. To the latter AH the weak interaction model was found to apply in which a molecule is divided into two units weakly interacting with each other.

INTRODUCTION

For a long time it was an open question whether there were organic molecules with spin multiplicities higher than triplet in the electronic ground state. This did not seem possible because the molecular symmetry of organic compounds is generally low in contrast to the case of ions of the transition-group elements in crystals or in ligands of metal complexes: From the group theoretical point of view, the number of the degeneracy of occupied molecular orbitals of organic compounds cannot be larger than two, which seems to violate Hund's rule.

In 1967, however, the author (1) and independently Wasserman et al. (2) found that the electronic ground state of the aromatic hydrocarbon, *m*-phenylene-bis-phenylmethylene, is the quintet state (S=2). This unusual molecule has the structure of type I in Fig. 1 with the phenyl group (C_6H_5) substituted for R.

Thereafter, a series of similar hydrocarbons with high spin multiplicities have been reported; *m*-phenylene-bis-methylene (I with R=H) in the quintet ground state (2), benzene-1,3,5-tris-phenylmethylene (II with R=C_6H_5) in the

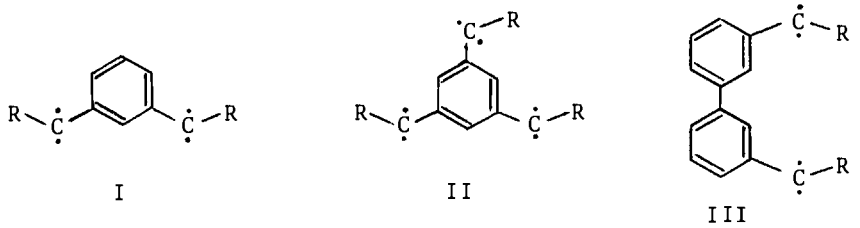

I II III

Fig. 1. Structures of aromatic hydrocarbons with high spin multiplicities.

septet ground state (3), and 1,3,5-benzenetryl[di(*p*-biphenyl)methyl] (II with $\dot{C}(biphenyl)_2$ substituted for $\dot{C}$-R) in the quartet ground state (4). The first two as well as *m*-phenylene-bis-phenylmethylene have divalent carbon atoms each having two unpaired spins. The investigations (1-3) by electron spin resonance (ESR) have shown that half of the parallel spins belong to the pi orbitals, while the other half is mainly localized in each of the non-bonding orbitals "n" of the divalent carbon atoms perpendicular to the pi orbitals. On the other hand, the last-mentioned hydrocarbon has parallel spins all of which belong to the pi electron system. The two high spin multiplet nitrenes isoelectronic to I and II were also reported (2,7). We are interested particularly in the hydrocarbons because they are of fundamental importance in quantum chemistry and can be dealt with using least ambiguous parameters in the calculation of the electronic structures.

GUIDING PRINCIPLE

The unusual spin multiplicity arises from the particular properties of zero-energy molecular orbitals or non-bonding molecular orbitals (NBMO's) in the pi system of conjugated alternant hydrocarbons which were already pointed out in 1950 by Longuet-Higgins (5), but the importance of the implication in molecular magnetism seems to have been overlooked until the discovery of the hydrocarbons described above. The rule of Longuet-Higgins states:

(1) An alternant hydrocarbon has at least $N - 2T$ NBMO's where N denotes the number of carbon atoms in the conjugated system and T the maximum number of double bonds occurring in any resonance structure.
(2) In the ground state there will be just one electron in each NBMO, and if there are two or more such electrons, their spins will be parallel.

For example, with the three hypothetical molecules, *o*-, *m*-, and *p*-$C_6H_4(\dot{C}H_2)_2$, the number of NBMO's is 2 for meta compound, while zero for para or ortho compounds. This is a clear demonstration that this orbital degeneracy of NBMO is determined by the sequence of carbon atoms forming the conjugated system. In this sense we may call this the topological symmetry and this degeneracy the topological degeneracy. This is an accidental degeneracy in view of the group theory but has some mathematical meaning within the simple LCAO-MO approximation. It is to be noted that this degeneracy does not depend on the assumption of equal or related resonance integrals for the various bonds, i.e., this rule is little affected by changes of molecular configurations. The above-mentioned rule for the simplest case of $N - 2T = 1$ is justified by the LCAO-SCF-MO calculation (7).

This theory has been found to apply remarkably well to the before-mentioned molecules. But our recent investigation has shown that it is too simple to account for all the experiments. The limitation of the theory will be discussed later.

Meanwhile, the electronic structure of methylene, $\dot{C}H_2$ is well known. Its stable spin multiplicity depends on the bond angle θ. In the gaseous phase the triplet state $^3\Sigma_g^-$ (or $^3B_1$) is stable for nearly linear methylene ($\theta \sim 180°$), while the singlet state $^1A_1$ is stable for bent methylene ($\theta = 103°$) (8). According to the theoretical calculation by Dixon using the intra-atomic correlation correction, the two spins occupying the pi orbital ($1b_1$) and the non-bonding orbital n ($3a_1$) are parallel for θ larger than ca 140° because the orbital energies are nearly degenerate (9). Recent *ab initio* calculations indicate that the ground state is the triplet ($^3B_1$) with the bond angle of $132 \sim 138°$ (10, 11). On the other hand, the ESR measurement of methylene-d_2 in xenon matrix at 4.2 K gave $\theta = 137.7°$ from the ^{13}C hyperfine structure (12) and 136° from the E/D value (13). These results indicate that the energy difference between the n and pi orbitals of the divalent carbon atom is small enough to align the two spins parallel. Therefore, if the topological degeneracy of NBMO's and the near degeneracy of n orbitals of divalent carbon atoms are taken into account, the number of parallel spins may be doubled provided that the bond angle is favorable to parallel spins.

ELECTRONIC STRUCTURES AND ESR SPECTRA OF ALTERNANT HYDROCARBONS WITH THE QUINTET AND SEPTET GROUND STATES

Figure 2 shows the electronic structure of the quintet molecule detected first in a series of similar molecules. R of I in Fig. 1 is replaced by the phenyl group in order to stabilize the molecule. Here the number of NBMO's is two and there are four nearly degenerate orbitals since the energy difference between the n orbital and NBMO may be small. Thus four spins are

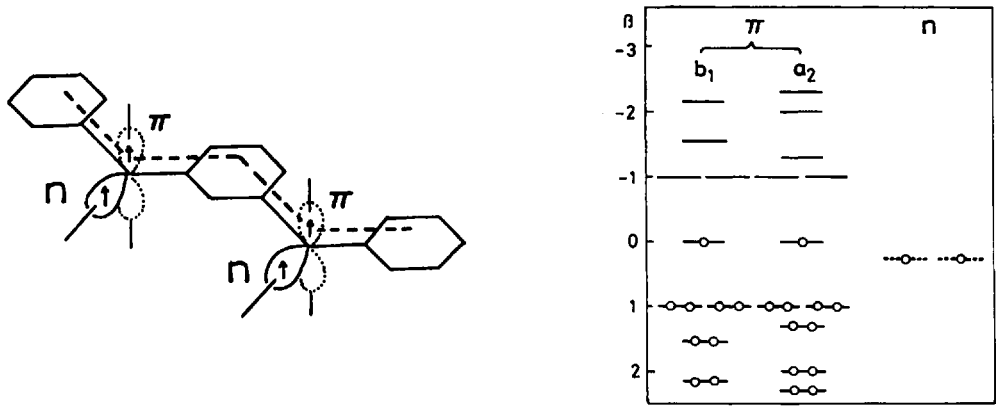

Fig. 2. Electronic structure of *m*-phenylene-bis-phenylmethylene

expected to be parallel according to Hund's rule. Two of them are localized in the n orbitals of the divalent carbon atoms, and the other two are delocalized over the whole molecule and exchange coupled strongly on the divalent carbon atoms, all the spins interacting in a common molecular space. It is interesting that this is similar to the s-d interaction of ferromagnetic metals.

The observed ESR spectra can be completely reproduced by the spin Hamiltonian

$$\mathcal{H} = g\beta\vec{H}.\vec{S} + D[S_Z^2 + S(S+1)/3] + E(S_X^2 - S_Y^2) \qquad (1)$$

with $S=2$, $g=2.0038$, $D=0.07137$ cm^{-1}, and $E=0.01963$ cm^{-1} (1). The terms of the type S_i^4, and $S_i^2.S_j^2$ $(i,j=X,Y,Z)$ were found to be negligibly small in this case. This is reasonable because the spin orbit interaction in hydrocarbons is much smaller than that in transition-metal ions for which these terms have some contribution. The observed parameters were in fair agreement with the theoretical prediction by Higuchi (14) for this electronic structure. In addition, temperature dependence of the ESR spectra confirmed this quintet state to be the ground state.

On the other hand, the topological isomer, *p*-phenylene-bis-phenylmethylene, showed an ESR signal indicating the triplet state (15). However, our recent investigation (16) revealed that this state is the thermally excited one located 202 cm^{-1} above the singlet ground state. The spin Hamiltonian is also given by Eq. (1) with $S=1$, $g=2.0025$, $D=+0.05005$ cm^{-1} and $E=+0.00159$ cm^{-1}. These parameters are reasonable for a triplet state in which two localized spins occupy the two different n orbitals. This is called the triplet state of the nn type (17). Thus this molecule has no singly occupied pi NBMO in contrast to the meta isomer. The meta and para isomers that have been detected experimentally constitute a good example of the theory of Longuet-Higgins described in the preceding chapter.

As an extension of this work, we have synthesized and detected benzene-1,3,5-tris-phenylmethylene (3) which has the structure II with R=C_6H_5 in Fig. 1. The ground state of this molecule is the septet which is the highest spin multiplicity amongst not only hydrocarbons but also a vast number of organic molecules known to date, togther with the septet nitrene, *sym*-$C_6(\dot{C}N)_3$ (6). It will be seen how well the spin Hamiltonian for the septet state reproduces the experimental results for this molecule which is dissolved in a single crystal of 1,3,5-tribenzoylbenzene.

Figure 3 shows the ESR spectrum recorded in the dispersion mode at liquid helium temperature after photolysis of the diazo precursor. The six lines $A^{\pm}$, $B^{\pm}$, and $C^{\pm}$ correspond to the six allowed transitions of the septet state. The other lines are due to the byproducts of the photolysis. The apparent deviation from the theoretical transition probabilities (3:5:6:6:5:3) is due to the Boltzmann distribution, from which the absolute sign of D was determined. The angular dependence of the six lines is shown in Fig. 4 as a function of the magnetic field. Here the solid line represents the calculated values using the spin Hamiltonian given by Eq. (1) with $S=3$, $g=2.0038$, $D=+0104158$ cm^{-1}, and $E=+0.01026$ cm^{-1} (the group theory allows terms up to the sixth

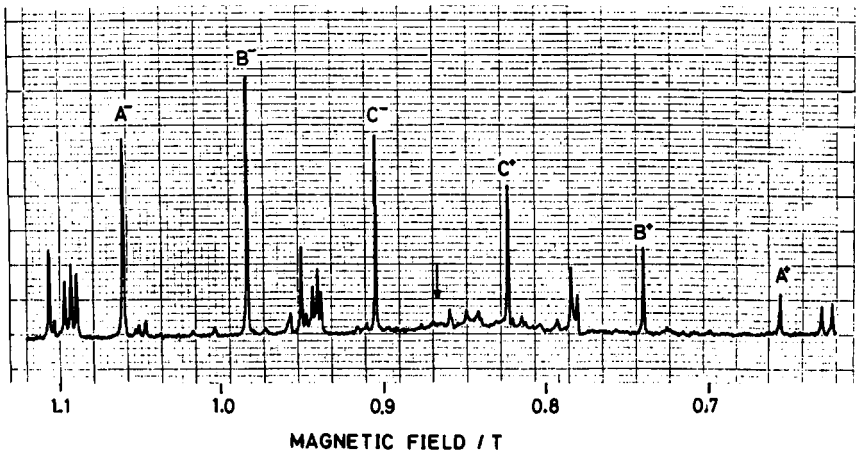

Fig. 3. ESR spectrum of benzene-1,3,5-tris-phenylmethylene recorded in the dispersion mode at 4.2 K. The magnetic field is parallel to the Z principal axis. The arrow indicates the position for g=2.0040.

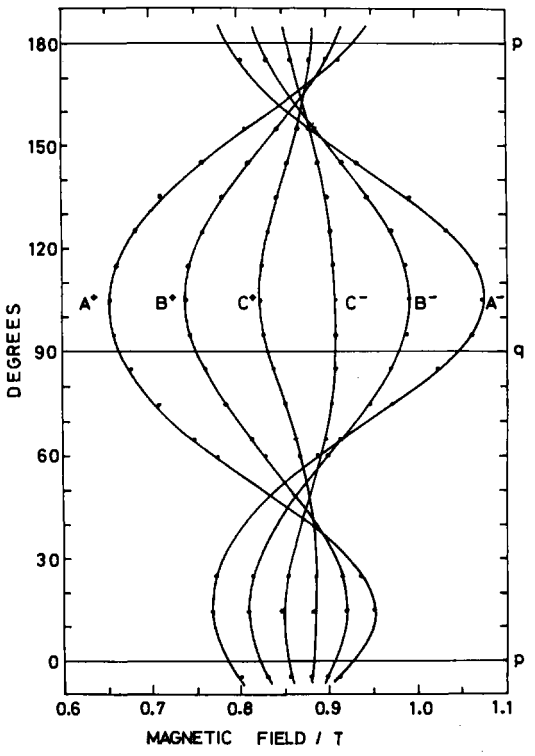

Fig. 4. Angular depencence of the resonance fields of the six lines for rotation of the magnetic field applied in the pq plane. The points represent the observed values, and solid lines the calculated ones.

power in $\vec{S}$ which were found, however, negligibly small similarly to the case of the quintet hydrocarbon). The remarkable agreement proves the existence of the septet state. In addition, the measurement of temperature dependence confirmed this to be the ground state.

The molecular configurations of the quintet and septet hydrocarbons have been found unsymmetrical from the ESR experiments. The most probable configurations are shown in Fig. 5. Higuchi estimated the bond angles of the divalent carbon

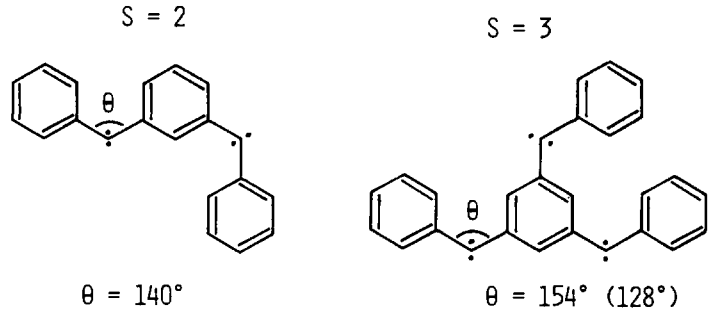

Fig. 5. Most probable configurations of the quintet and septet hydrocarbons.

atoms which are consistent with the observed fine structure parameters D and E. They are about 140° (18) and 154° (19) for the quintet and septet hydrocarbons, respectively, which are to be compared with the values for the $^1B_1$ state of methylene (10-13).

It may be interesting at this stage to classify the molecules with high spin multiplicities according to their magnitude of the spin-spin interaction. Most of the molecules mentioned before belong to the nπ type, and their $(2S-1)|D|$ value ranges from 0.2 to 0.3 cm^{-1}. In contrast to these, the ππ type molecule, 1,3,5-benzenetriyl [di(*p*-biphenyl)methyl], has a very small value of 0.00824 cm^{-1} (4). Yang's biradical (S=1) having oxygen atoms in the pi system also belongs to this category, and has a value of 0.0032 cm^{-1} (20). These small values are due to the particular property of the spin distribution of the NBMO where the spin density appears on alternating carbon atoms, so that the ππ interaction between the spins occupying the NBMO's is of long-range type and small. This is the same for the nπ type molecules as far as the ππ interaction is concerned. The large values for the nπ type molecules are, however, essentially due to the one-center nπ type interaction on the divalent carbon atoms. On the other hand, in the case of the nn type molecule, *p*-phenylene-bis-phenylmethylene, the interaction (0.05005 cm^{-1}) is simply a long-range one between the two localized spins.

It seems natural to extend this theory to polymers which are composed of these unusual molecules as units. The possible electronic structure of these polymers was discussed by Mataga previously (21).

NEW TYPE OF ALTERNANT HYDROCARBON

The electronic structure of the alternant hydrocarbon having the structure of type III in Fig. 1 is interesting because the spins on the divalent carbon atoms couple through a biphenyl ring in contrast to the case treated in the preceeding chapter where spins couple through a benzene ring. According to the above-mentioned rule and experimental results, molecules of type III are also expected to have the quintet ground state. Recently, we have investigated the ESR of biphenyl-3,3'-bis-phenylmethylene (BBPM) with the structure shown in Fig. 6a (22). This alternant hydrocarbon was formed at 4.2 K or 20 K by the photolysis of its diazo precursor, 3,3'-bis(α-diazobenzyl)biphenyl, oriented in single crystals of benzophenone. By the analysis of angular dependence and

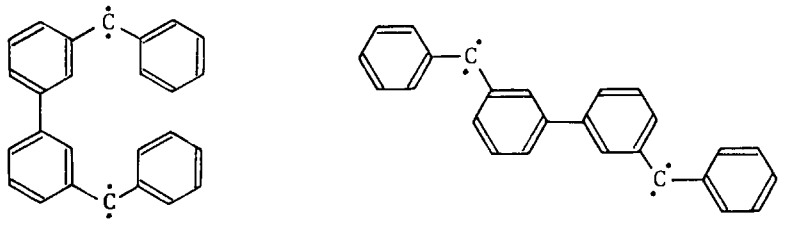

Fig. 6. Chemical structure (a) and molecular configuration (b) of biphenyl-3,3'-bis-phenylmethylene.

temperature dependence of the ESR spectra, we confirmed that the lowest energy levels are nearly degenerate singlet, triplet, and quintet states in the order of increasing energy in spite of the above-mentioned simple expectation. In addition, there are two isomers of BBPM with different configurations in the host crystal. The isomer designated L is stable at low temperature and changes irreversibly into another isomer H at 140 K. Therefore, the irreversible spectral change corresponding to

$$T_L\ ,\ Q_L \xrightarrow{140\ K} T_H\ ,\ Q_H$$

was observed, where T and Q stand for the triplet and quintet states, respectively.

As before the spin Hamiltonian given by Eq. (1) fully accounts for the angular dependence of the ESR spectra of all the four paramagnetic species. The parameters experimentally determined are listed in Table 1. This table indicates

TABLE 1. Fine structure parameters and g values for T_L, Q_L, T_H, and Q_H of biphenyl-3,3'-bis-phenylmethylene. The principal axes of the fine structure tensors for T_L and Q_L and also for T_H and Q_H coincide with each other.

$S = 1$	$S = 2$
T_L: $D = -0.29583 \pm 0.00010\ cm^{-1}$	Q_L: $D = 0.10349 \pm 0.00009\ cm^{-1}$
$E = 0.06032 \pm 0.00010\ cm^{-1}$	$E = -0.01457 \pm 0.00009\ cm^{-1}$
$g = 2.0040$	$g = 2.0040$
T_H: $D = \pm 0.23895\ cm^{-1}$	Q_H: $D = \pm 0.08329 \pm 0.00008\ cm^{-1}$
$E = +0.06452\ cm^{-1}$	$E = \mp 0.02114 \pm 0.00008\ cm^{-1}$
$g = 2.0040$	$g = 2.0040$

the three characteristic features of the fine structure tensors. Firstly, the principal axes of the fine structure tensors for $T_{L(H)}$ and $Q_{L(H)}$ coincide with each other. Secondly, the D and E values of $T_{L(H)}$ are almost three times as large as those of $Q_{L(H)}$. Thirdly, the absolute signs of the D and E values are opposite between T_L and Q_L (unfortunately the absolute sign for T_H and Q_H could not be determined because of the small population at low temperature). In addition, the g values of the triplet and quintet states are almost isotropic and equal.

These features were found to be nicely accounted for by the following weak interaction model. BBPM may be regarded as composed of two diphenylmethylene units connected with each other at the meta position of each benzene ring (see Fig. 6a). The spin densities at the bridge carbon atoms connecting these units are zero for the spins occupying the NBMO's. Therefore, concerning the four spins occupying the two NBMO's and the two n orbitals, their interactions between the two diphenylmethylene units may be considered to be much smaller than the nπ interaction within each unit in good approximation. Since the ground state of diphenylmethylene is the triplet state(23), the composite system is expected to have one quintet, one triplet, and one singlet state as low-lying energy levels.

The spin Hamiltonian for a system consisting of weakly interacting units a and b may be written as

$$\mathcal{H} = \mathcal{H}^a(1) + \mathcal{H}^b(2) + \mathcal{H}^{ab}(1,2) \tag{2}$$

where the Hamiltonians for each unit are

$$\mathcal{H}^a(1) = \beta \vec{H} \cdot \underset{\sim}{g}^a \cdot \vec{S}_1 + \vec{S}_1 \cdot \underset{\sim}{D}^a \cdot \vec{S}_1 \tag{3}$$

$$\mathcal{H}^b(2) = \beta \vec{H} \cdot \underset{\sim}{g}^b \cdot \vec{S}_2 + \vec{S}_2 \cdot \underset{\sim}{D}^b \cdot \vec{S}_2 \tag{4}$$

and the Hamiltonian for the interaction is

$$\mathcal{H}^{ab}(1,2) = J\vec{S}_1.\vec{S}_2 + \vec{S}_1.\underset{\sim}{D}^{ab}.\vec{S}_2 \tag{5}$$

For the present model $S_1 = S_2 = 1$, and in good approximation $\underset{\sim}{g}^a = \underset{\sim}{g}^b = g$ (isotropic). If the exchange energy is large compared with the other spin energies, $\mathcal{H}$ can be rewritten with the total spin $\vec{S} = \vec{S}_1 + \vec{S}_2$ as

$$\mathcal{H} = E_S + g\beta\vec{H}.\vec{S} + \vec{S}.\underset{\sim}{D}_S.\vec{S} \tag{6}$$

where

$$E_S = (J/2)[S(S+1) - 4] \tag{7}$$

$$\underset{\sim}{D}_S = [(3S^2 + 3S - 11)/2(2S-1)(2S+3)](\underset{\sim}{D}^a + \underset{\sim}{D}^b) + [(S^2 + S + 8)/2(2S-1)(2S+3)]\underset{\sim}{D}^{ab} \tag{8}$$

using the transformation properties of angular momentum and tensor operators (24). E_S is J, $-J$, and $-2J$ for $S = 2$, 1, and 0, respectively, and $\underset{\sim}{D}_S$ for $S = 2$, and 1 is given by

$$\underset{\sim}{D}_2 = (1/6)(\underset{\sim}{D}^a + \underset{\sim}{D}^b) + (1/3)\underset{\sim}{D}^{ab} \tag{9}$$

$$\underset{\sim}{D}_1 = (-1/2)(\underset{\sim}{D}^a + \underset{\sim}{D}^b) + \underset{\sim}{D}^{ab} \tag{10}$$

In this system $\underset{\sim}{D}^{ab}$ may be much smaller than $\underset{\sim}{D}^a$ and $\underset{\sim}{D}^b$ which are very large because of the large one-center $n\pi$ interaction, so that we finally obtain $\underset{\sim}{D}_1 = -3\underset{\sim}{D}_2$. All the above-mentioned characteristic features of the fine structure tensors are interpreted by this relation.

Consequently, if J values determined independently from the triplet and quintet signals are equal and positive, all the above-mentioned experimental results are explained by the weak interaction model. In order to confirm the mechanism the signal intensity for the H isomer times temperature is plotted in Fig. 7.

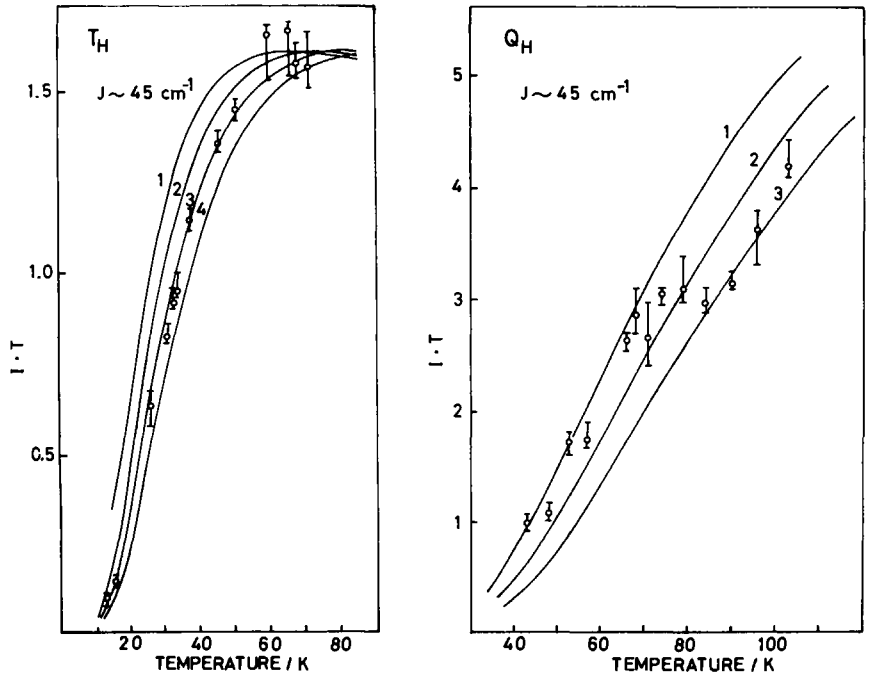

(a) (b)

Fig. 7. Plots of the signal intensity for T_H and Q_H times temperature as a function of temperature. The circles and the vertical lines represent the experimental values and their uncertainties, respectively. The solid lines represent the theoretical values calculated from the above-mentioned model for the following J values: (a) 1(35 cm^{-1}), 2(40 cm^{-1}), 3(45 cm^{-1}), 4(50 cm^{-1}); (b) 1(40 cm^{-1}), 2(45 cm^{-1}),3(50cm^{-1}).

as a function of temperature and compared with the theoretical values calculated from the model. The plots for both T_H and Q_H give the same J value of 45 ± 5 cm^{-1} independently. Similarly, the J value for the L isomer was determined to be + 20 cm^{-1}.

As we have seen, every phase of the present experiment supports the weak interaction model. Therefore, it may be concluded that the four spins in this molecule couple strongly with ferromagnetic J, and that each pair of spins further couples weakly with antiferromagnetic J. As a result, the simple prediction by theory of Longuet-Higgins does not apply to this molecule.

The reason for the value of J being positive may be accounted for as follows. The spin distribution of NBMO for BBPM in the simple LCAO-MO approximation is such that there is no spin density on the bridge carbon atoms. However, since the direct long-range exchange interactions between carbon atoms other than the bridge carbons are very small, the observed weak exchange interaction is probably due to the spin densities induced on the bridge carbon atoms. If this is the case, the weak antiferromagnetic coupling seems reasonable from the nature of the exchange interaction between. Figure 8 shows the behavior of J between two pπ orbitals on adjacent carbon atoms

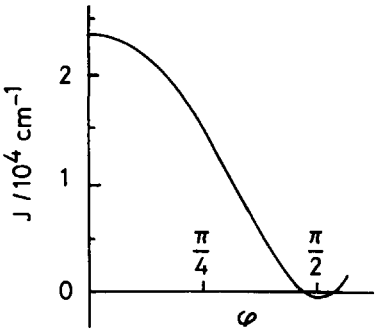

Fig. 8. J value vs. angle of bond twist φ between two p orbitals on adjacent carbon atoms. The value for $\varphi=0$ is estimated from the singlet-triplet transition energy of ethylene and that for $\varphi=\pi/2$ is from Kotani's table (about -200 cm^{-1}).

when the angle of bond twist is varied. Here the positive sign corresponds to the antiferromagnetic coupling from the definition of the exchange energy in the spin Hamiltonian given by Eq. (5). The J value for $\varphi=0$ may be approximated by the singlet-triplet transition energy of ethylene. As φ increases, J decreases and changes its sign at an angle very close to $\pi/2$. For $\varphi=\pi/2$ J reduces simply to the negative of the exchange integral, $-(pp'|e^2/r|p'p)$, which is very small between the p orbitals perpendicular with each other (about -200 cm^{-1} was estimated from Kotani's table). Negative J values would be obtained only if two benzene planes of the biphenyl group are very nearly perpendicular with each other. If we consider the size of BBPM molecule, such a configuration may be impossible not only in the host crystal but also in other matrices. Moreover, a recent *ab initio* CI calculation by Iwata (25) suggests that J is always positive if electron correlations are taken into account. The positive J value is , therefore, reasonable for other type-III molecules as well as BBPM. On the other hand, the calculation of the spin-spin interaction suggests that BBPM takes an unsymmetrical and stretched configuration as shown in Fig. 6b.

Our experimental results on the alternant hydrocarbons which are expected to have high spin multiplicities from their topological symmetry may be summarized as follows. The alternant hydrocarbons of the type (A) and (B) in Fig. 9 have parallel spins in the ground state. For these molecules the starred carbon atom coincides with the active carbon atom where "active" means the non-zero spin density on that carbon atom. On the other hand, for the type (C) molecule the set of the starred carbon atoms and that of the active carbon atoms do not coincide with each other. In other words, in this category of alternant hydrocarbons the spin distribution is not alternant, and there are always two adjacent carbon atoms with zero spin densities in NBMO's. The molecule may, therefore, be regarded as separated at the boundary concerning the interaction between the spins occupying the NBMO's. For this group of

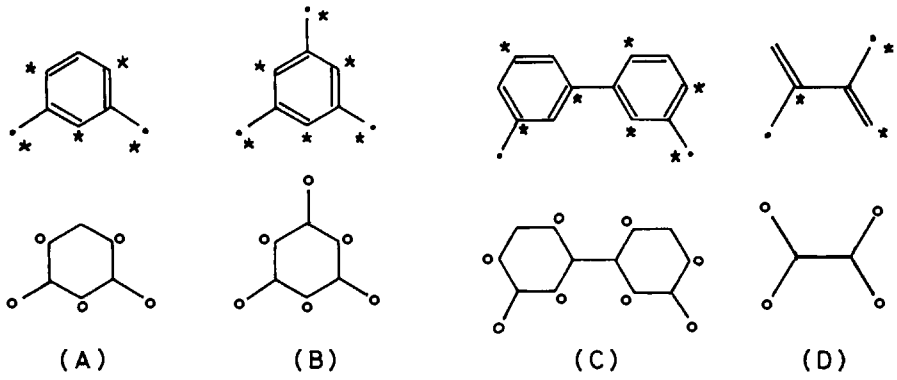

Fig. 9. Diagram showing the starred (*) and active (o) carbon atoms of the alternant hydrocarbons which are expected to have high spin multiplicities. Hydrogen atoms are neglected in this diagram.

molecules the weak interaction model is better suited and their ground states are expected to be singlet. The still hypothetical molecule, tetramethylene ethylene, shown as (D) in Fig. 9 and originally suggested by Longuet-Higgins, may also belong to this group.

Acknowledgements - The author wishes to acknowledge to Prof. J. Higuchi of Yokohama National University for his stimulating discussion. He is also indebted to Dr. T. Takui and to the several doctoral candidates who have done much of the experimental work described herein.

REFERENCES

1. K. Itoh, Chem. Phys. Letters 1, 235 (1967).
2. E. Wasserman, R. W. Murray, W. A. Yager, A. M. Trozzolo and G. Smolinsky, J. Am. Chem. Soc. 89, 5076 (1967).
3. T. Takui and K. Itoh, Chem. Phys. Letters 19, 120 (1973).
4. J. Brickman and G. Kothe, J. Chem. Phys. 59, 2807 (1973).
5. H. C. Longuet-Higgins, J. Chem. Phys. 18, 265 (1950).
6. E. Wasserman, K. Schueller and W. A. Yager, Chem. Phys. Letters 2, 259 (1968).
7. H. C. Longuet-Higgins, A. J. Pople, Proc. Phys. Soc. (London) A58, 591 (1955).
8. G. Herzberg, Proc. Roy. Soc. (London) A262, 291 (1961).
9. R. N. Dixon, Mol. Phys. 8, 201 (1964).
10. J. F. Harrison and L. C. Allen, J. Am. Chem. Soc. 91, 807 (1969); J. F. Harrison and R. C. Liedtke, J. Chem. Phys. 58, 3106 (1973).
11. C. F. Bender and H. F. Schaefer III, J. Am. Chem. Soc. 92, 4984 (1970).
12. R. A. Bernheim, H. W. Bernard, P. S. Wang, L. S. Wood, and P. S. Skell, J. Chem. Phys. 54, 3223 (1971).
13. E. Wasserman, V. J. Kuck, R. S. Hutton and W. A. Yager, J. Am. Chem. Soc. 92, 7491 (1970)
14. J. Higuchi, J. Chem. Phys. 38, 1237 (1963).
15. A. M. Trozzolo, R. W. Murray, G. Smolinsky, W. A. Yager and E. Wasserman, J. Am. Chem. Soc. 85, 2526 (1963).
16. M. Asano, T. Takui and K. Itoh, to be published.
17. J. Higuchi, J. Chem. Phys. 39, 1847 (1963).
18. J. Higuchi, Bull. Chem. Soc. Japan 43, 3773 (1970).
19. J. Higuchi, private communication.
20. R. Kreilick, J. Chem. Phys. 43, 308 (1965); K. Mukai, T. Mishina and K. Ishizu, J. Chem. Phys. 66, 1680 (1977).
21. N. Mataga, Theoret. Chim. Acta (Berl.) 10, 372 (1968).
22. Details will be published elswhere.
23. E. Wasserman, A. M. Trozzolo, W. A. Yager, R. W. Murray, J. Chem. Phys. 40 2408 (1964); R. W. Brandon, G.L. Closs, C.E. Davoust, A. Hutchison Jr. B. E. Kohler, R. Silbey, J. Chem. Phys. 43, 2006 (1965).
24. B. R. Judd, Operator Techniques in Atomic Spectroscopy, McGraw-Hill(1963).
25. S. Iwata and K. F. Freed, to be published.

Pure & Appl. Chem., Vol. 50, pp. 1261-1271.
Pergamon Press Ltd. 1978. Printed in Great Britain.

0033-4545/78/1201-1261 $02.00/0

NON-STOICHIOMETRY AND STRUCTURAL DISORDER IN SOME FAMILIES OF INORGANIC COMPOUNDS

Arne Magnéli

Arrhenius Laboratory, University of Stockholm, S-106 91 Stockholm, Sweden

Abstract - The structural background of non-stoichiometry in some families of inorganic compounds is discussed. The materials described include oxygen deficient tungsten trioxides at different degrees of reduction, and potassium intergrowth tungsten bronzes. The article stresses the importance of structural studies combining investigations by X-ray and electron diffraction and by electron-optical imaging.

INTRODUCTION

During the first decade of the 19th century one of the most intense controversies in the history of chemistry took place. The two combatants were French by birth - one Joseph Louis Proust being professor in Madrid and the other count Claude Berthollet holding a chair in Paris. It had become a generally accepted idea among chemists during the 18th century that a pure chemical compound has a constant composition. This was stated by Proust as a general law of constant proportions of a compound chemical species. The law was vigorously opposed by Berthollet who argued that the composition could vary within certain limits and depend on the conditions of formation. Hardly any experimental evidence to support either standpoint was presented, which is quite natural considering the state of the art of chemical analysis at the time. However, Proust became considered the winner of the fight as his view was generally accepted by the chemists. This outcome was largely due to the advent of Dalton's atomic theory, which so nicely seemed to explain the laws of constant and multiple proportions. These laws became the undisputed foundations for the science of stoichiometry. That chemical compounds could be non-stoichiometric, i.e. violate the law of constant proportions, was hardly considered possible by chemists for more than a century.

In 1914, however, the Russian chemist Kurnakov reported on results from studies of equilibria in binary metallic systems. He had found several instances of intermediary phases with compositions varying by several atomic percent of the components. He concluded from such observations that the stoichiometric compounds, which he called daltonides, may be looked upon as a special class of phases. Compounds of variable atomic composition - the non-stoichiometric compounds - form a more general class of phases, and Kurnakov called these berthollides.

Non-stoichiometry has since been found to be frequently occurring in non-molecular solid compounds. Kurnakov stated that this was a new, unexplored field of research giving promise of rich scientific progress, and this has certainly turned out to be true.

Research on non-stoichiometry has been conducted along various lines. Important results have been obtained with thermodynamic methods. Frenkel, Schottky and Wagner were among the pioneers in that field. The application of X-ray diffraction techniques gave the possibilities for crystallographic studies of the structural basis of non-stoichiometry. Among the several investigators who were active in such research, Hägg performed extensive studies on the mechanisms of non-stoichiometry in several groups of inorganic compounds, e.g. the sodium tungsten bronzes (Ref. 1). These materials were first prepared in the early nineteenth century by reduction of sodium polytungstates. The strange products with their extreme chemical inertness and beautiful colours ranging from glittering gold via red and purple to dark blue had attracted the interest of many chemists who tried to rationalize these materials as a series of distinct chemical compounds. Hägg by his X-ray powder diffraction investigations showed that this is rather an instance of an extraordinary wide range of non-stoichiometry.

Irrespective of the composition the crystal structure contains a three-dimensional framework made up of tungsten and oxygen atoms which are arranged as WO_6 octahedra mutually linked by corners (cf. Fig. 1). The big holes in the tungsten-oxygen skeleton are partially occupied by sodium atoms distributed at random. The occupancy may almost reach 100 percent, but also be as low as about 35 percent. The formula of this berthollide material may accordingly be

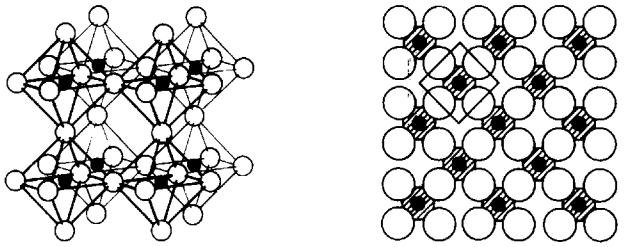

Fig. 1. The tungsten-oxygen network of the cubic sodium tungsten bronzes viewed in perspective and in projection along a cube axis.

written Na_xWO_3 with x values ranging from 1/3 to unity. From the structural point of view the sodium tungsten bronzes may be looked upon as formed by addition of sodium atoms in a ReO_3-type arrangement of WO_6 octahedra, i.e. in an idealized tungsten trioxide structure. Alternatively, they may be described as formed by subtraction of sodium atoms from an $NaWO_3$ structure of perovskite type.

STRUCTURE ANALYSIS BY X-RAY DIFFRACTION AND BY ELECTRON MICROSCOPY

Tungsten trioxide upon moderate reduction gives a dark blue product. The composition or formula of this product was, however, not well known; some investigators concluded from X-ray powder studies that the product is non-stoichiometric and that oxygen vacancies are likely to account for the deficiency in oxygen. A crystal structure investigation performed some 30 years ago, using X-ray diffraction data obtained from single crystals found in the blue reduction product, gave an entirely different result (Ref. 2).

The structure thus arrived at (Fig. 2) is rather like that of tungsten trioxide: the metal atoms have six oxygen neighbours octahedrally arranged and the WO_6 octahedra thus formed are mutually linked by corners as in the ReO_3-type of structure. However, in the blue reduced oxide there are deviations from this simple pattern of linking. Some of the WO_6 octahedra share edges among themselves instead of corners, and the edge-sharing is arranged in such a way that groups of six octahedra are formed. Such groups of six edge-sharing octahedra are arranged at parallel planes extending through the crystal. The ReO_3-type patterns

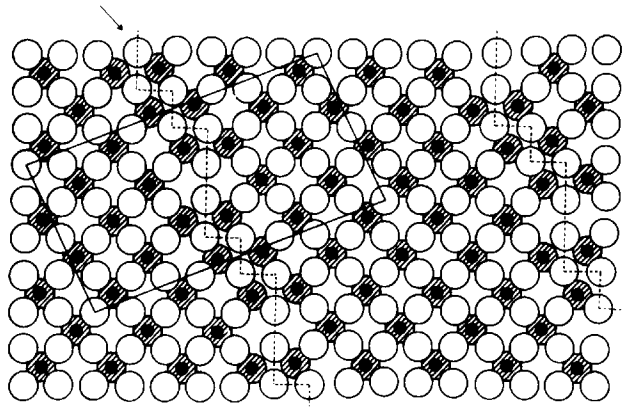

Fig. 2. Projection of the structure of $W_{20}O_{58}$ with dashed lines indicating edge-sharing between WO_6 octahedra at {103} crystallographic shear planes and arrow showing direction of characteristic width of ReO_3-type slabs (n = 20 WO_6 octahedra).

on each side of such planes are "out of phase" with respect to one another and this is the reason for the designation crystallographic shear (CS) later introduced to describe this phenomenon. The oxygen atoms which are engaged in edge-sharing at the shear planes are common to three WO_6 octahedra and thus account for the deficiency in oxygen compared to the WO_3 stoichiometry. The direction of the shear planes is {103} with respect to the basic WO_3 structure.

The complete X-ray crystallographic structure determination directly gave the formula of the reduced oxide. It turned out to be $W_{20}O_{58}$, i.e. exactly $WO_{2.90}$. The reason why the formula is written $W_{20}O_{58}$ and not $W_{10}O_{29}$ is that 20 represents the number of WO_6 octahedra between two consecutive shear planes if the structure is viewed in the particular direction indicated in the figure.

The oxide studied in these experiments was prepared by heating mixtures of tungsten trioxide and tungsten dioxide in sealed tubes. Slight variations of the proportions of the starting materials did not lead to any shifts of the positions of the lines of the X-ray powder patterns of the products. This was taken as evidence that the $W_{20}O_{58}$ phase has a constant daltonide composition.

Results of X-ray structural studies of several binary molybdenum oxides and ternary molybdenum tungsten oxides of compositions lower in oxygen than trioxide stoichiometry are shown in Fig. 3 (Ref. 3 and 4). These phases contain crystallographic shear in a basic ReO_3-type structure, but the edge-sharing takes place within groups of four octahedra instead of six as is the case in the $W_{20}O_{58}$ structure. The shear plane is {102} in these structures whereas it is {103} in the binary tungsten oxide.

The molybdenum oxides and the mixed molybdenum tungsten oxides form a series of analogously built structures, differing only with respect to the width of the ReO_3-type slabs, which extend between the shear planes. The series of oxides comprises Mo_8O_{23}, Mo_9O_{26}, $(Mo,W)_{10}O_{29}$, $(Mo,W)_{11}O_{32}$ etc. The general formula of this "homologous" series of apparently daltonide

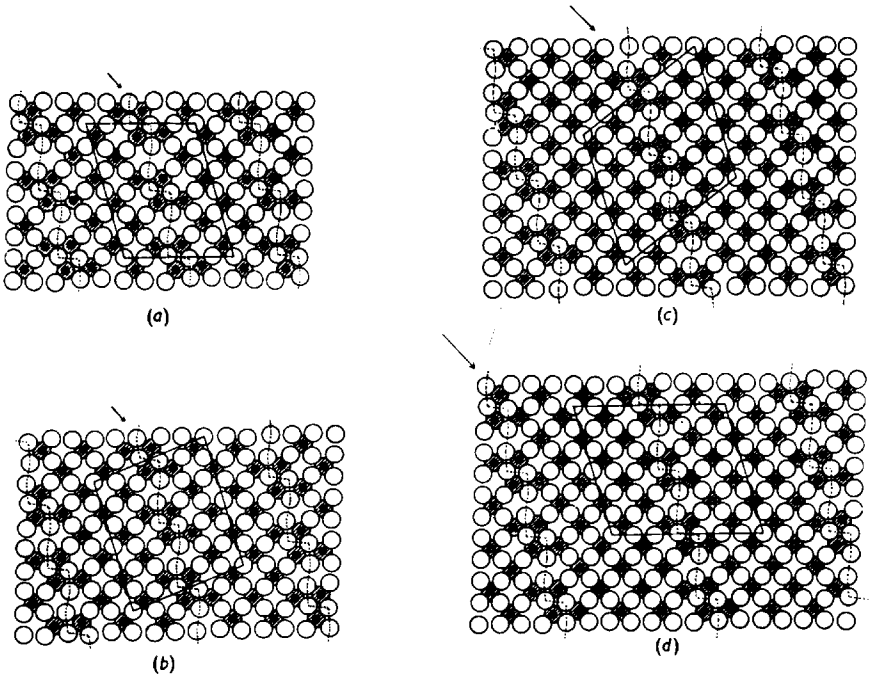

Fig. 3. Homologous series of molybdenum tungsten oxides M_nO_{3n-1} (n = 8, 9 10 and 11) with {102} crystallographic shear.

phases is M_nO_{3n-1}, where n with an observed maximum value of 14 represents the width of the slabs, i.e. the number of metal-oxygen octahedra between consecutive shear planes (Ref. 5).

Studies on other transition metal oxide systems such as titanium and vanadium oxides gave further evidence of the importance of crystallographic shear as a structural mechanism to accommodate a moderate reduction while still preserving the nearest coordination of oxygen around the metal atoms. These oxide systems were also found to contain long homologous series of daltonide phases.

For smaller degrees of reduction, i.e. for increasing distances between the shear planes, the difficulties to interpret the X-ray diffraction data were found to increase. It became evident that the structural problems set by such systems were approaching the limits of applicability of the X-ray techniques.

The way out of these difficulties was entered when Wadsley and others some ten years ago applied the electron microscope for lattice imaging of complex niobium oxides (Ref. 6). The availability of microscopes with a resolution of 3.5 Å or better and the advances in the theory of the image formation (Ref. 7 and 8) have helped to develop this technique into a means of imaging structures of crystals, applicable to large groups of chemical compounds.

In this connection it should be pointed out that the meaning of "structure" as obtained from electron microscope studies may differ considerably from that of X-ray diffraction structure. The single crystals used in X-ray experiments may seem very small, typically measuring thousandths or hundredths of a millimeter on an edge. This little volume, however, contains an enormous number of unit cells, and the crystal structure derived from the X-ray diffraction data represents an average structure of these unit cells, which individually may deviate more or less from the average. The image in the high resolution electron microscope shows the structure on the atomic level and is formed by a volume of the crystal which is less than the one used in the X-ray experiment by a factor of something like 10^{14}. The electron microscope is thus able to give detailed information about local deviations and defects in the crystal structure and also about local compositional variations.

ORDER AND DISORDER IN REDUCED TUNGSTEN TRIOXIDE

Reduced tungsten trioxide gives ample evidence of the applicability of electron microscopy for studies of non-stoichiometry and disorder. Research in that field has been reported by several authors in recent years. The present survey will mainly describe results obtained by M. Sundberg in investigations of samples of compositions WO_{3-x} ($0 < x < 0.13$) mostly heated at temperatures above 1000°C for periods up to several weeks. The study, which was started as an attempt to prepare homologues of $W_{20}O_{58}$ and to determine structural characteristics of such phases, has since been considerably widened in its scope. The investigations of the reduced tungsten trioxide samples include characterization by X-ray powder photographs, single crystal X-ray structure determination whenever suitable crystals are obtained, and electron microscope studies involving electron diffraction and imaging of very thin crystal fragments.

An X-ray structure analysis of a single-crystal of a sample of approximately $WO_{2.92}$ composition had given a structure rather similar to that of $W_{20}O_{58}$ (Fig. 4a), with {103} crystallographic shear in a basic ReO_3-type structure (Ref. 9). The difference lies in the thickness of the slabs between the shear planes. This corresponds to n = 25 WO_6 octahedra in the new phase, which gives the formula $W_{25}O_{73}$ ($WO_{2.92}$). The structure image is shown in the top picture of Fig. 4b. The texture of the areas between the dark dotted bands has the dimensions and orientation required by tungsten atoms arranged as in an ReO_3-type structure. These parts of the structure are obviously resolved. The dark bands are in an {103} orientation and comprise the groups of six tungsten atoms in edge-sharing octahedra. The tungsten atoms of the groups are not resolved but the interstices between them are visible. The micrograph thus gives a clear picture of the projection of the atomic arrangement in the direction of the electron beam.

However, a detailed analysis of the image shows that the spacing of the shear planes is not entirely uniform. The bottom picture of Fig. 4b is an interpretation of the area in the box in terms of WO_3 octahedra. Values of n = 25 are most frequent, but deviating n values are often found. The crystallite is thus not strictly stoichiometric in character and shows compositional deviations on the microlevel associated with variations in the thickness of the ReO_3-type slabs (Wadsley defects).

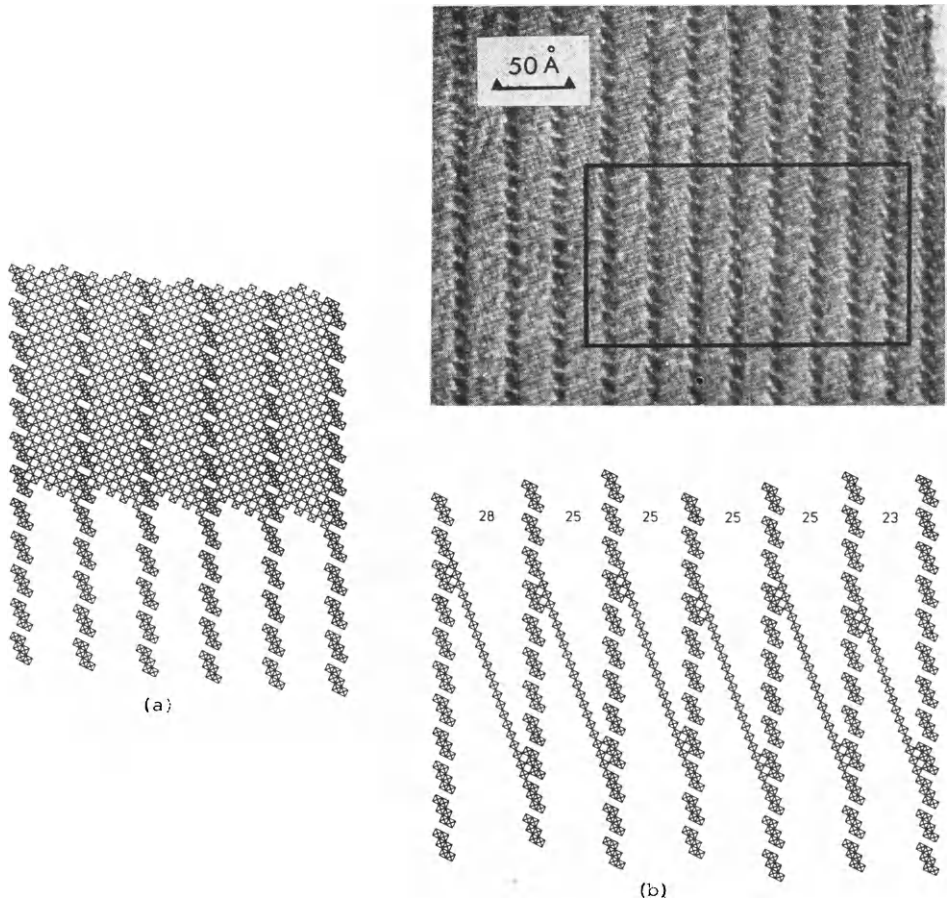

Fig. 4. Structure of $W_{20}O_{58}$ as formed by WO_6 octahedra (left). Structure of $W_{25}O_{73}$ (right). Top picture shows electron-optical image and bottom picture interpretation in terms of WO_6 octahedra of portion within box (Ref. 9).

The $W_{25}O_{73}$ structure is easily identified by the electron diffraction pattern shown in Fig. 5a. The substructure of ReO_3-type is clearly visible, and the rows running in the [103] direction, consisting of fairly sharp, weaker reflections at intervals of 1/25 of the unit length in that direction, identify the crystallite as containing the n = 25 member of the W_nO_{3n-2} series. Electron diffraction studies of a large number of crystallites, however, show that some are characterized by n values other than 25, viz. in decreasing order of frequence 24, 23, 22 and 26. Some crystallites give diffraction patterns of two different n values, mostly 25 and 24 and should thus consist of $W_{25}O_{73}$ and $W_{24}O_{70}$ domains grown together in a coherent way.

The results obviously answer in the affirmative the question if homologues other than $W_{20}O_{58}$ exist in the series. However, it is also obvious that at higher n-values crystals of different homologues may form simultaneously and that there is a tendency towards compositional deviations by crystals containing Wadsley defects.

Crystallites from a sample of the composition $WO_{2.97}$ give a quite different diffractogram (Fig. 5b). It does not exhibit rows of fairly distinct spots in the [103] direction but rather continuous streaks pointing in the [102] direction. The structure image is shown in Fig. 6. The shear planes are in {102} orientation, which means that edge-sharing takes place within groups of four WO_6 octahedra. The variation of the spacings between the shear

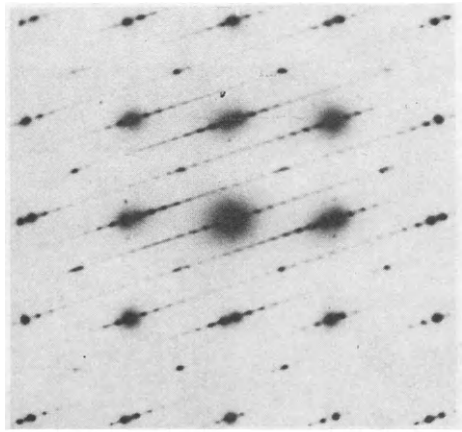

(a)

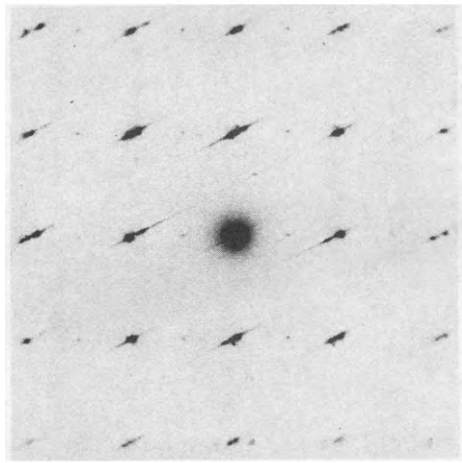

(b)

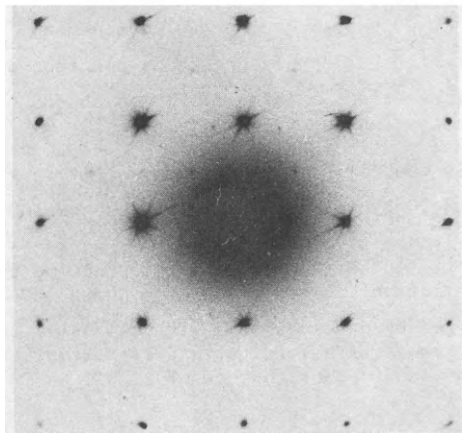

(c)

Fig. 5. Electron diffraction patterns of crystallites of compositions (from top) $WO_{2.92}$, $WO_{2.97}$ and $WO_{2.99}$ (Ref. 10).

planes is very large. The average n value for the crystal fragment (n = 33-34) gives an average composition of $WO_{2.97}$. The local compositional variations are considerable in spite of the long heating time at the synthesis. It seems appropriate to describe the material as substoichiometric berthollide tungsten trioxide. The deficiency in oxygen is associated with parallel but irregularly spaced crystallographic shear planes.

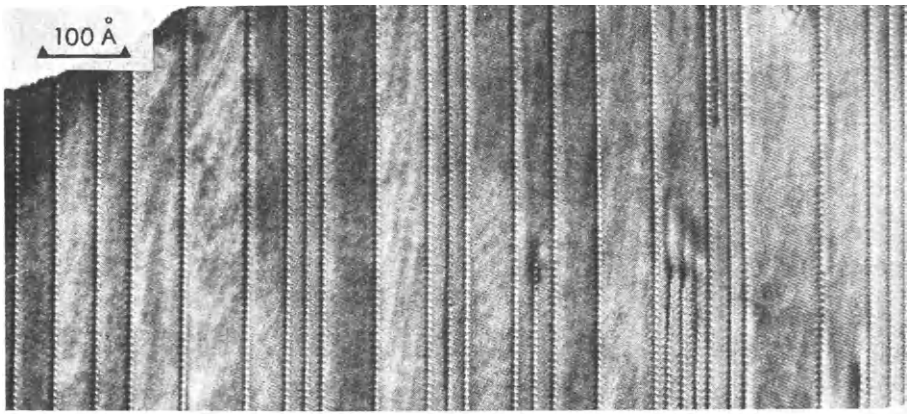

Fig. 6. Structure image of $WO_{2.97}$ crystallite. Shear planes ending within the crystal are likely to have formed under the influence of the electron beam in the microscope (Ref. 10).

For still smaller degrees of reduction the picture changes further. Fig. 5c gives the electron diffractogram of a crystallite of the approximate composition $WO_{2.99}$. The reflections are only those of tungsten trioxide but they show streaking by faint continuous rays protruding in all four equivalent directions $\lfloor 102 \rceil$, $[201]$, $[\bar{1}02]$ and $\lceil \bar{2}01 \rceil$. The structure image is shown in Fig. 7. It contains shear planes in all those four orientations with large and irregular spacings. It should be pointed out that tungsten trioxide, which is monoclinic at room temperature, is actually tetragonal at the temperature of formation of the reduced crystal. This may be the reason why shear planes appear with all possible orientations at small degrees of reduction. In this connection it is interesting to note that crystallographic shear in all orientations and with irregular spacing was observed by Gadó (12) in studies of the reduction of WO_3 to $W_{20}O_{58}$ at far-off-equilibrium conditions.

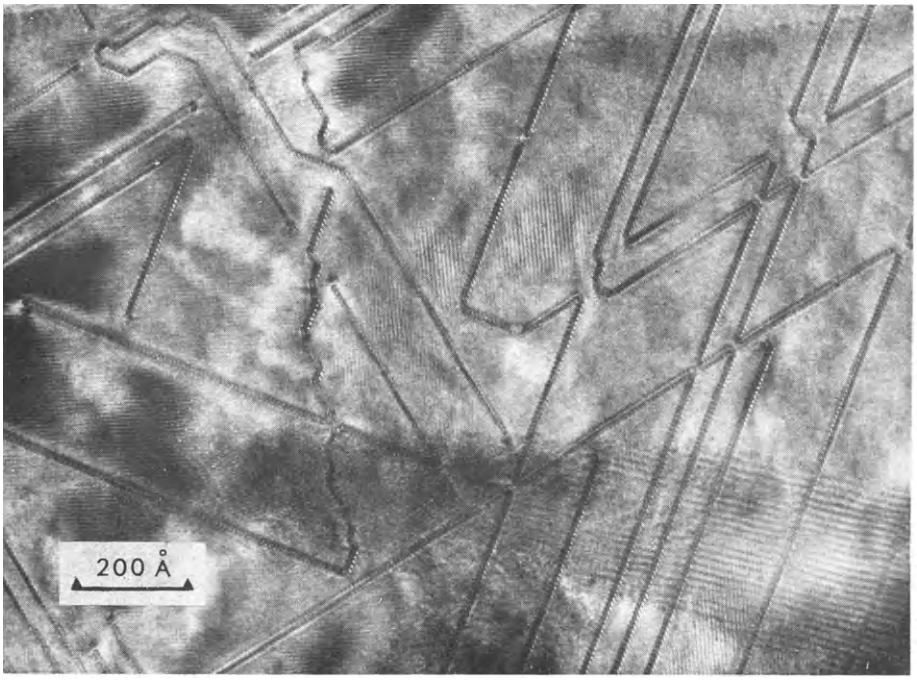

Fig. 7. Structure image of $WO_{2.99}$ crystallite (Ref. 11).

In conclusion it may be stated that the present knowledge of the mechanism of reduction in substoichiometric tungsten trioxide in its main lines is as follows: Slight reduction at elevated temperatures introduces crystallographic shear of {102} type in all possible directions and with irregular spacing. Further reduction suppresses all but one of the orientations of the shear planes, but they remain irregularly spaced and the nonstoichiometric character is preserved. Upon further reduction the shear planes change to an {103} orientation. This implies a higher reduction at the planes and serves to increase the spacing between them. As the reduction continues there is an increasing tendency of formation of discrete phases with narrow ranges of homogeneity and eventually phases approaching daltonide character.

Further experiments will be needed to add more detail to the picture of the structural mechanism of substoichiometry in tungsten trioxide. It may be mentioned that structure image studies have shown the transition from {102} to {103} crystallographic shear to be dependent not only on the degree of reduction but also on the temperature (Ref. 13).

INTERGROWTH TUNGSTEN BRONZES

For the alkali atoms larger than sodium, bronze structures occur which are different from the simple cubic structure referred to above. However, also these bronzes exist over considerable ranges of composition A_xWO_3 and are instances of non-stoichiometry due to high concentrations of point defects. The hexagonal and tetragonal potassium tungsten bronzes illustrated in Fig. 8, both contain networks of WO_6 octahedra linked by corners. The tetragonal bronze structure contains pentagonal as well as square tunnels wherein the alkali atoms reside (Ref. 14). The potassium content may approach the theoretical upper limit of $K_{0.6}WO_3$, which corresponds to 100 percent occupancy of the sites in both types of tunnels. For lower x values the potassium atoms preferably occupy positions in the wider pentagonal tunnels (Ref. 15).

In the hexagonal bronze the potassium ions are situated within the wide six-sided tunnels formed by the WO_6 octahedra (Ref. 16) with average occupancies ranging from about 0.5 to unity. It has recently been shown (Ref. 8) that local variations in the potassium concentrations in the tunnels may be demonstrated by means of the lattice image technique.

A potassium tungsten bronze lower in alkali than the hexagonal phase has recently been found by Kihlborg and Hussain (Ref. 17). The new material which has been obtained within the compositional range K_xWO_3 ($0.05 < x < 0.10$) (cf. Fig. 9) is described as an intergrowth tungsten bronze (ITB) for reasons to be presented in the following. It exhibits bronze characteristics such as metallic lustre, bluish black in colour, and chemical resistance towards attack by alkali solutions and strong acids.

The structural characterization of the new bronze was not made by X-rays but rather by means of electron diffraction and in particular electron-optical image techniques. Only at a later stage it was possible to obtain a suitable single crystal and to perform an X-ray structure analysis. This investigation fully confirmed the electron microscope results (and gave structural data of higher accuracy) (Ref. 17).

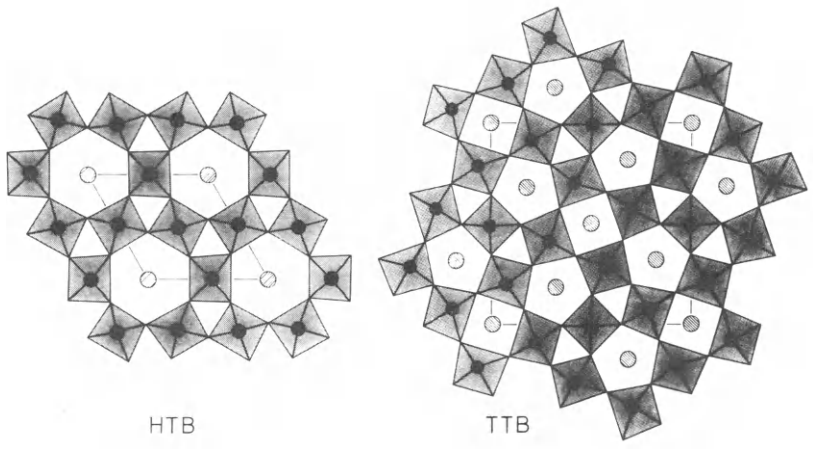

Fig. 8. Structures of hexagonal (HTB) and tetragonal (TTB) potassium tungsten bronzes.

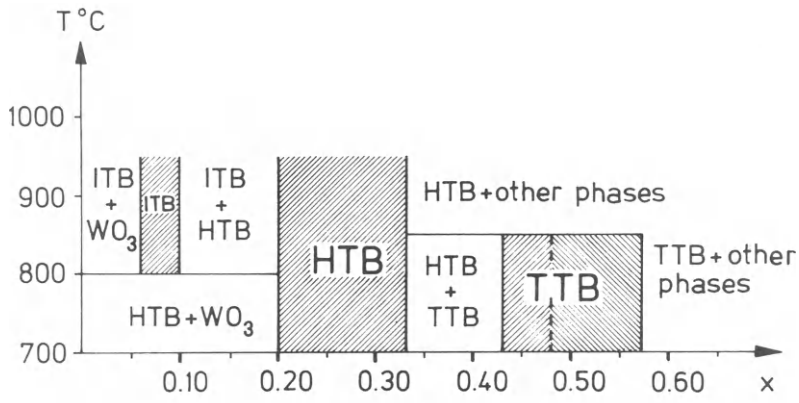

Fig. 9. Areas of formation of tetragonal (TTB), hexagonal (HTB) and intergrowth (ITB) tungsten bronzes in the K_xWO_3 system (Ref. 18).

The structure image of an ITB crystallite is given in Fig. 10. It is a very regular picture. The texture and dimensions of the lighter bands are in accordance with the tungsten atom arrangement in a resolved tungsten trioxide structure viewed along a pseudo-cube axis. The intermediary very marked double strings of "beads" may be interpreted as not entirely resolved tungsten atoms arranged in the same way as around the tunnels of the hexagonal tungsten bronze.

The resulting structure is illustrated in Fig. 11 in terms of WO_6 octahedra linked by corners. With potassium atoms occupying sites within the six-sided tunnels these should be approximately half-filled, which is roughly the same occupancy as in the hexagonal bronze at its minimum alkali content.

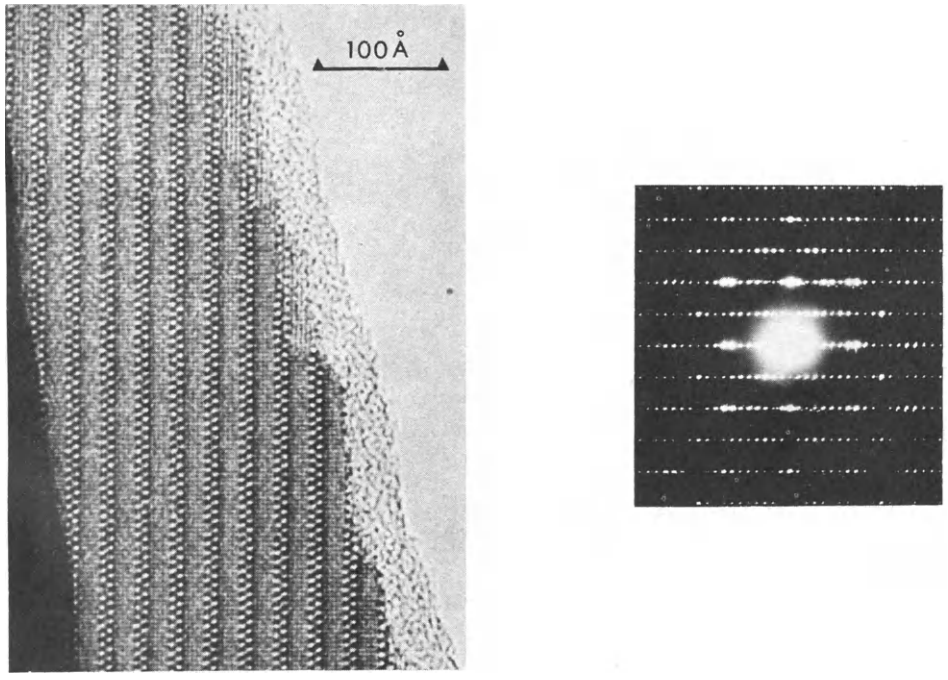

Fig. 10. Structure image and electron diffraction pattern of a crystallite of potassium intergrowth tungsten bronze.

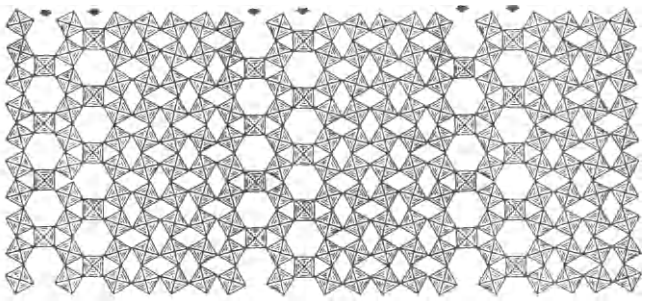

Fig. 11. Interpretation in terms of WO_6 octahedra of structure imaged in Fig. 10.

The structure may be described as an ordered intergrowth of slabs of hexagonal bronze type with slabs of distorted WO_3 type. The correctness of the structure has been confirmed by theoretical calculation of a synthetic electron microscope image from the structure model and, as mentioned above, also by a crystallographic structure determination based on single crystal X-ray data.

Families of analogous structures may be derived by changing the widths of the two types of slabs. Two of the structures in Fig. 12 also contain double rows of hexagonal tunnels but differ with respect to the thickness of the WO_3 slabs. Both types of structure have been identified in ITB samples by means of the electron microscope. As a matter of fact the very complicated X-ray powder patterns of the ITB preparations are completely accounted for if the sample is assumed to be a mixture of all three phases.

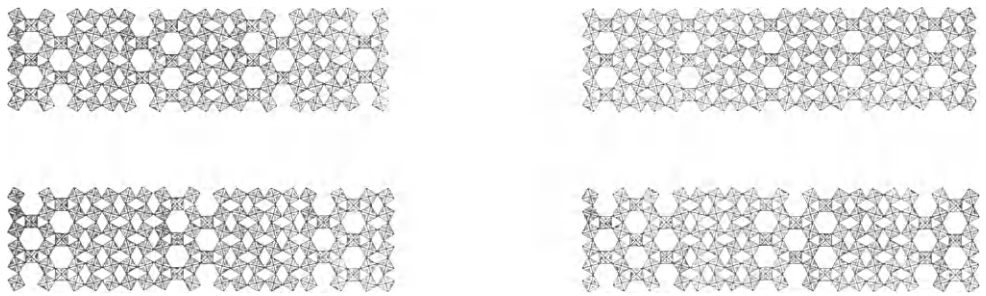

Fig. 12. ITB-type structures exhibiting different widths of WO_3 slabs (left) and of HTB slabs (right).

Structures deviating with regard to the widths of the hexagonal bronze slabs (cf. Fig. 12) have not been observed in ITB samples except as faults in structures of the type described above. The structure image of a crystallite of a rubidium intergrowth tungsten bronze (Fig. 13) shows a highly disordered structure with differing widths of the WO_3 slabs and instances of single as well as triple rows of hexagonal tunnels.

The combined studies by X-ray crystallography and electron microscopy techniques have shown that products formed within the ITB area of the diagram presented in Fig. 9 invariably are composite in character. The components are members of a series of closely related structures formed by an ordered intergrowth of slabs of WO_3 and HTB structure, the various members differing by the widths of the slabs. Attempts to prepare homogeneous samples of individual members of the series have so far been unsuccessful. The small crystals of the preparations, however, often contain just one type of structure with a moderate content of structural defects due to the local presence of slabs of deviating thickness. This suggests that the various structures form under similar conditions and once formed, a structure does not easily react to transform into a structural homologue.

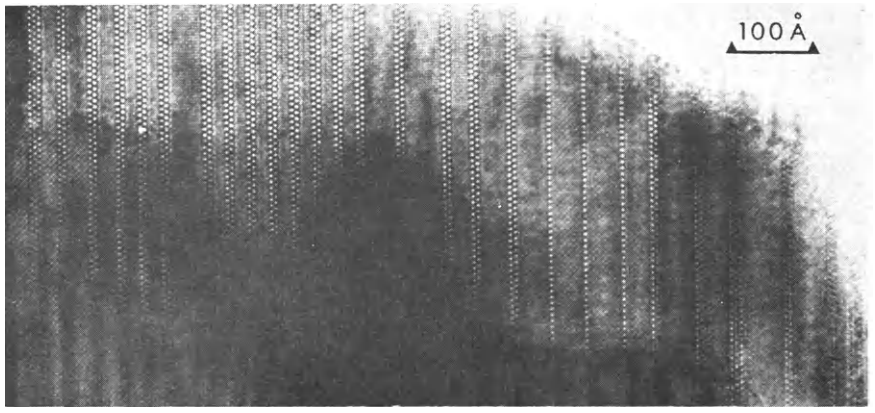

Fig. 13. Image of disordered structure of rubidium intergrowth tungsten bronze.

The mechanism of non-stoichiometry in the intergrowth tungsten bronze structures is twofold. It evidently combines the features of extended defects, similar to the Wadsley defects, with gross point defects due to partial occupancy of the alkali atom positions in the hexagonal tunnels. Further research will be necessary to evaluate the combined effects on the non-stoichiometry of these two kinds of structural disorder.

CONCLUDING REMARKS

The instances of non-stoichiometry described above should serve to illustrate the importance of detailed structural knowledge for the appreciation of the often very intricate relations between daltonide and berthollide character in transition metal oxides. Structure image electron microscopy as a means to study structural defects and compositional variations on the atomic level has brought a most powerful complement to the structural knowledge obtainable with diffraction methods. The present rapid development of electron microscopes with higher resolution and the increasing insight in the theory of the image formation will certainly make the new technique applicable to further groups of compounds to provide knowledge of importance in correlating composition and structure with chemical and physical properties of materials.

REFERENCES

1. G. Hägg, Z. Phys. Chem. B29, 192-204 (1935).
2. A. Magnéli, Arkiv Kemi 1, 513-523 (1949).
3. A. Magnéli, Acta Chem. Scand. 2, 501-517 (1948).
4. B. Blomberg, L. Kihlborg and A. Magnéli, Arkiv Kemi 6, 133-138 (1953).
5. A. Magnéli, Acta Cryst. 6, 495-500 (1953).
6. J.G. Allpress, J.V. Sanders and A.D. Wadsley, Acta Cryst. B25, 1156-1164 (1969).
7. S. Iijima, J. Appl. Phys. 42, 5891-5893 (1971).
8. J.M. Cowley and S. Iijima, Phys. Today, March, 32-40 (1977).
9. M. Sundberg, Acta Cryst. B32, 2144-2149 (1976).
10. M. Sundberg. Unpublished results.
11. L. Kihlborg and M. Sundberg, Siemens Rev. 43, 3-8 (1976).
12. P. Gadó, Acta Cryst. A16, 182 (1963).
13. M. Sundberg and R.J.D. Tilley, J. Solid State Chem. 11, 150-160 (1974).
14. A. Magnéli, Arkiv Kemi 1, 213-221 (1949).
15. L. Kihlborg and A. Klug, Chemica Scr. 3, 207-211 (1973).
16. A. Magnéli, Acta Chem. Scand. 7, 315-324 (1953).
17. A. Hussain and L. Kihlborg, Acta Cryst. A32, 551-557 (1976).
18. A. Hussain and L. Kihlborg. Unpublished results.

Pure & Appl. Chem., Vol.50, pp.781-783
Pergamon Press Ltd.1978, Printed in Great Britain.

0033-4545/78/0801-0781 $02.00/0

MOLECULAR REACTION DYNAMICS BY THE CROSSED MOLECULAR BEAM TECHNIQUE: A FEW RECENT EXAMPLES

Richard B. Bernstein

Department of Chemistry, Columbia University, New York, N.Y. 10027, U.S.A.
and The University of Texas, Austin, TX 78712, U.S.A.

Abstract - Several recent examples are presented of experimental studies by the author and his co-workers on the microscopic chemical dynamics of elementary reactions via the crossed molecular beam technique. The reactions investigated include the following:

$M + XCH_3 \rightarrow MX + CH_3$ ($M \equiv Rb,K$; $X \equiv I,Br$)

$MF + K \rightarrow M + FK$ ($M \equiv Cs,Rb$)

$Hg + IX \rightarrow HgI + X$ ($X \equiv I,Br$)

$Hg(^3P_0) + Br_2 \rightarrow HgBr^*(B) + Br$

$N + XY \rightarrow NX + Y$ ($X,Y \equiv I,Br,Cl$)

INTRODUCTION

The subject of molecular dynamics is concerned with the microscopic, molecular mechanism of elementary chemical reactions (Ref. 1). Fundamental details of the intimate process of reaction via collision of atoms and molecules can be provided from experiments which make use of the crossed molecular beam method. Typically, measurements are made of the angular and recoil velocity distributions of the nascent products of a binary molecular reaction, from which a number of important features of the intermolecular potential energy hypersurface can be deduced fairly directly.

At the previous IUPAC Congress the author reviewed the mutual interplay of theory with experiment in the field of molecular reaction dynamics (Ref. 2). The present paper is devoted to the presentation of a few case studies, examples of elementary reactions investigated by the crossed beam technique in the author's laboratory, which have been subjected to detailed theoretical-computational analysis.

RESULTS

The first of these examples consists of a precise quantitative measurement of the translational energy dependence of the total reaction cross section for a direct-mode, rebound reaction, $Rb + ICH_3 \rightarrow RbI + CH_3$ (Ref. 3), serving as a test of various theoretical predictions. A quantitative determination of the ratio of the cross section for this reaction to that of the closely related reaction with potassium over a wide energy range has been carried out (Ref. 4), allowing comparison with several theoretical dynamical calculations in the literature. These experiments, taken together with previously published results, have confirmed the existence of small translational energy thresholds E_0 for these reactions, beyond which the reaction cross section $\sigma_R(E_{tr})$ rises to a maximum with increasing translational energy E_{tr} and then declines to a minimum at energies $\gtrsim$0.9 eV.

Very recent experiments on the reactions of K and Rb with CH_3Br (Ref. 5) have shown clear evidence for appreciable energy thresholds (ca. 0.1-0.2 eV), corresponding to substantial activation barriers. These results account for the very small thermal cross sections for the exoergic CH_3Br-alkali family of reactions.

The second study deals with the complex-mode reactions $CsF,RbF + K \rightleftarrows [CsFK,RbFK] \rightarrow Cs,Rb + FK$. The branching ratios for the decay of the collision complexes have been measured as a function of the relative translational energy (Ref. 6), and the influence of the rotational energy of the diatomic reagent has been directly determined (Ref. 7 & 8). It is of interest

to note that for the CsF reaction, which is endoergic, the reactive branching fraction F_R increases with E_{tr}, and the reactivity is enhanced by reagent rotational energy, E_{rot}, while for the exoergic RbF reaction, F_R decreases with E_{tr} and with E_{rot} as well. The results have been interpreted in terms of the RRKM-Herschbach (RRKMH) model for formation and decay of a long-lived triatomic complex (Ref. 9).

The third investigation involves first the endoergic (1.15 eV) reaction $Hg + I_2 \rightarrow HgI + I$, for which the translational energy threshold, E_0, has been experimentally determined (Ref. 10). It is found that E_0 is essentially equal to the endoergicity, implying that the intrinsic activation barrier for the reaction is, for practical purposes, zero. Evidence is presented from angular distribution measurements over a wide range of translational energies that the reaction proceeds via the insertion of Hg into I_2 to form the normally stable IHgI molecule, which must decay (because of its excess internal energy) either into the products HgI + I or the reactants $Hg + I_2$. The onset of collision-induced dissociation (at 1.54 eV) is observed (Ref. 11). An empirical potential energy surface for this system has been deduced (Ref. 12) from these results. The entire body of experimental data can be understood in terms of an extended version of the RRKMH theory, assuming the presence of a barrier of ca. 0.5 eV in the entrance channel. Confirmatory experiments have been carried out for the analogous reaction of Hg with IBr (Ref. 13); the (different) thresholds for the formation of both HgI and HgBr products have been overcome by translational excitation.

The fourth investigation deals with the reaction of metastable Hg atoms, i.e., $Hg(6^3P_0) + Br_2 \rightarrow HgBr^*(B^2\Sigma^+) + Br$, observed in a crossed beam experiment via the chemiluminescence of the $HgBr^*$ product at 500 nm (Ref. 14). The cross section is smaller by more than an order of magnitude than that reported in the literature for the analogous reaction with $Hg(6^3P_2)$ atoms. This difference in reactivity is apparently a spin-orbit effect, suggesting a potential energy barrier for the $^3P_0$ reaction which is absent for the $^3P_2$ case.

The final example consists of a series of bimolecular beam reactions of atomic nitrogen (Ref. 15). Five reactions of the type $N + XY \rightarrow NX + Y$ (where $X,Y \equiv I,Br,Cl$) have been observed using the crossed molecular beam scattering technique. The NX product is mass spectrometrically detected over a range of scattering angles. From the product intensities it is concluded that the cross sections (for the exoergic reactions) are large (i.e., essentially gas-kinetic). A number of other reactions of atomic nitrogen reported in the literature on the basis of flame, discharge and other types of bulk, gas phase, experiments occurred with only negligible cross sections when the experiment was carried out under single-collision (beam vs. beam) conditions. Few of them appear to be bimolecular elementary reactions.

CONCLUDING REMARKS

This paper has reviewed a few examples of elementary chemical reactions studied recently by the author and his co-workers by means of the crossed molecular beam technique. Due to considerations of brevity, it has, unfortunately, been impractical to refer to the many significant contributions of other molecular beam laboratories around the world. It should be emphasized, however, that molecular beam chemistry is an activity now being actively pursued in many laboratories scattered throughout IUPAC-land, and the combined knowledge derived from such molecular dynamics studies is of great value in providing an understanding of the microscopic mechanism of elementary chemical reactions.

Acknowledgment - This work received financial support from the National Science Foundation (Grant CHE73-04940 A03) and the R. A. Welch Foundation (Grant F-567).

REFERENCES

1. R.D. Levine and R.B. Bernstein, Molecular Reaction Dynamics, Clarendon Press, Oxford (1974); Japanese edition, H. Inouye, Editor, Tokyo Press (1976).
2. R.B. Bernstein, 25th IUPAC Congress, Jerusalem; Israel J. Chem. 14, 79 (1975).
3. S.A. Pace, H.F. Pang and R.B. Bernstein, J. Chem. Phys. 66, 3635 (1977).
4. K.T. Wu, H.F. Pang and R.B. Bernstein, J. Chem. Phys. (submitted).
5. H.F. Pang, K.T. Wu and R.B. Bernstein (to be published).
6. S. Stolte, A.E. Proctor and R.B. Bernstein, J. Chem. Phys. 65, 4990 (1976).
7. S. Stolte, A.E. Proctor, W.M. Pope and R.B. Bernstein, J. Chem. Phys. 66, 3468 (1977).
8. L. Zandee and R.B. Bernstein (to be published).
9. S. Stolte (to be published).

10. B.E. Wilcomb, T.M. Mayer, R.B. Bernstein and R.W. Bickes, Jr., J. Amer. Chem. Soc. 98, 4676 (1976).
11. T.M. Mayer, B.E. Wilcomb and R.B. Bernstein, J. Chem. Phys. 67, (1977), in press.
12. T.M. Mayer, J.T. Muckerman, B.E. Wilcomb and R.B. Bernstein, J. Chem. Phys. 67, (1977), in press.
13. S. Hayashi, T.M. Mayer and R.B. Bernstein (unpublished).
14. S. Hayashi, T.M. Mayer and R.B. Bernstein, Chem. Phys. Lett. (submitted).
15. R.L. Love, J.M. Herrmann, R.W. Bickes, Jr. and R.B. Bernstein, J. Amer. Chem. Soc. (submitted).